

Investigation of Measurement Techniques for Obtaining Airborne
Antenna Spectrum Signatures

J. E. Ferris, S. E. Stone and R. L. Wolford

Technical Report AFAL-TR-65-104

May 1965

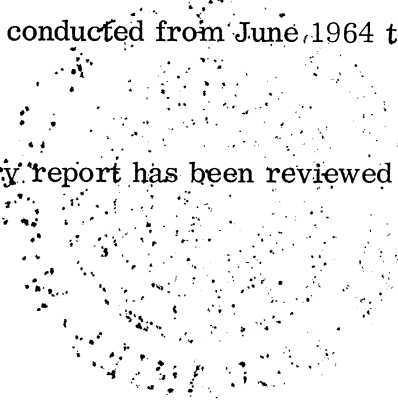
Final Report

FOREWORD

This report was prepared by The University of Michigan under USAF Contract No. AF33(615)-1964. The contract was initiated under Proj. No. 4357, "Electromagnetic Compatibility Techniques" and Task No. 435703, "RF Interference Measurement Techniques". The work was administered under the direction of the Electronic Warfare Division, Air Force Avionics Laboratory at Wright-Patterson Air Force Base, Ohio with Mr. H. M. Bartman as Project Manager and Mr. K. W. Tomlinson as Contract Monitor.

This report covers work conducted from June 1964 to March 1965.

This technical documentary report has been reviewed and is approved.


Ronald L. Stimmel
LIONEL W. ROBERTS
Lt Colonel, USAF
Chief, Electronic Warfare Division

ABSTRACT

This report presents measurement techniques applicable for determining the three-dimensional spectral radiation patterns of antennas installed in airborne vehicles.

There are six possible measurement techniques that may be followed to obtain spectrum signatures of airborne antennas. These techniques are characterized by the type of models used, namely, 1) full-scale models, 2) full-scale partial mock-ups, 3) instrumented flying aircraft, 4) precision scale models, 5) simplified scale models, and 6) simplified partial models. The data obtained for electromagnetic compatibility analysis is normally required to be in a statistical form, therefore, a discussion of the instrumentation required to obtain data suitable for statistical analysis will also be presented.

TABLE OF CONTENTS

	ABSTRACT	ii
I	INTRODUCTION	1
II	CONVENTIONAL TECHNIQUES	5
	2.1 Full-Scale Models	5
	2.2 Partial Full-Scale Models	11
	2.3 Instrumented Aircraft	13
	2.4 Precision Scale Models	17
III	SIMPLIFIED TECHNIQUES	21
	3.1 Simplified Scale Models	21
	3.2 Simplified Partial Models	41
	3.2.1 Introduction	41
	3.2.2 Derivation of Approximation	57
	3.2.3 Analysis of the Far Field	60
	3.2.4 Uncorrected Results (First Set of Numerical values)	65
	3.2.5 Analytical Derivation of Correction Term	73
	3.2.6 Corrections to the Arcs of IV	76
	3.2.7 Numerical Results (Second Set of Numerical values)	81
	3.2.8 Limiting Case of Large R	86
	3.2.9 Conclusions Concerning the Numerical Results	86
IV	INSTRUMENTATION	88
V	CONCLUSIONS AND RECOMMENDATIONS	89
	REFERENCES	91
	ACKNOWLEDGMENTS	93
	APPENDIX A - Determining Aspect Angles from Photographs	94
	APPENDIX B - $g_1(\xi)$ vs $(kR = 4.19, 2)$	102

I

INTRODUCTION

Demand for the use of the electromagnetic spectrum has increased both nationally and internationally since World War II. This demand will undoubtedly continue and at an accelerated pace in view of present and future space program requirements. As the number of transmitters and receivers placed in service increases, so will the probability of interference between systems. A principal cause for interference in addition to the fundamental frequency being transmitted and received is that due to spurious and harmonic frequencies. Because of this interference source, the efficient use of the electromagnetic spectrum has been reduced. Other associated factors that contribute to the interference problem are: transmitted power level, frequency assignments, equipment bandwidth, antenna radiation characteristics, etc.

Because the radiation characteristics of airborne antennas are an essential part of the present electromagnetic compatibility program, a study of antenna pattern measurement techniques is being conducted by The University of Michigan. The purpose of this study is to determine feasible measurement techniques for obtaining three-dimensional RF spectrum signature data of airborne antennas in the 100 Mc - 20 Gc frequency range at the fundamental, spurious, and harmonic frequencies.

Before discussing the various measurement techniques, some antenna types that may be associated with airborne vehicles will be considered. Turner (1959) characterized the antennas normally used in airborne systems as follows: in the 100-500 Mc range, the antennas are low-gain (less than +7 db with respect to an isotropic source) broad beam unidirectional or split beam omnidirectional

antennas. Typical 100-500 Mc antennas are: stubs, biconicals, helices, spirals, logarithmic periodic structures, etc. In the 500 Mc - 10 Gc frequency range, both low- and high-gain antennas are employed, and at frequencies above 10 Gc high-gain antennas are typical. Examples of high-gain antennas are: parabolic reflectors, lenses, planar arrays, horns, etc.

The radiation characteristics of low- and high-gain antennas are altered, first because of the surface currents (Fig. 1) and secondly, by shadowing effects (Fig. 2) associated with the vehicle. Since the shadowing effect can be handled reasonably well by analytical means, it was concluded that emphasis should be on measurement techniques applicable to low-gain antennas.

The feasibility of using standard antenna measurement procedures for obtaining the desired spectrum signature data was first considered. Measurement procedures that have been employed in the past are characterized by the type of models used, namely: 1) full-scale models, 2) full-scale partial models, 3) instrumented flying aircraft, and 4) precision scale models.

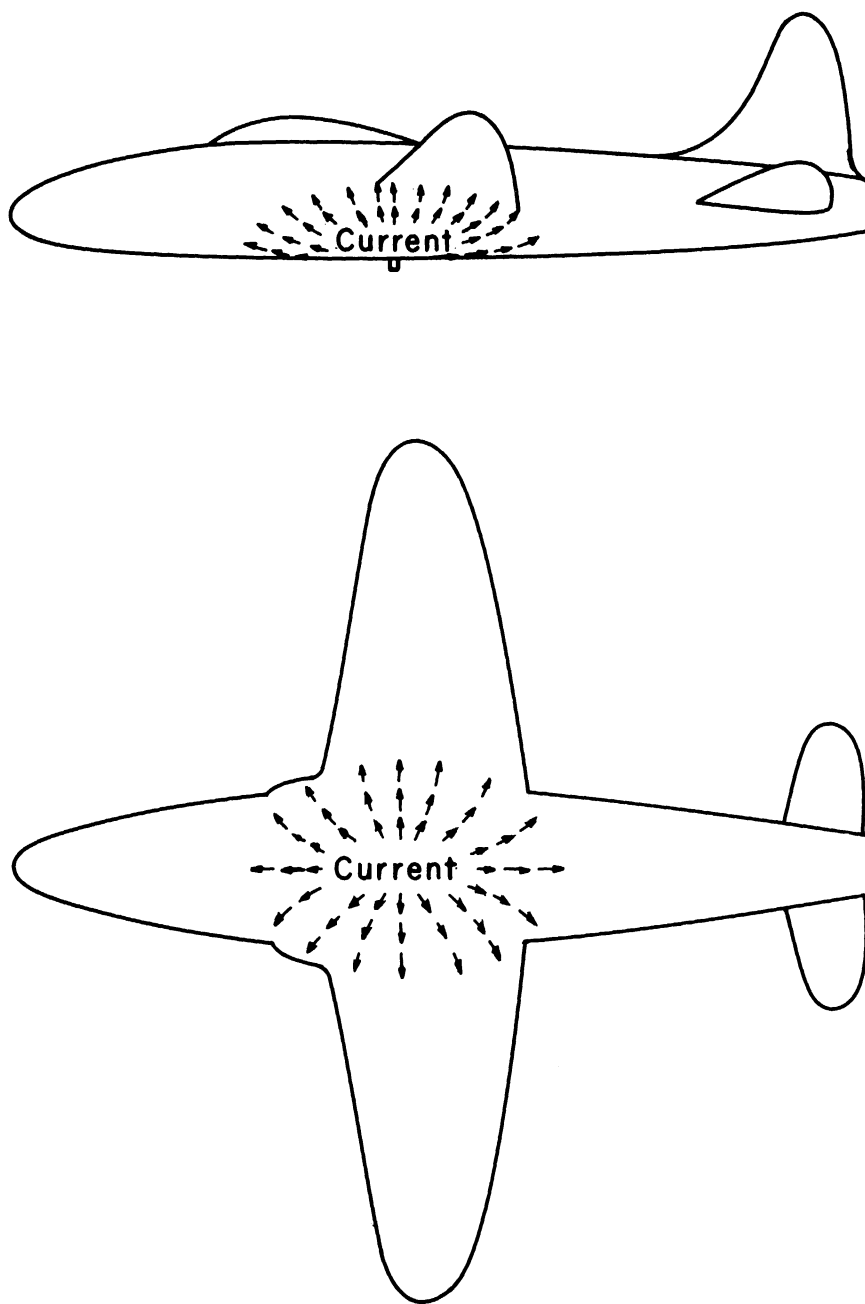


FIG. 1: AIRFRAME SURFACE CURRENTS.

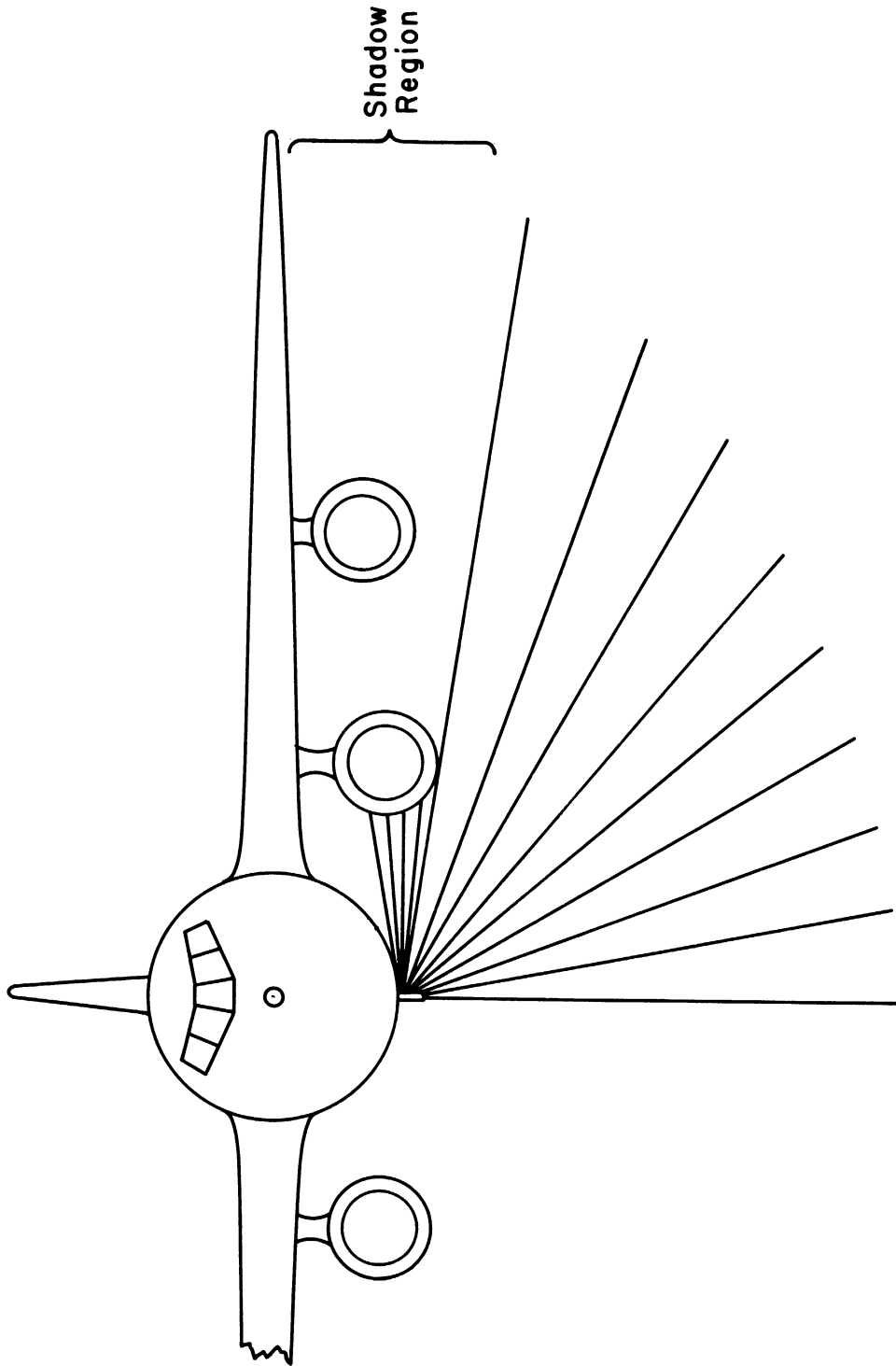


FIG. 2: SHADOWING EFFECT.

II

CONVENTIONAL TECHNIQUES

Procedures, problems, and typical costs associated with the above four measurement techniques as applied to low-gain low-frequency antennas will be considered in the following discussion.

2.1 Full-Scale Models

Full-scale airborne models have been used by several laboratories in the design and development of airborne antennas (North American Aviation, 1964; Goodyear Aerospace Corporation, 1964; Melpar, Incorporated⁺). For large airborne systems, such as airplanes, space capsules and missiles, the model consists of a metal covered rib structure, such that the exterior contour is within the allowable tolerances of the true vehicle. The metallic covering may consist of either thin sheet aluminum or copper wire screening and the rib structure of either aluminum or wood framing material as illustrated in Fig. 3. The useful life of such models may range from 5 to 10 years. The time required to fabricate a typical full-scale model of a reconnaissance type aircraft has been estimated to be 1000 manhours at a cost of \$ 10,500 including material.

Full-scale models are generally employed to obtain either antenna coupling or impedance data and are occasionally used in measuring radio frequency interference and antenna pattern data. Since the majority of the antennas installed on airplanes are located on the underside of the fuselage, the models are erected in an upside down position, as shown in Fig. 4, to minimize ground effects. As a general rule, both transmitting and receiving antennas are tested in the receiving

⁺ Personal experience of one of present authors, former employee, Melpar, Inc.

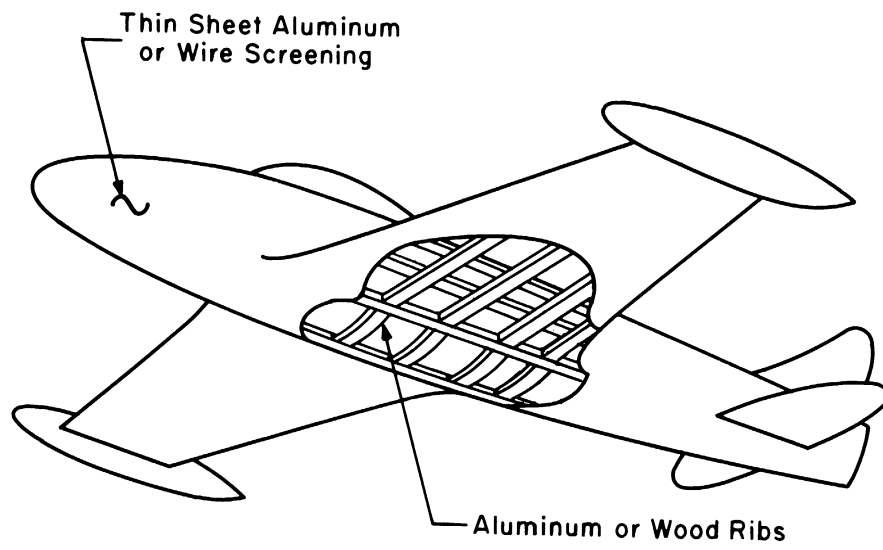


FIG. 3: FULL-SCALE MODEL.

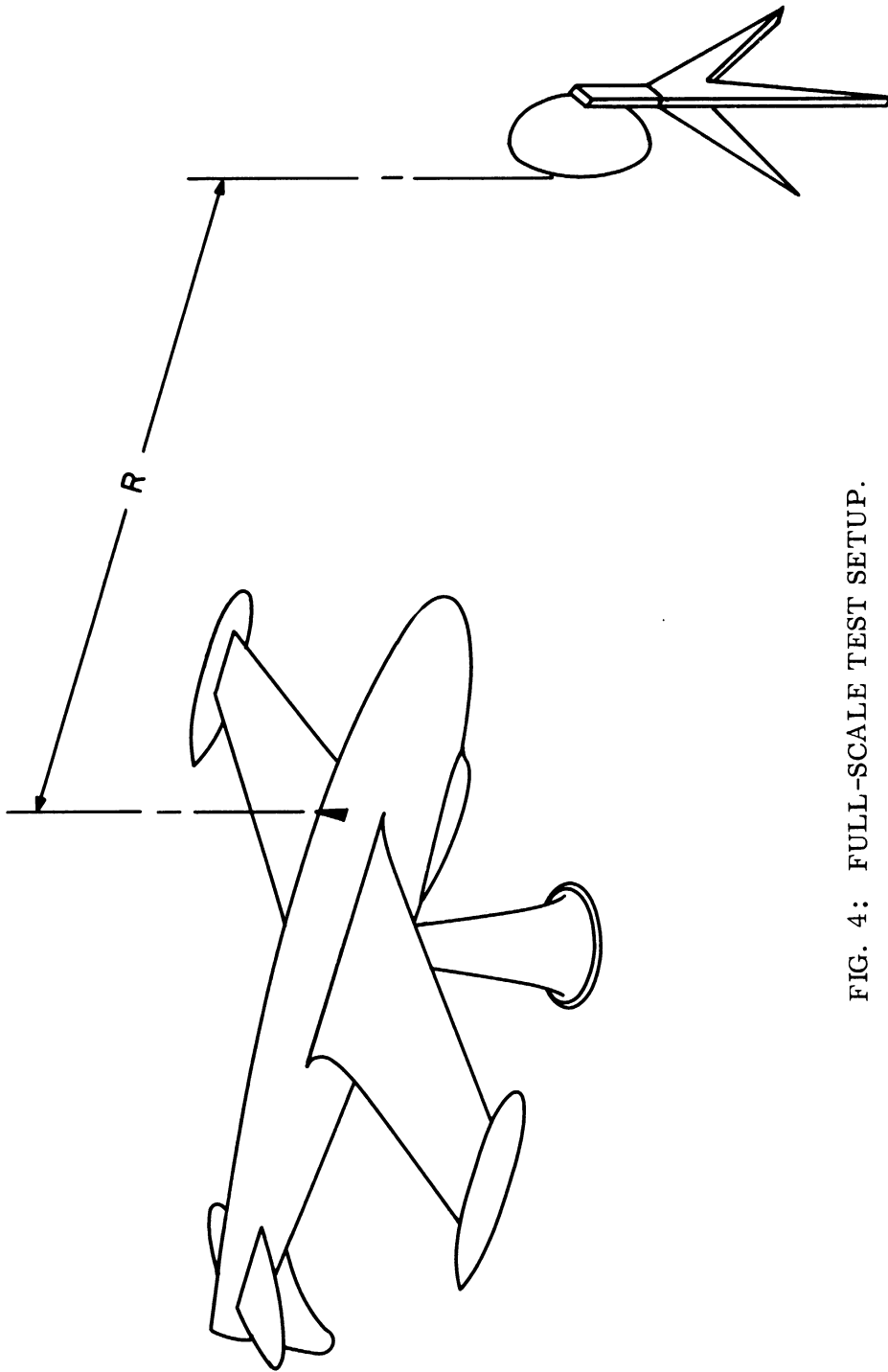


FIG. 4: FULL-SCALE TEST SETUP.

sense as the model is rotated in the horizontal plane with respect to earth. The model is illuminated from a tower located a distance, R , from the model (Fig. 4) where

$$R = \frac{2D^2}{\lambda}$$

and D and λ are the antenna effective aperture size and the operating wavelength, respectively. In the event several antennas operating at different frequencies are to be tested, the above equation must be evaluated for each condition such that an optimum-range length may be chosen.

When using a full-scale model to obtain three-dimensional antenna spectrum signatures, it is desirable to reposition either the illuminating antenna or the airplane model so that variable ϕ patterns may be recorded at various θ angles referred to in Fig. 5. Past experience has shown that the feasibility of either of the above is dependent upon the size of the full-scale model. For example, when considering reconnaissance type aircraft, bombers and fighters, it is very difficult to obtain reasonably accurate three-dimensional signature data without the use of an expensive and elaborate model rotator similar to that shown in Fig. 6. However, when considering smaller models such as missile nose cones or Piper-type airplanes, conventional model rotators have been successfully employed to obtain antenna pattern data. An alternate approach to obtaining data from large systems is to move the illuminating antenna (see Fig. 5) such that variable θ patterns are recorded at various ϕ angles. Blimps, planes (Jones, 1948), balloons (Keay and Gray, 1963), satellites (Bruckmann, 1963), etc., have been suggested as vehicles from which patterns may be recorded. However, costs and time required to obtain the desired three-dimensional data for interference analysis may be prohibitive.

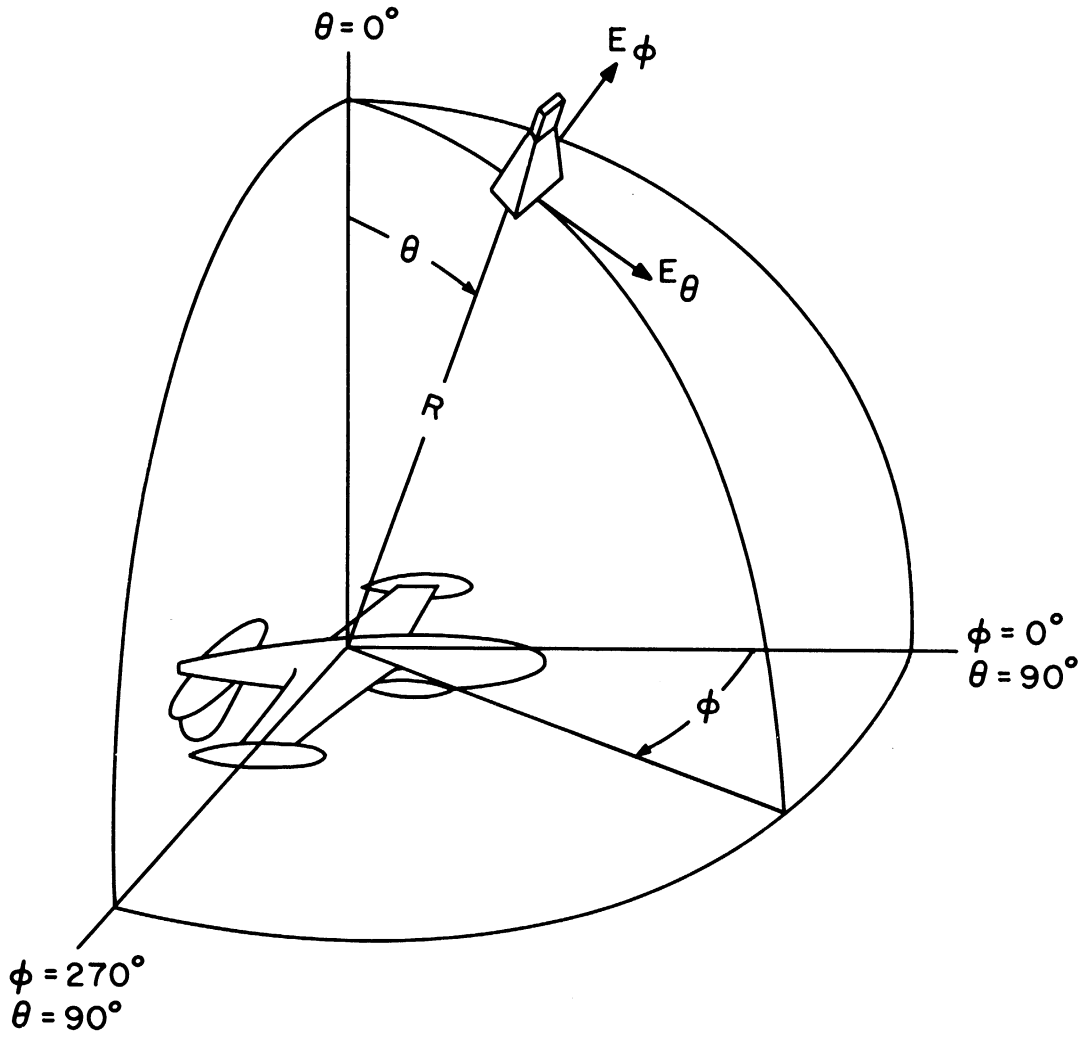


FIG. 5: SPHERICAL COORDINATE SYSTEM

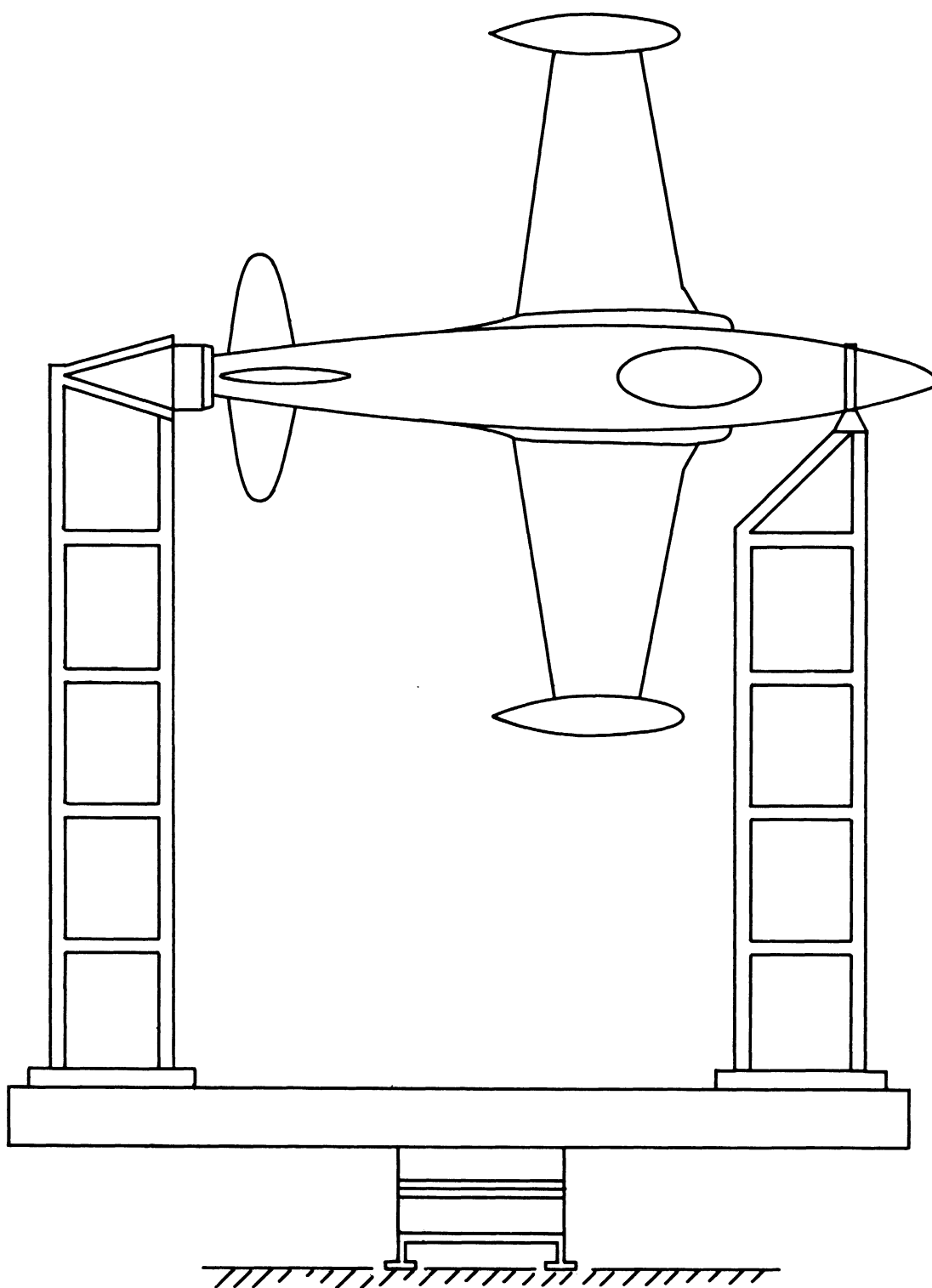


FIG. 6: ROTATOR FOR FULL-SCALE MODEL. (SCIENTIFIC-ATLANTA).

Another factor that must be considered when using full-scale models is reflections from the earth and nearby objects such as buildings, vehicles, trees, etc. Past experience has shown that this form of interference can be minimized through the judicious positioning of microwave absorbing material. However, it often requires several man hours to position the material until acceptable radiation patterns can be achieved. To justify the accuracy of the patterns, a precision scale model of the full-scale system is generally employed. From this scale model a set of reference data is obtained for comparison to the full-scale model data. It has generally been found desirable to repeat the above procedure for each frequency at which data is to be obtained, further increasing the costs.

Because of the high costs and complex procedures associated with the use of full-scale models of large airborne systems (e. g. bombers, manned space capsules) their use for obtaining spectrum signature data is not recommended.

2.2 Partial Full-Scale Models

In addition to the use of full-scale airborne models, partial full-scale models have been employed in the design and development of airborne antenna systems, their principal use being to obtain impedance and occasional pattern data. The fabrication of the partial model is identical to that of the full-scale model, with cost dependent on model size. To obtain reasonably accurate pattern data, it has been found advisable to model all parts of the aircraft within 5 wavelengths of the antenna under test (Dorne and Lazarus, 1947) as shown in Fig. 7. In general, this technique is applicable to airborne systems employing relatively few antennas, thus placing a limitation on this technique, e. g. in the case of a reconnaissance vehicle a hundred or more antennas may be installed in the airframe, thus dictating the need for several partial models of the aircraft, the total cost of which may be greater than one full-scale model.

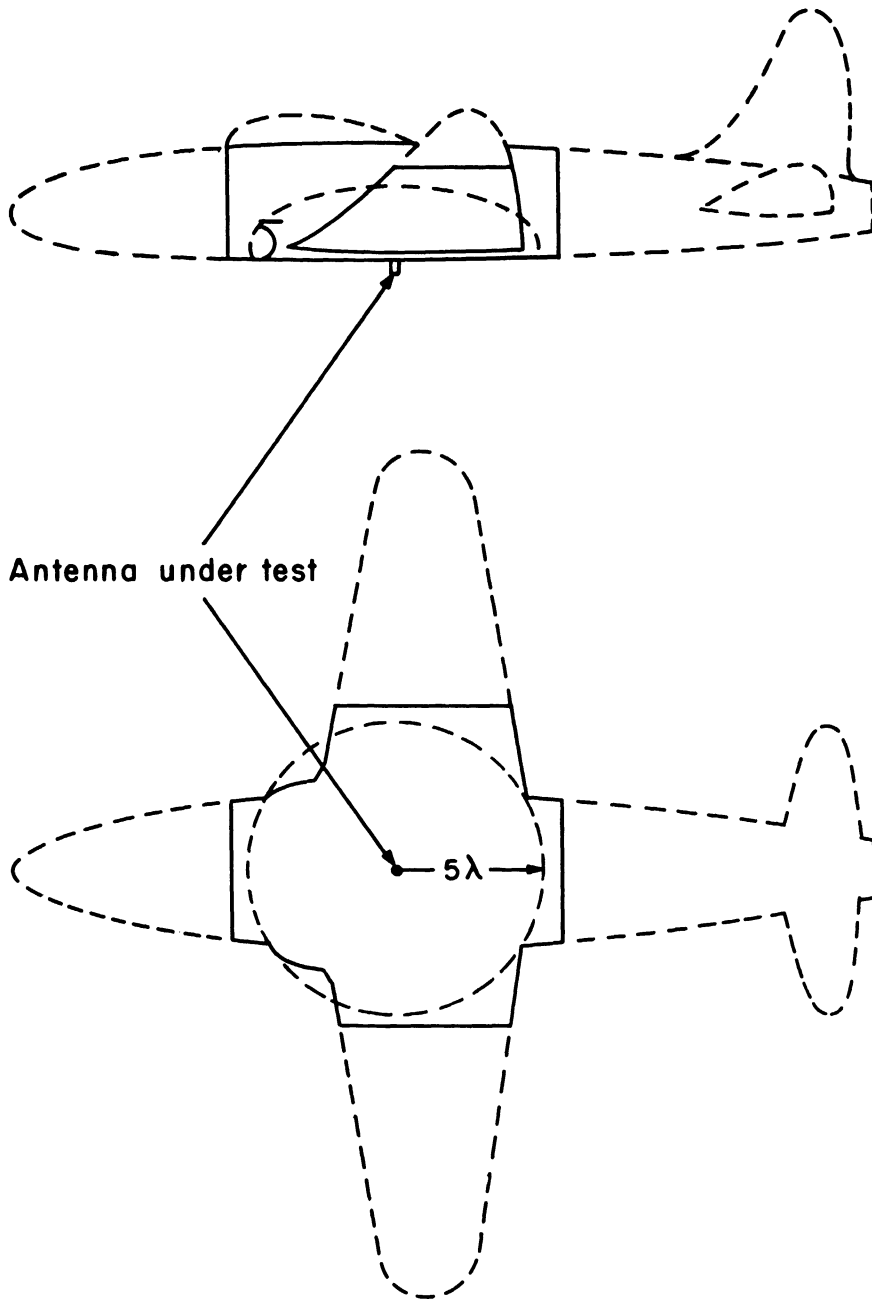


FIG. 7: PARTIAL FULL-SCALE MODEL.

Another limitation of partial models is the feasibility of obtaining signature data from a complex array (complex denotes that the elements of the array are spaced many wavelengths apart as in the case of an interferometer antenna). Airborne arrays of this type often have elements located in the wings on either side of the fuselage, thus requiring that large portions of the aircraft, and often the entire airframe, be modeled. However, partial models offer the advantage of employing conventional antenna measurement techniques, negating the need for special model rotators or other costly measuring techniques as required with full-scale models.

2.3 Instrumented Aircraft

In Section 2.1 several limitations to the use of the full-scale model were noted which hampered their use for obtaining spectrum signature data. In Section 2.2 it was noted that in some instances it may be necessary to build up several partial models to adequately test the antennas located on a typical reconnaissance vehicle. Because of these limitations, workers have also given consideration to the employment of instrumented aircraft to obtain pattern data. In employing this technique, an aircraft typical of one in which the antennas are to be located must be instrumented with the necessary equipment to obtain pattern data.

Each of the antennas from which patterns are required is operated in the receiving sense, whether it is a transmitting or receiving antenna. Data are obtained on a point-by-point basis from which the pattern can be traced. It was noted above that several antennas may be located on the aircraft, and it is conceivable that more than one antenna could be tested simultaneously through the use of elaborate computer and switching techniques. However, in the following discussion only one antenna will be considered. It is also to be noted that the pattern normally measured using an instrumented aircraft is an azimuthal cut of $\theta \approx 90^\circ$, (Fig. 5). Other cuts may be obtained by appropriately choosing a series of ground reference

points such that a series of θ cuts would be obtained as shown in Fig. 8. As may be reasoned from the above, patterns would be limited to the lower hemisphere since it would not be practical to obtain upper hemisphere patterns without requiring that the aircraft be flown upside down or some other complex measurement procedure devised.

A procedure that has been employed to obtain pattern data from an instrumented aircraft will now be discussed. The range should typically be several miles in length to enable a $\theta \approx 90^\circ$ cut to be recorded. A transmitting tower and antenna are located at one end of the range and a reference point located on the ground at the other end of the range. The reference point must be readily visible to the pilot from the air. Initially, it will be necessary to adjust the height, h , of the ground station transmitting antenna to insure that the elevation pattern shown in Fig. 9 is obtained. Because of the long range, the ground station antenna will have a specular reflection from the ground, thus producing a diffraction pattern similar to that illustrated in Fig. 9. It will be desirable to have the major lobe of the diffraction pattern positioned on the aircraft since it will have a higher gain and a better defined beam than will the minor lobes. Since the diffraction pattern is dependent upon the specular reflection from the ground, it is advisable to fly the aircraft first over the reference point several times at a constant altitude and at the same heading so that the height of the transmitting antenna may be adjusted to position the major lobe of the diffraction pattern on the aircraft. The time required to adjust the antenna height may be as much as two to three hours for each frequency of interest. A more thorough discussion of the use of the ground plane type of antenna range is presented by Cohen and Maltese (1961).

The aircraft must be equipped with the necessary instrumentation to insure a constant altitude flight path and to record data to correct for roll, yaw and pitch. Typically, a 24 cloverleaf pattern is flown such that 20 to 30 points are

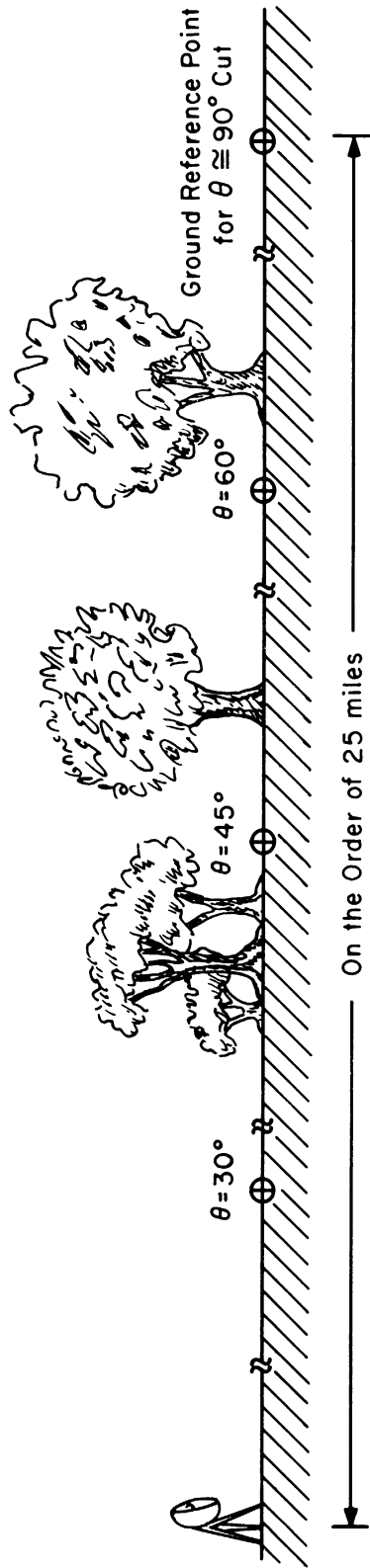


FIG. 8: SETUP FOR OBTAINING θ CUTS IN INCREMENTS.

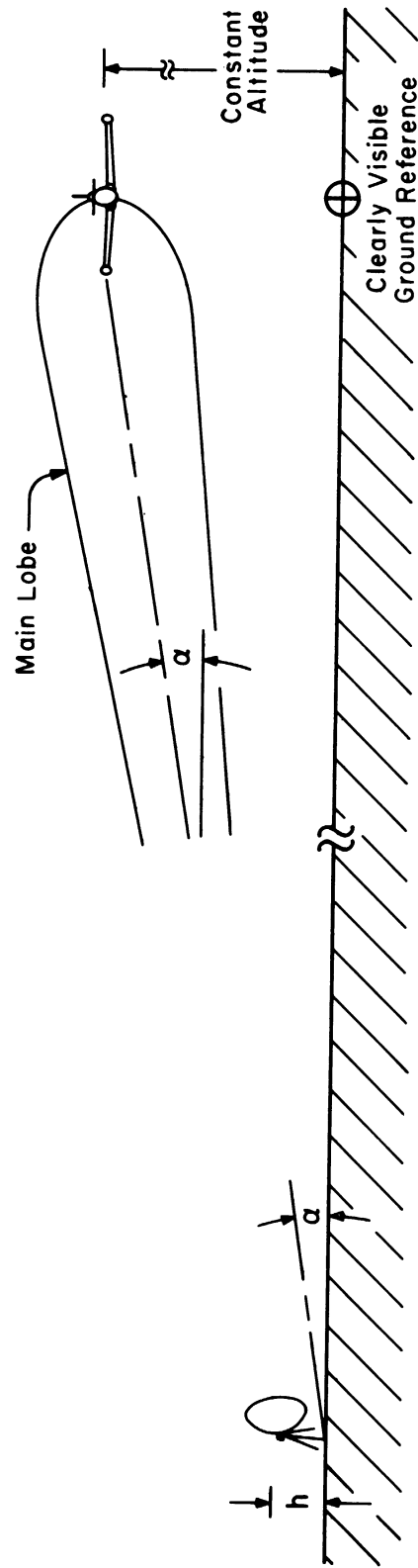


FIG. 9: FIXED STATION DIFFRACTION PATTERN.
(NOTE: α IS A FUNCTION OF h .)

measured. When an operational reconnaissance aircraft has been used, data has been obtained in 2 - 1/2 hours flying time, and reduction of these data to an antenna pattern requires several days when employing hand techniques. However, data reduction time may be reduced considerably through the use of computer techniques. The estimated cost of obtaining patterns as described above (excluding data reduction) employing an operational reconnaissance aircraft has been estimated to be in excess of \$ 18,000 per hour of flying time. In addition to the cost of the instrumented aircraft, one must add the cost of necessary special test equipment, radar tracking time and computer time required to obtain and to reduce the data to an actual pattern.

In the above discussion the pilot has been required to fly the aircraft in a pre-defined flight pattern. This tends to minimize both the complexity of supporting ground equipment and the data reduction time, because the aspect angle of the aircraft is known. However, it should be noted that it is not mandatory that a pre-defined flight pattern be followed. A procedure for determining the aspect angle of a free-flying aircraft is presented in Appendix A. Because of the cost and time required to obtain individual pattern cuts, the use of an instrumented aircraft is not recommended for obtaining spectrum signature data.

2.4 Precision Scale Models

The feasibility of using precision models in tests of antennas on ships, aircraft, and missiles has long been established and the principles involved have been appropriately described by Sinclair (1947) and others. It has been shown that if an antenna is scaled down in size by a factor, P , and the test frequency scaled up by the same factor, the radiation pattern is essentially unchanged. However, there is a limitation to this technique. Care must be exercised to insure that the conductivity, permeability and dielectric constant of the metallic and non-metallic parts

of the full-scale vehicle are related by $\sigma = P\sigma'$, $\omega' = \omega$ and $\epsilon = \epsilon'$; where the primed values are associated with the scale model. The conductivity of metals employed in radiating systems generally approximates an infinite value, thus the condition $\sigma' = P\sigma$ is a priori satisfied. Because of this fact, the large amount of antenna work that has been done by scaling has been found to be effectual. However, there is at present no satisfactory method for handling the scaling problems associated with non-metallic parts of antennas. This is a limitation to the use of scaling techniques for spectrum signature work.

Another factor that must be considered is the antenna types that may be installed on the aircraft and require scaling. For example a reconnaissance aircraft may employ several antenna types to cover the frequency range from 50 Mc to 50 Gc. During this study antennas operating in the 100 Mc - 10 Gc frequency range have been considered. A spiral antenna is typical for this frequency range. The scaling factor by which the spiral antenna may be modelled must be carefully considered. For example, it may be feasible to scale a 300 Mc - 600 Mc spiral by a factor of 10 but not feasible to scale a 1000 Mc - 2000 Mc spiral by this same factor because of the fabrication limitations. Therefore, if the aircraft from which spectrum signature data are required contains spiral antennas, care must be exercised in choosing the scaling factor such that the antennas may be accurately scaled and fabricated.

When scale models are fabricated, as noted above, the scale factor must also be applied to the tolerances applicable to the full-scale model. For example, full-scale tolerances may be of the order of .250 inch, but when scaled by a factor of 10, the tolerances considered must be .025 inch. Because of this tolerance factor, the cost of fabricating scale models may become high as the scale factor becomes large. This, then, places an additional limitation on the use of precision

scale models for obtaining spectrum signature data. Scaling is also limited generally to those models in which dielectric materials may be avoided and not scaled, as has been done in this study. Dielectric parts, such as radomes and windows, have not been considered. Figure 10 shows a precision 1/8 scale model in a typical test set-up.

The cost of a fifth-scale model of a reconnaissance aircraft has been estimated to be approximately \$2,000. This may be considered relatively low cost for a model. However, if one is concerned with obtaining spectrum signature data from the many types of aircraft in use today, the high cost of models needs to be considered.

Because of the limitations associated with each of the above measurement techniques, an alternate technique has been considered which has shown much promise for obtaining spectrum signature data in an economical and practical manner. This technique will be discussed in the following two sections.

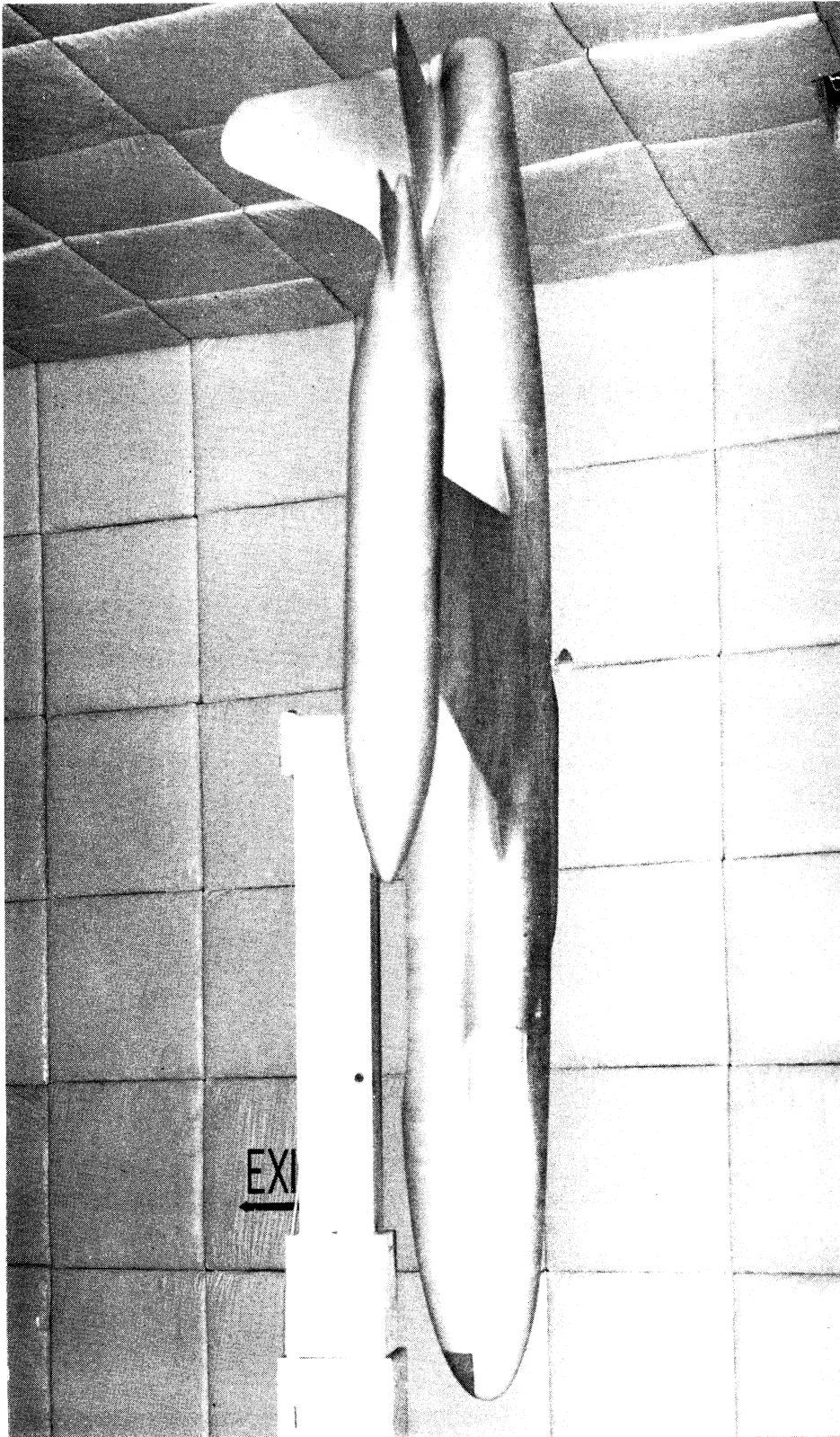


FIG. 10: PRECISION T-33 MODEL.

III

SIMPLIFIED TECHNIQUES

Procedures, typical costs and theory associated with simplified techniques as applied to low-gain, low-frequency antennas will now be considered.

3.1 Simplified Scale Models

An investigation has been made to determine the degree to which a scale model may be simplified and still represent an aerodynamically-shaped aircraft model with sufficient accuracy to produce adequate far-field patterns. For the purpose of interference studies, it is assumed that one is primarily concerned with the general contour of the antenna pattern. Thus the determination of this contour is adequate and the pattern's fine structure is of only secondary interest. Data have been obtained which shows that to satisfy the above criteria, it is necessary to model only the basic aircraft configuration and not the aerodynamic contours.

The model used experimentally is thus a "Simplified Model" derived from the simple geometric shapes employed in its construction. The fuselage is represented by a metallic cylinder having a diameter approximately equal to the mean diameter of the aerodynamically shaped fuselage. The wings and tail structure are formed by thin flat metallic planar surfaces having the approximate outline of the true components. The overall size of the simplified model approximates the size of its precision model counterpart. Figure 11 is a simplified version of the precision scale model shown in Fig. 10 from which the data to be discussed below were obtained. The precision model serves as a reference for evaluation of the simplified modeling technique.

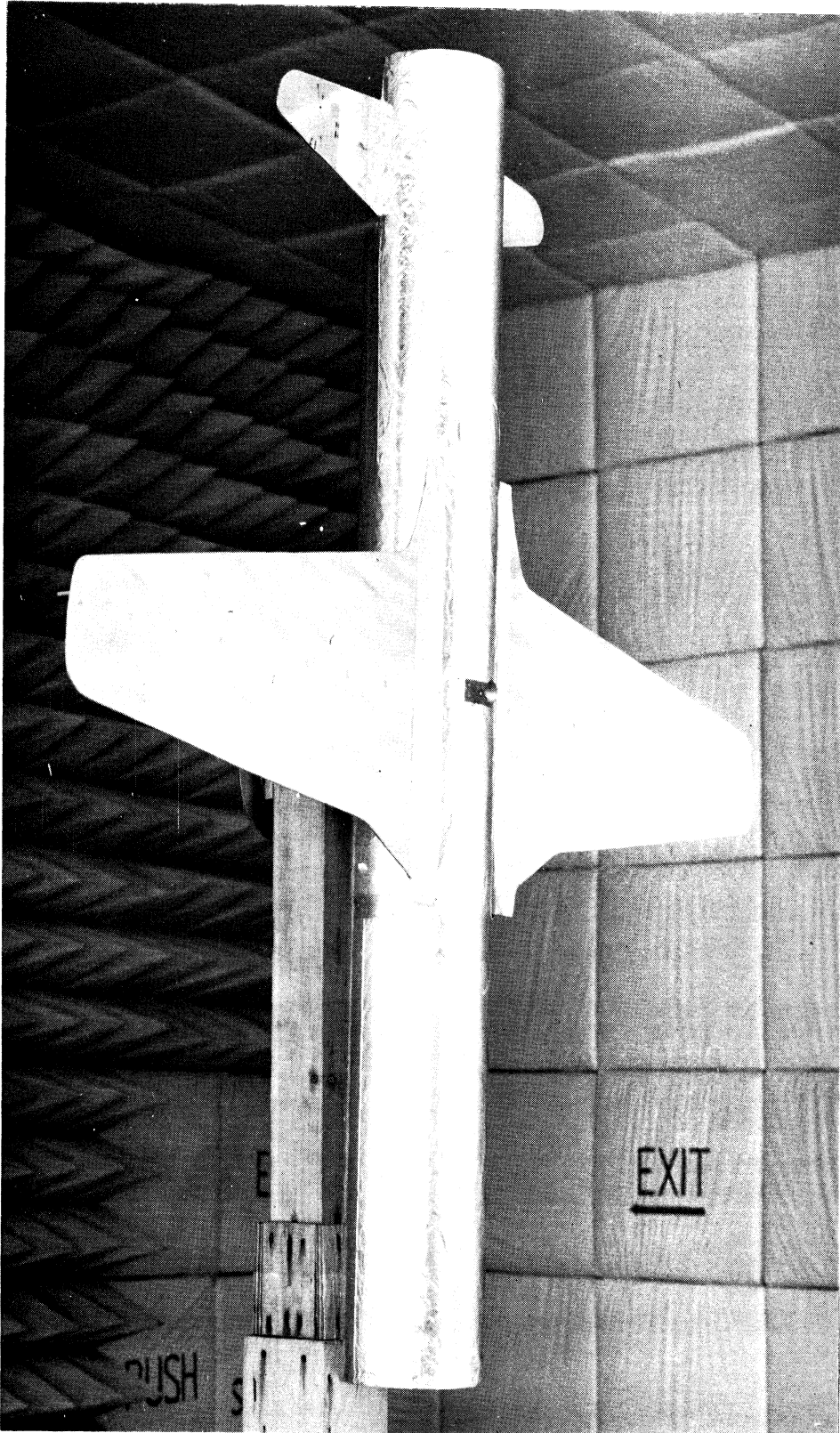


FIG. 11: SIMPLIFIED T-33 MODEL.

The two scaled antennas employed in the investigation of this technique are of the monopole type. The first antenna is a 1/8 scale model of a modified monopole; the full scale version is a typical aircraft communications antenna operating in the 200-400 Mc range. The model antenna, located on the underside of the fuselage centered between the leading and trailing edges of the wings, can be seen in Figs. 10 and 11. This location permits the evaluation of the antenna radiation characteristics in the presence of the wings and surrounding fuselage structure. A complete set of the three-dimensional antenna patterns recorded for the modified monopole mounted on the precision and simplified models establishes the feasibility of the simplified modeling technique. This is evidenced by the very favorable pattern agreement between the simplified model and the reference (precision) model as shown in Figs. 12 through 21. These patterns, recorded at the model fundamental frequency (2.4 Gc) and the first four harmonic frequencies, are for the transverse elevation cut only⁺, but are typical of the data collected. The above pattern data, when reduced to statistical data in the form of cumulative gain distributions, again exhibit very good agreement over the full range of interest as shown in Figs. 22 through 26.

To further verify the feasibility of the simplified modeling technique, radiation patterns were obtained with a standard $\lambda/4$ monopole, scaled to the model fundamental frequency (2.4 Gc). The antenna is shown mounted on the underside of the fuselage of the precision and simplified models in Figs. 27 and 28. This location, near the nose of the aircraft, i. e. approximately 2 feet forward of the former location of the modified monopole, affords an evaluation of antenna characteristics in the presence of a significant dissimilarity of fuselage contour. From

⁺ ($\phi = 90^\circ$ and 270° ; θ variable; see Fig. 5)

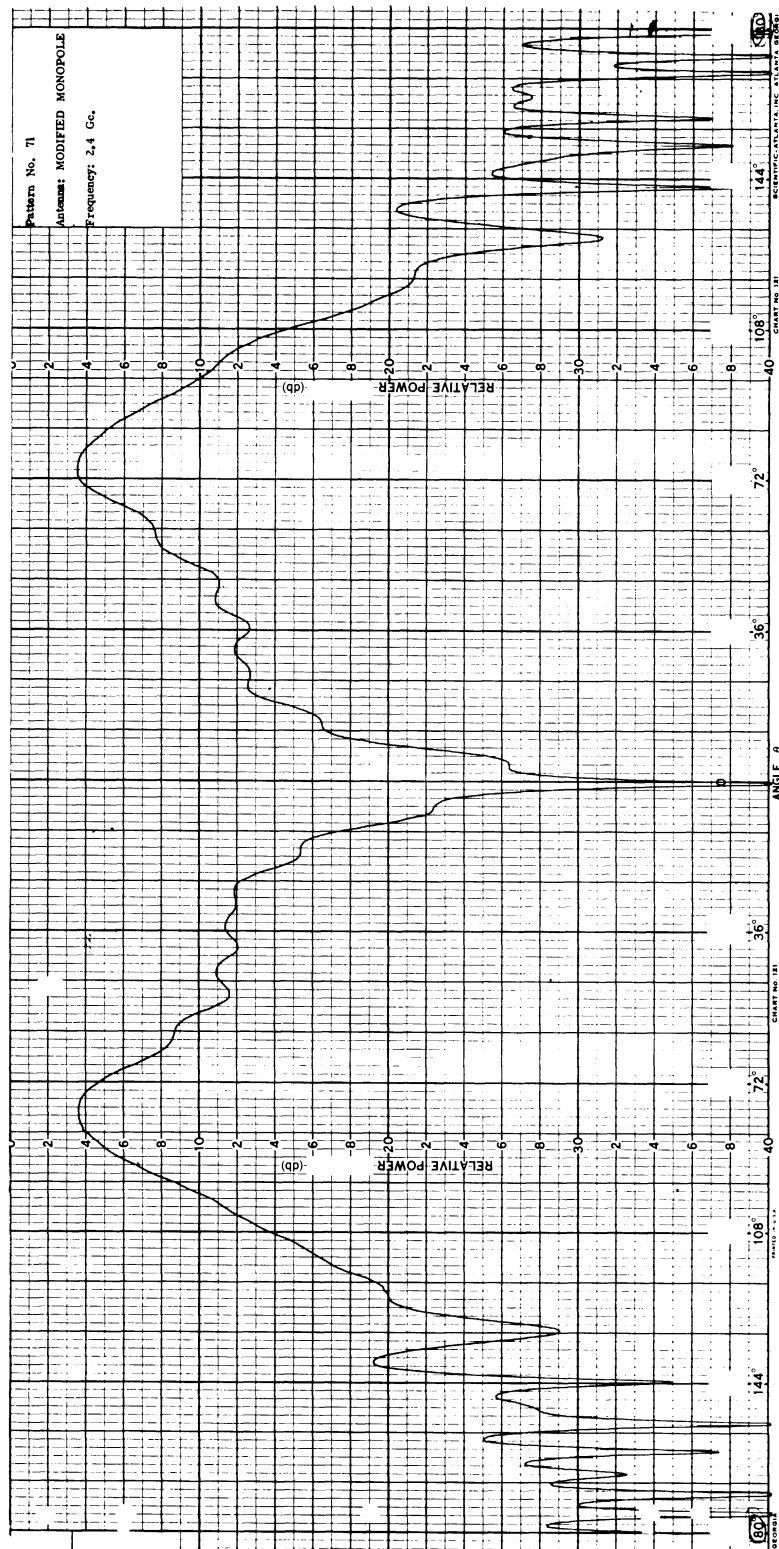


FIG. 12: PRECISION T-33 MODEL (LESS WING TANKS). FREQ. = 2.4 Gc.

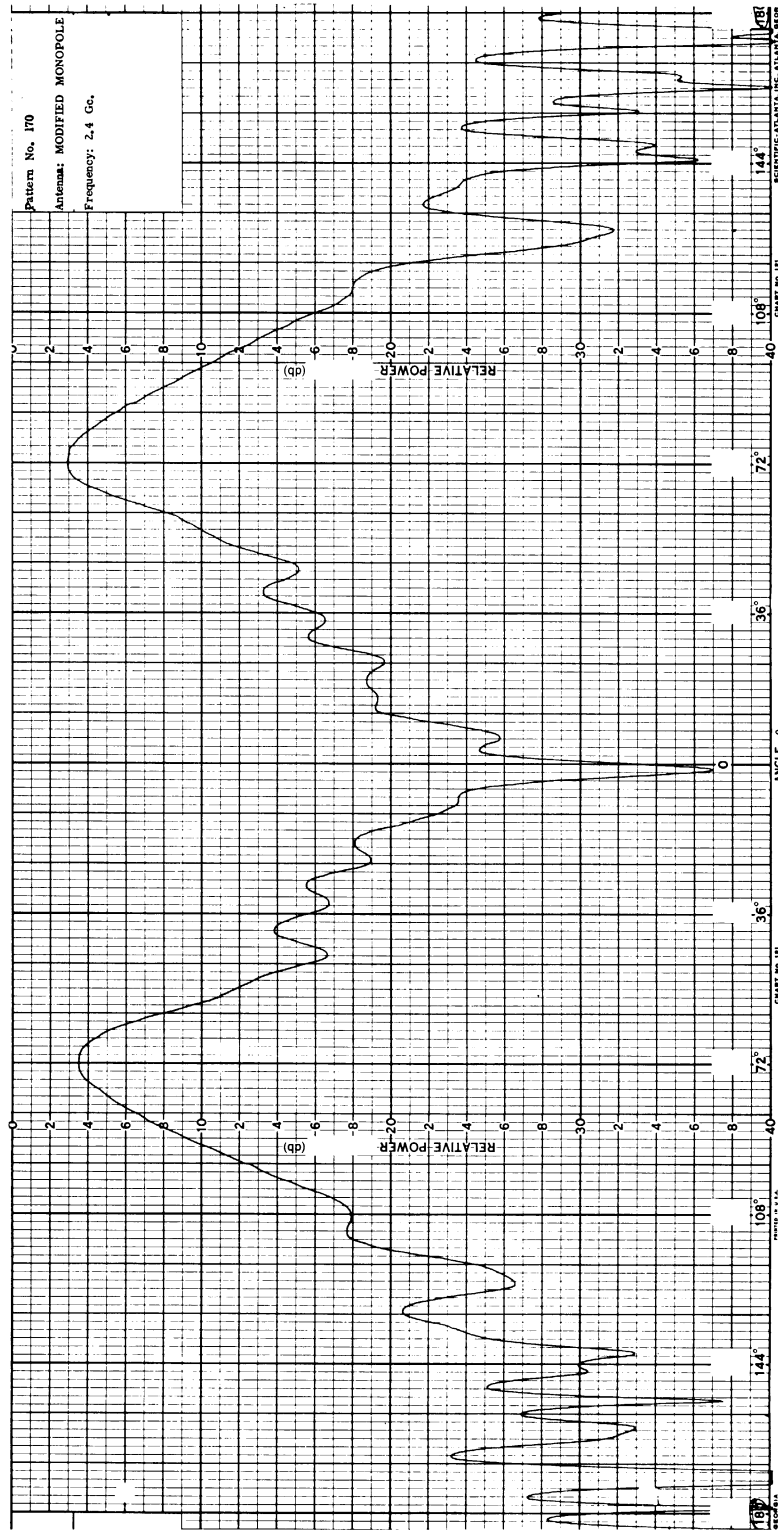


FIG. 13: SIMPLIFIED T-33 MODEL. FREQ. = 2.4 Gc.

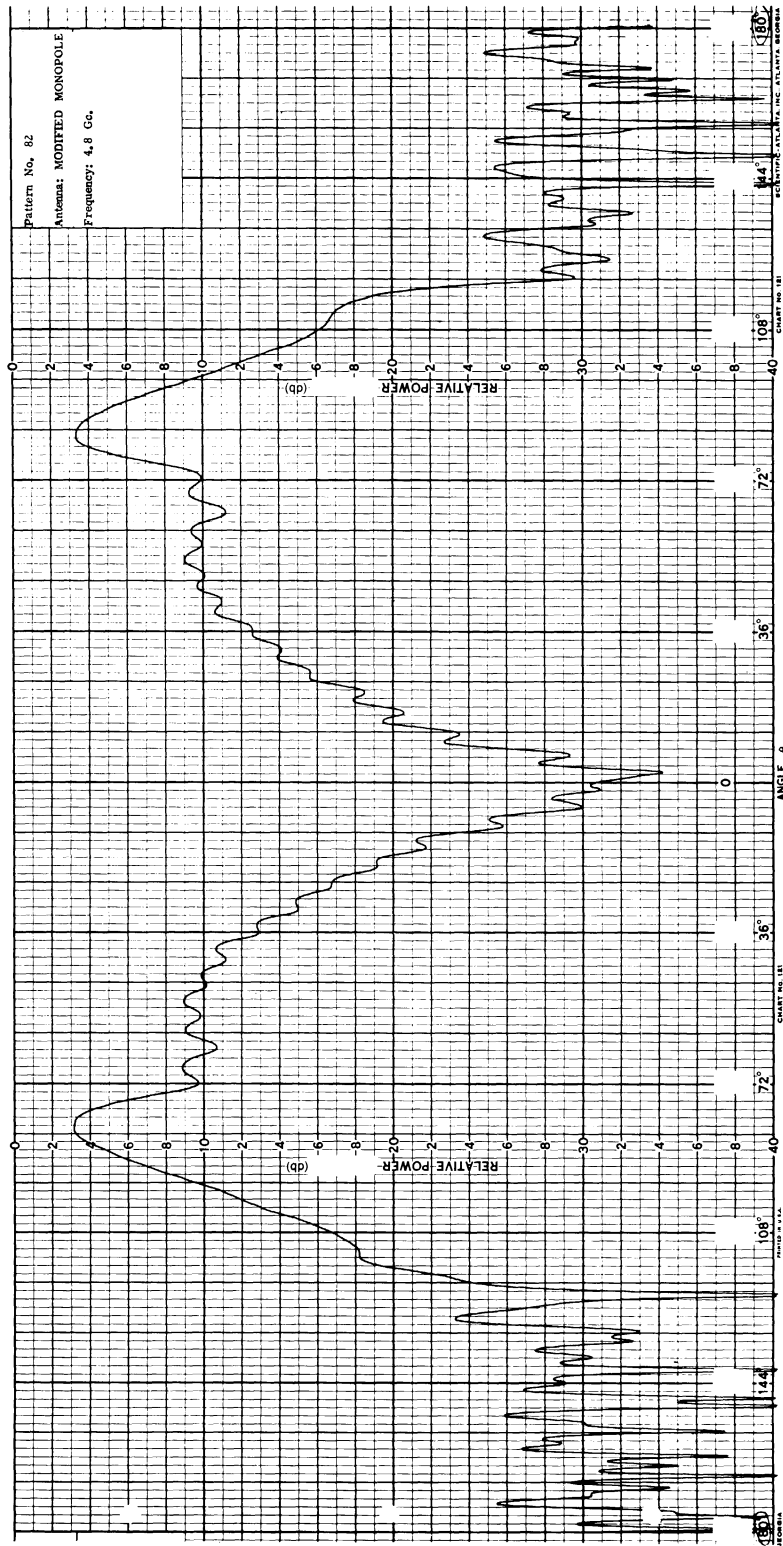


FIG. 14: PRECISION T-33 MODEL (LESS WING TANKS). FREQ. = 4.8 Gc.

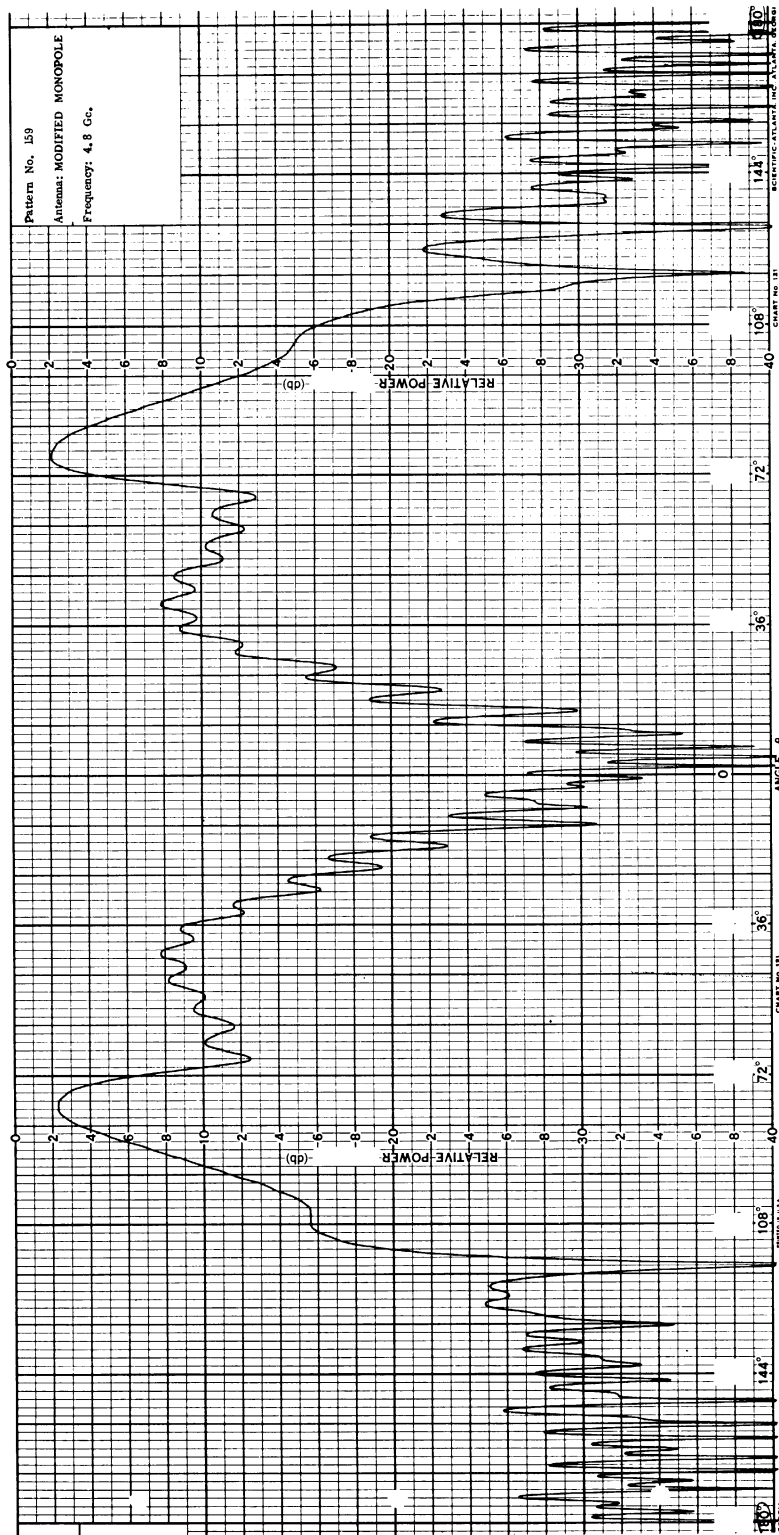


FIG. 15: SIMPLIFIED T-33 MODEL. FREQ. = 4.8 Gc.

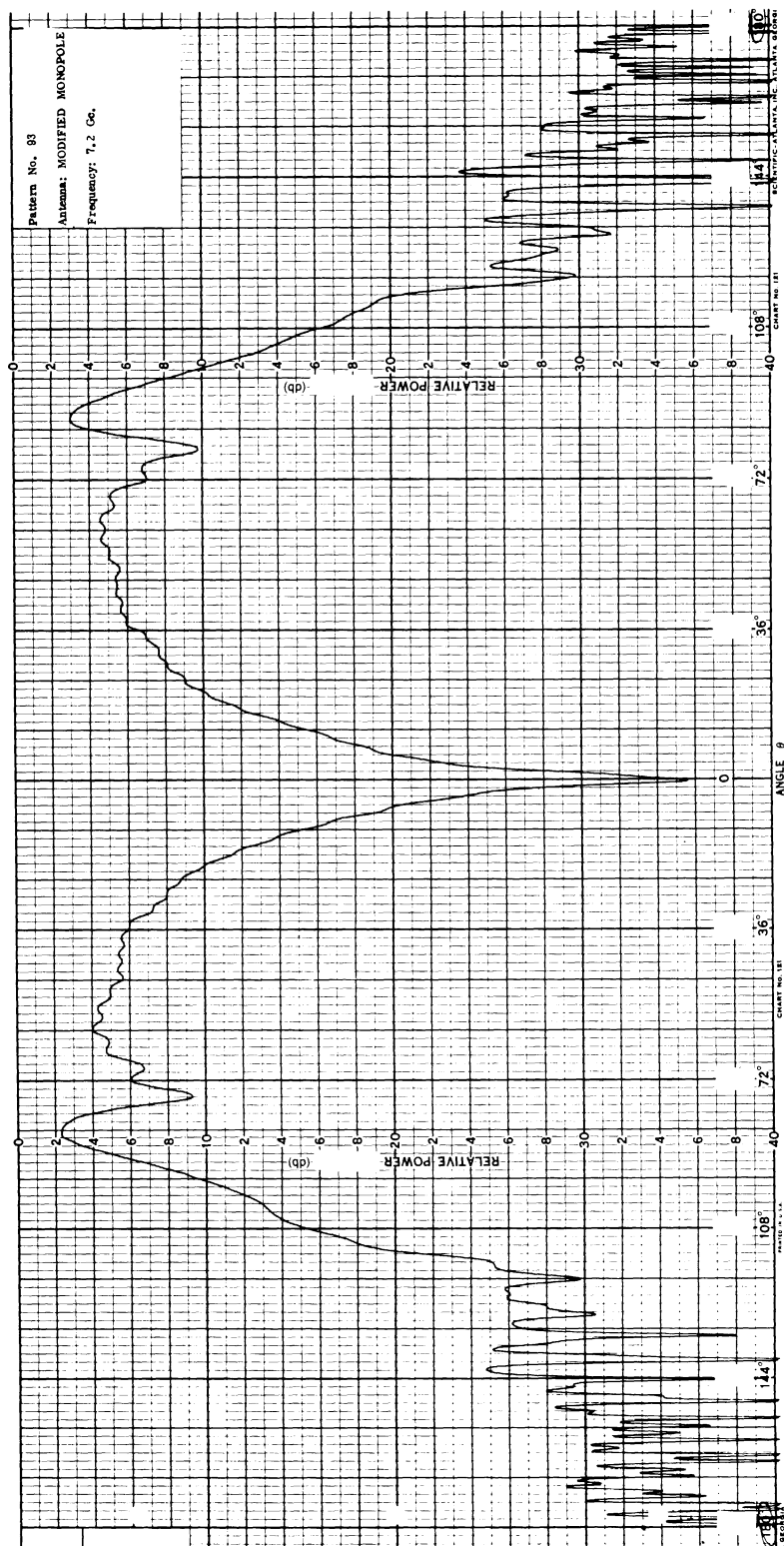


FIG. 16: PRECISION T-33 MODEL (LESS WING TANKS). FREQ. = 7.2 Gc.

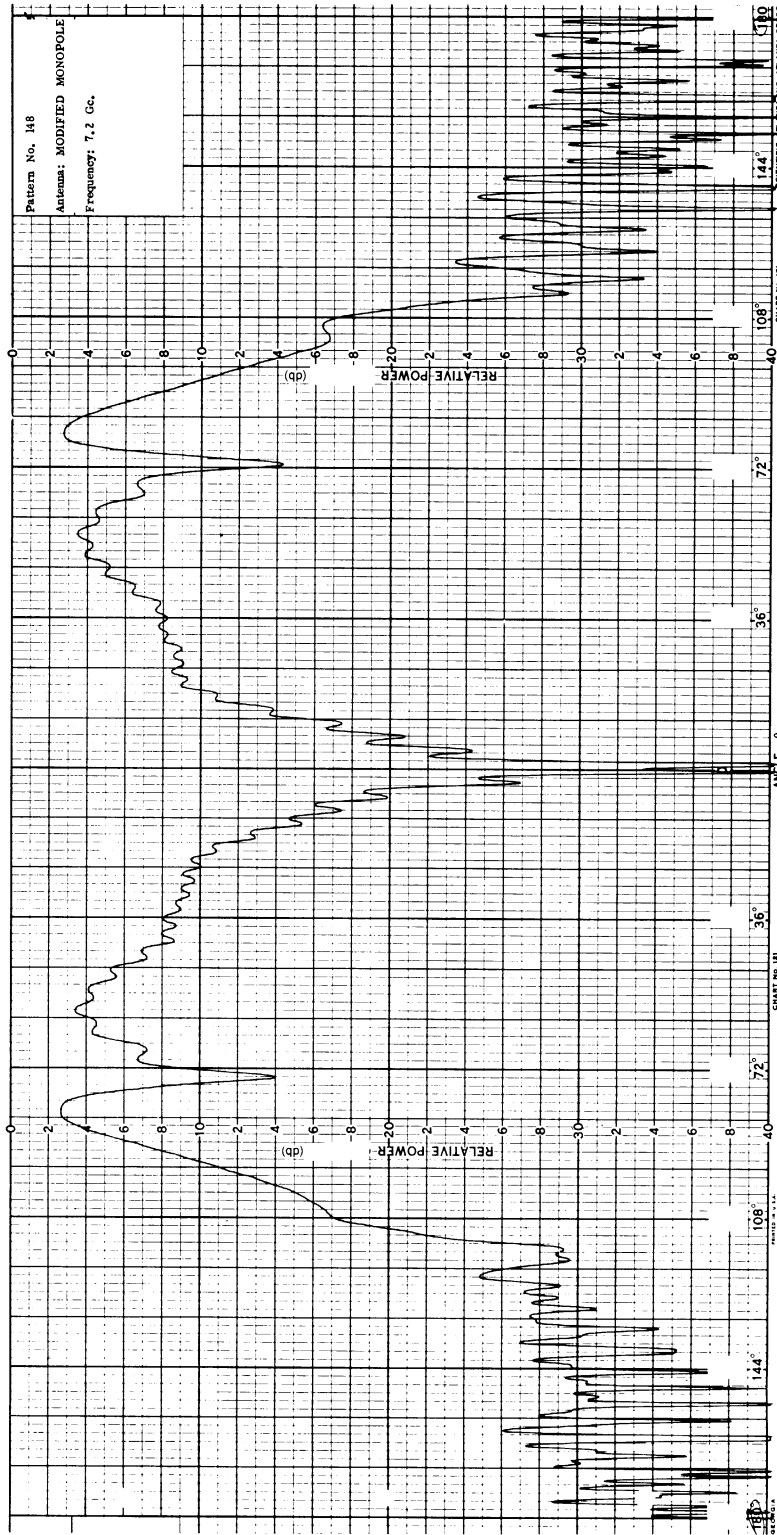


FIG. 17: SIMPLIFIED T-33 MODEL. FREQ. = 7.2 Gc.

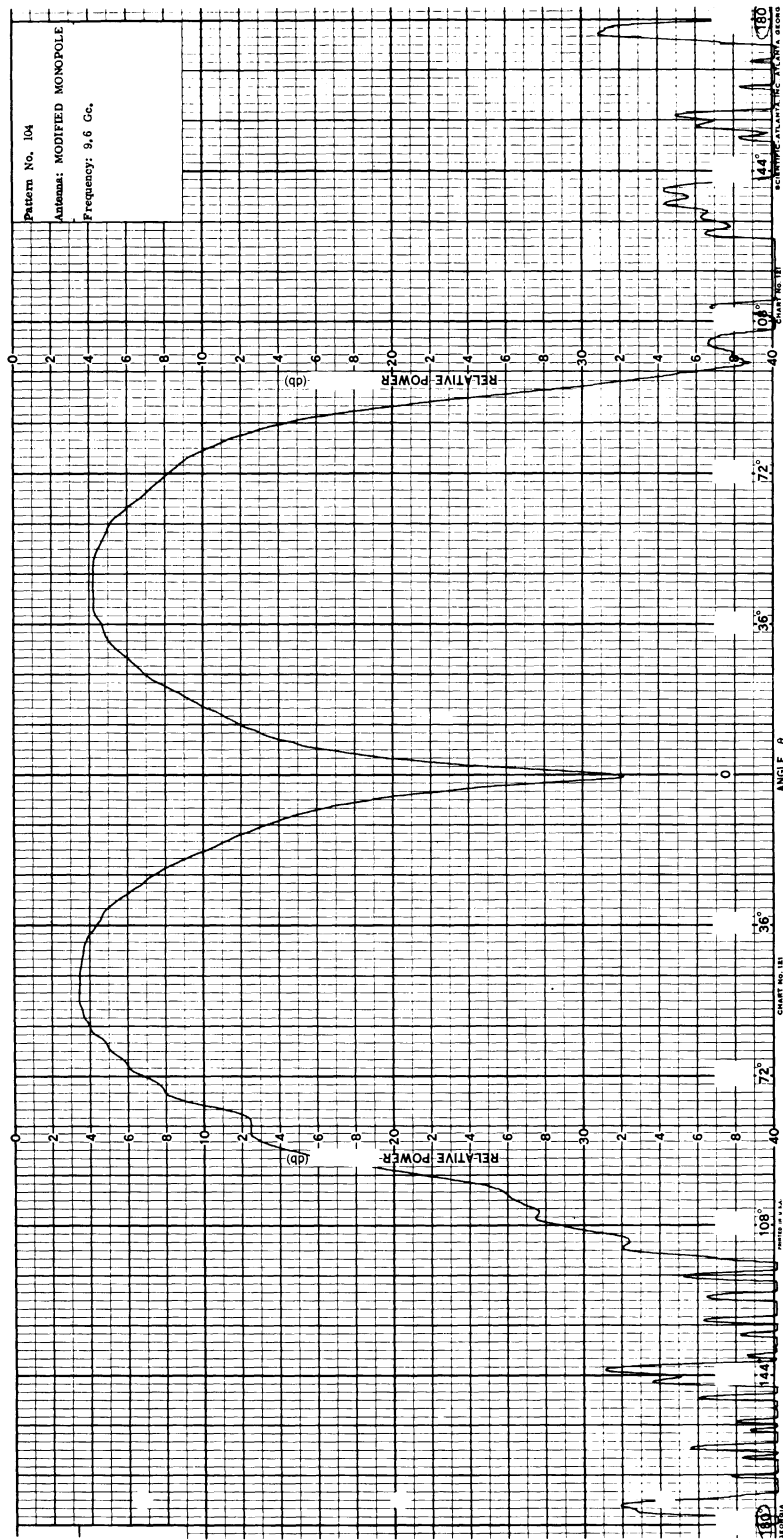


FIG. 18: PRECISION T-33 MODEL (LESS WING TANKS). FREQ. = 9.6 Gc.

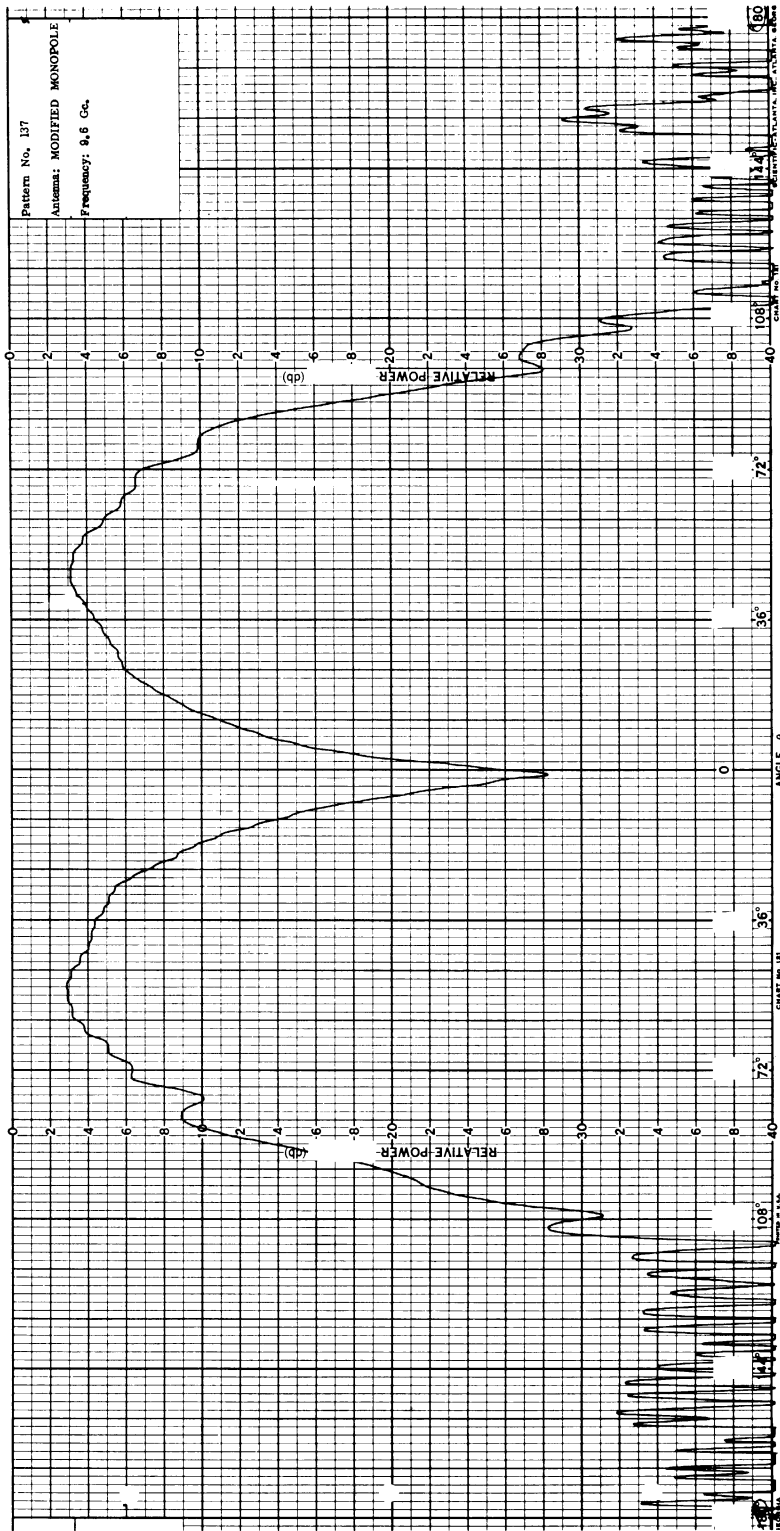


FIG. 19: SIMPLIFIED T-33 MODEL. FREQ. = 9.6 Gc.

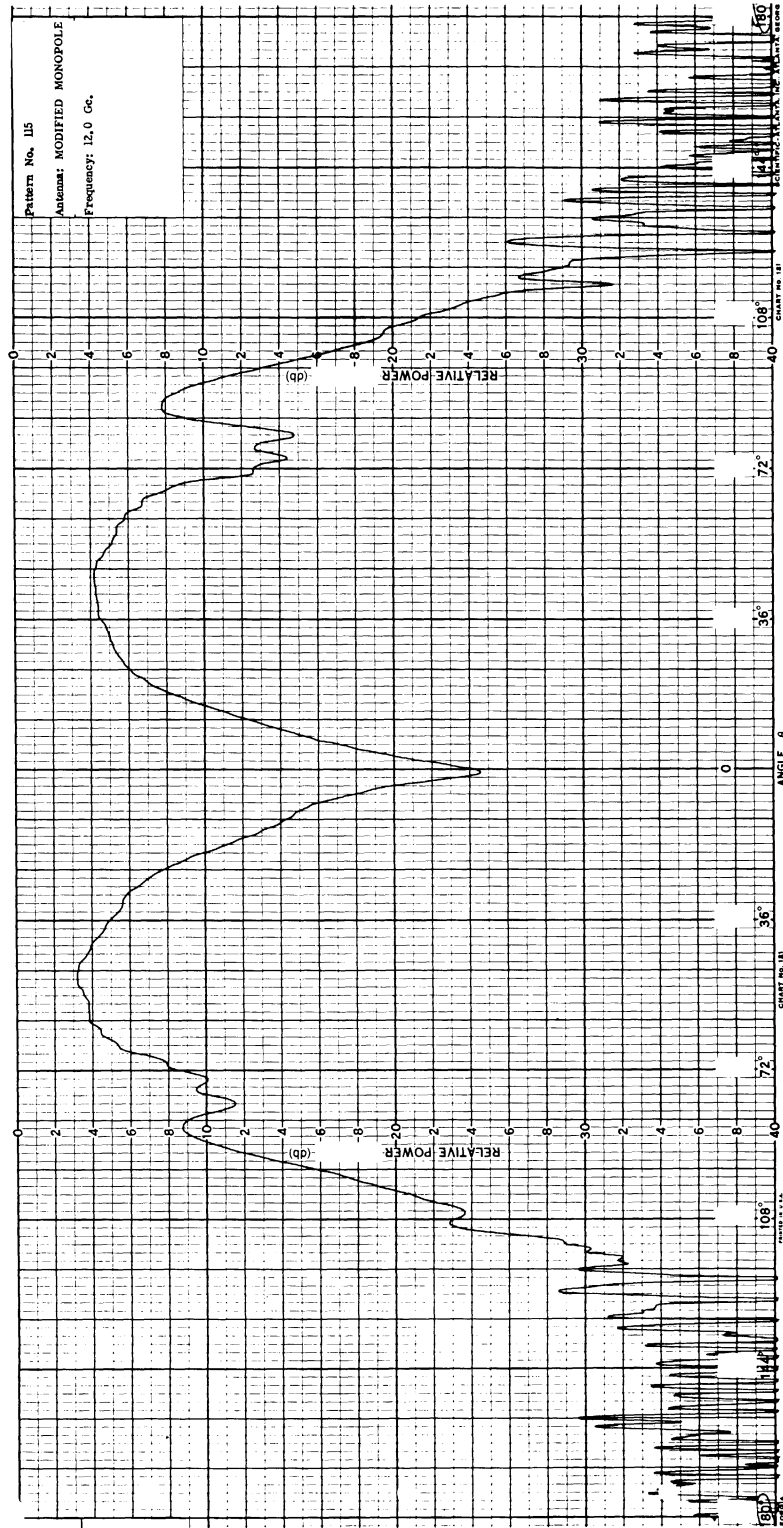


FIG. 20: PRECISION T-33 MODEL (LESS WING TANKS). FREQ. = 12.0 Gc.

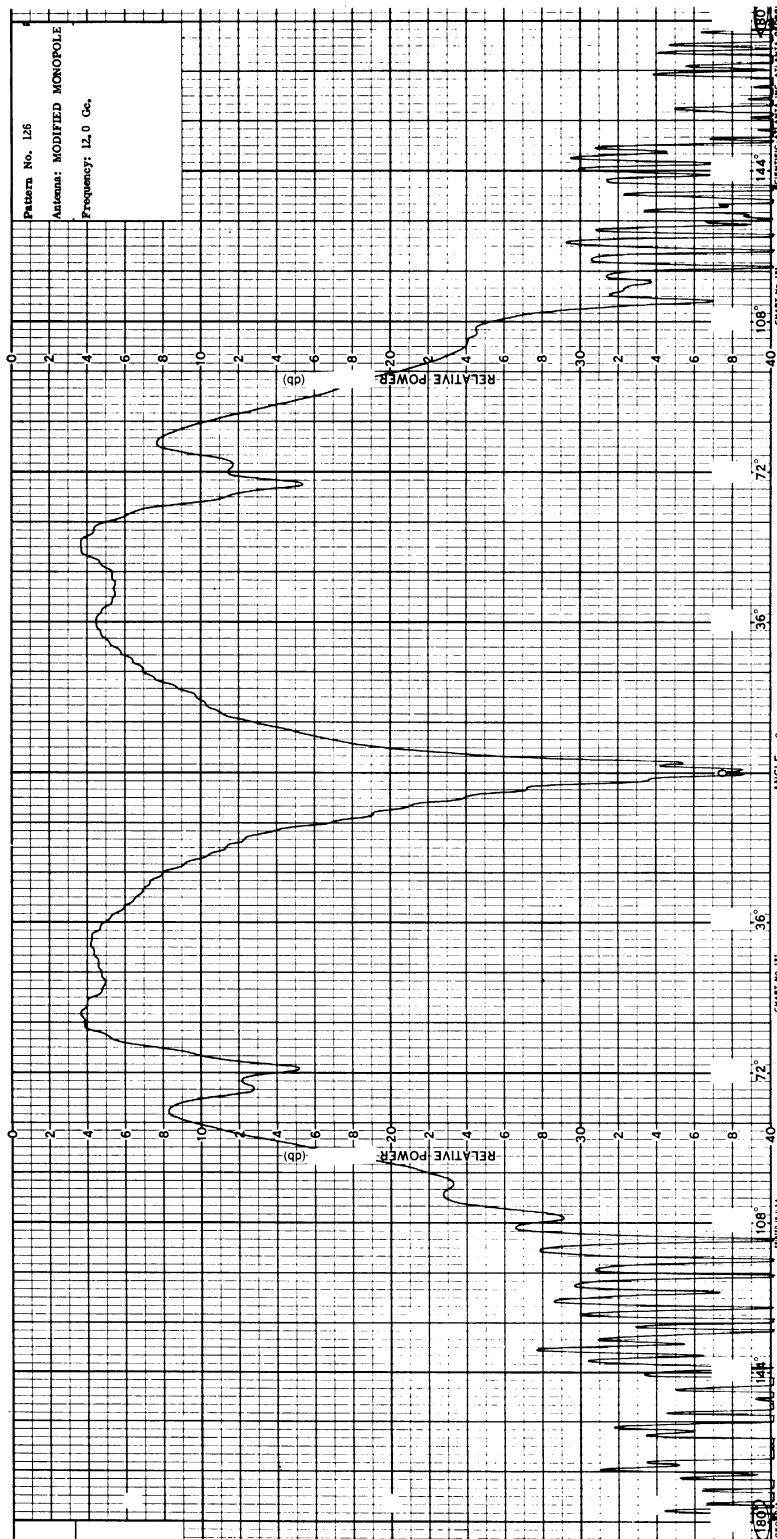


FIG. 21: SIMPLIFIED T-33 MODEL. FREQ. = 12.0 Gc.

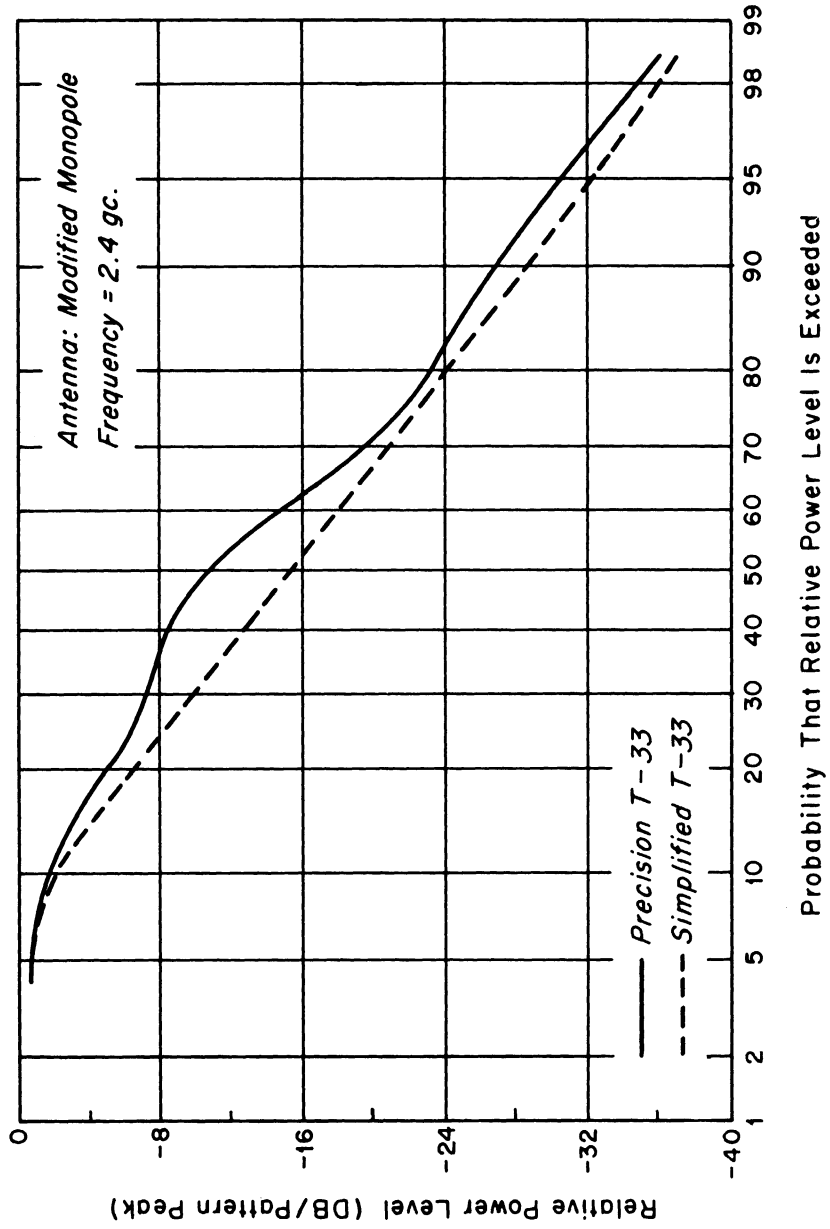


FIG. 22: CUMULATIVE GAIN DISTRIBUTIONS OF PRECISION AND SIMPLIFIED MODELS.

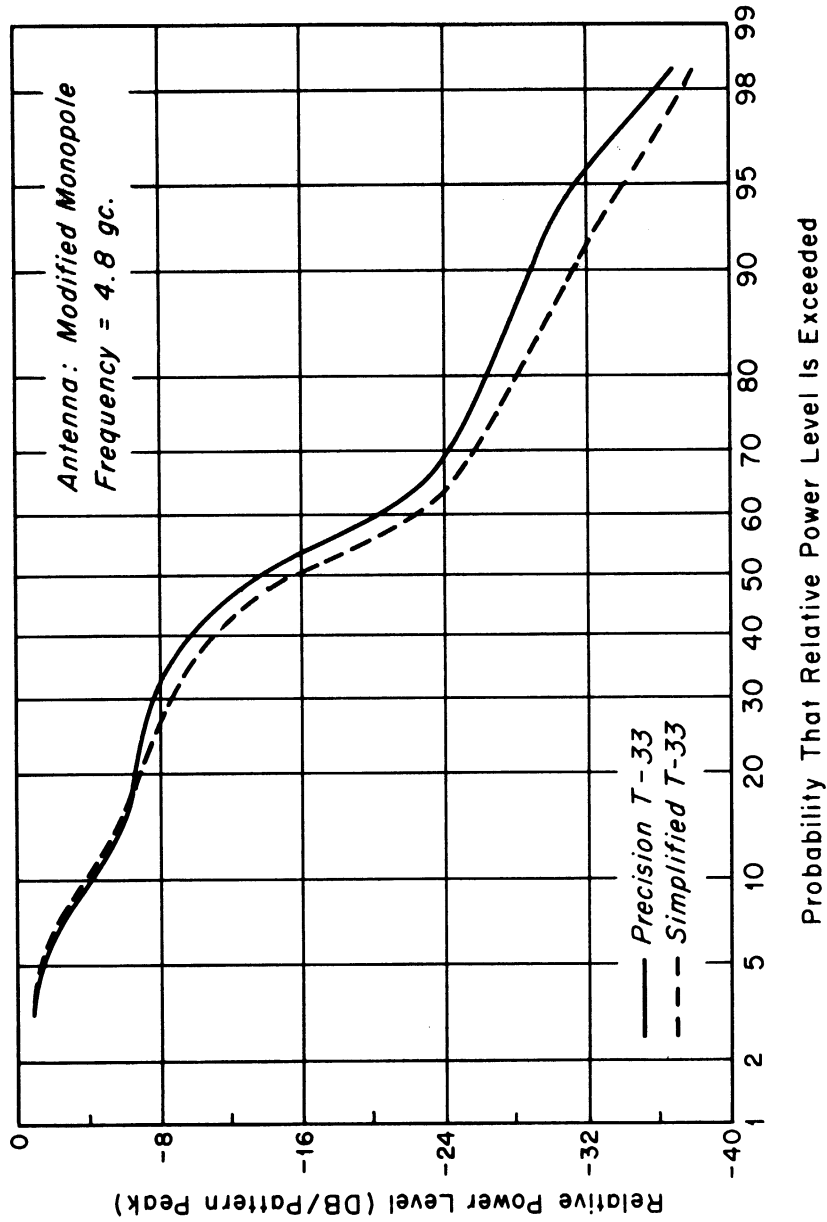


FIG. 23: CUMULATIVE GAIN DISTRIBUTIONS OF PRECISION AND SIMPLIFIED MODELS.

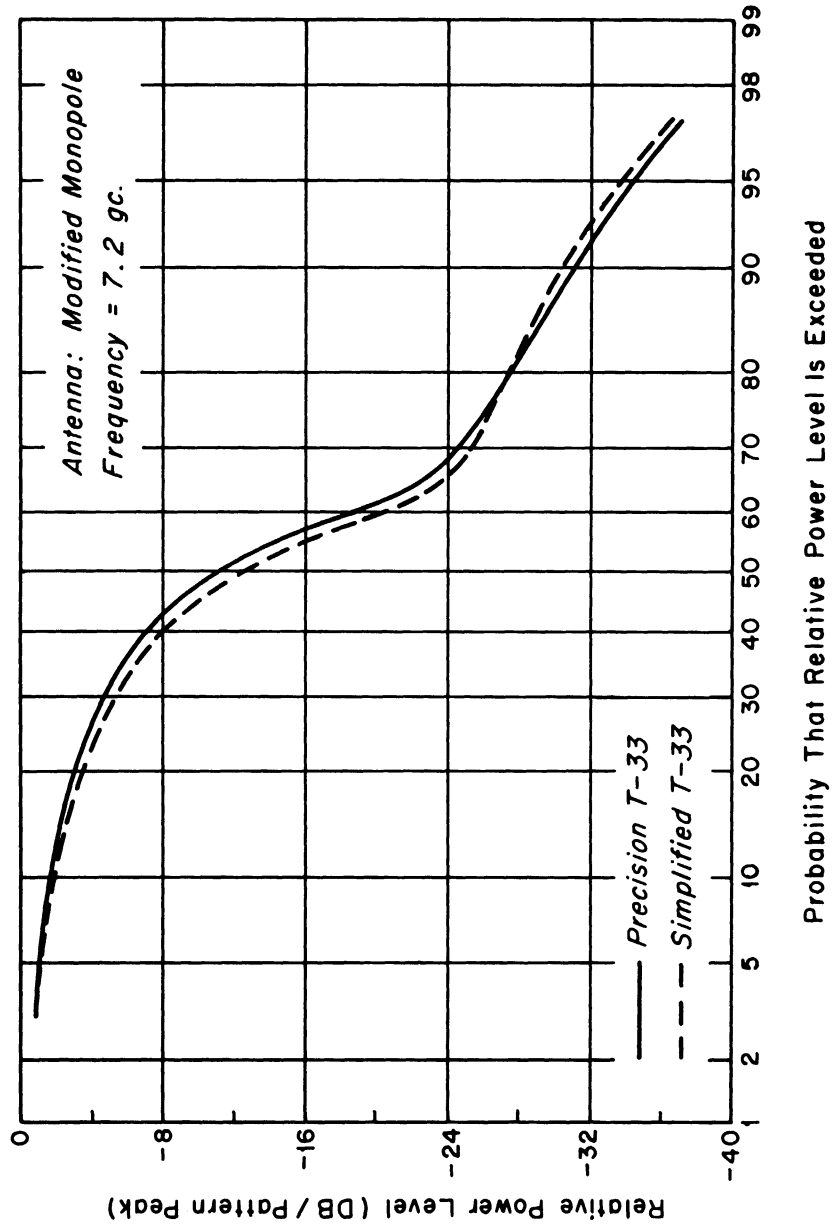


FIG. 24: CUMULATIVE GAIN DISTRIBUTIONS OF PRECISION AND SIMPLIFIED MODELS.

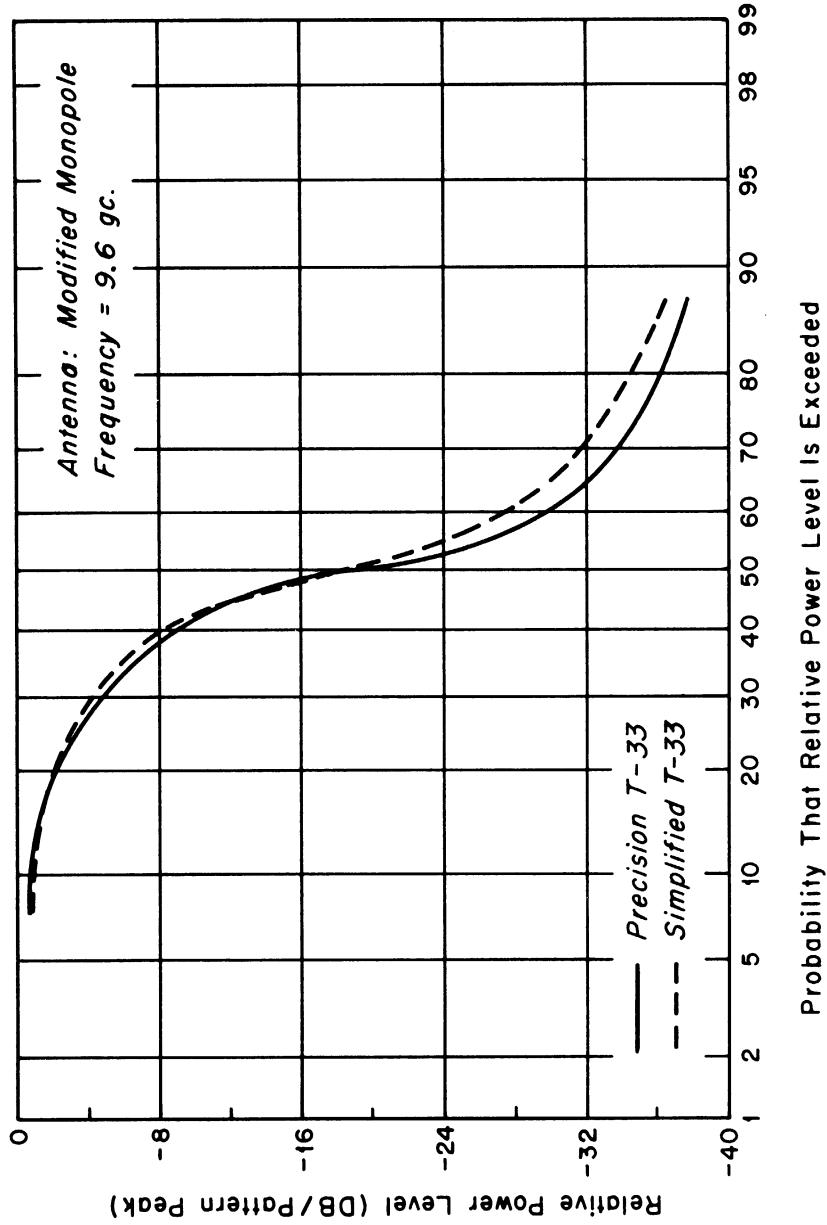


FIG. 25: CUMULATIVE GAIN DISTRIBUTIONS OF PRECISION AND SIMPLIFIED MODELS.

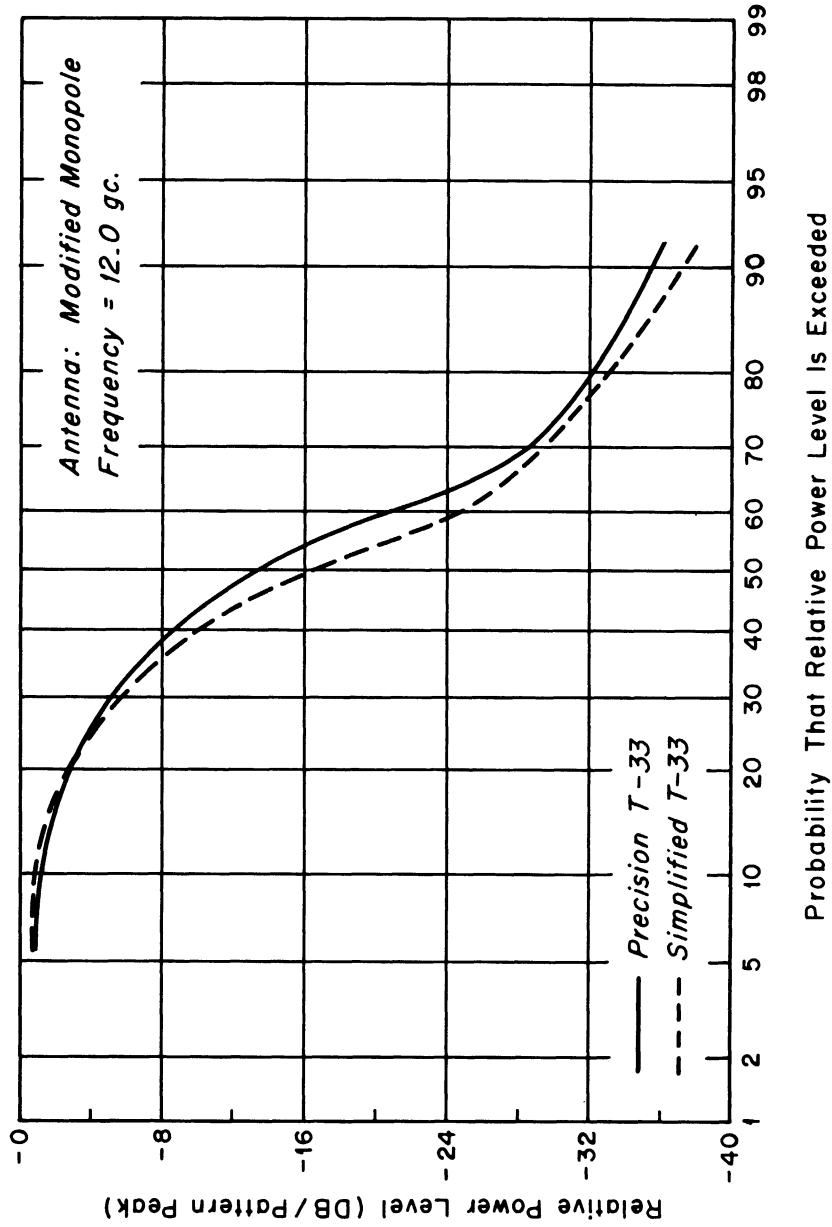


FIG. 26: CUMULATIVE GAIN DISTRIBUTIONS OF PRECISION AND SIMPLIFIED MODELS.

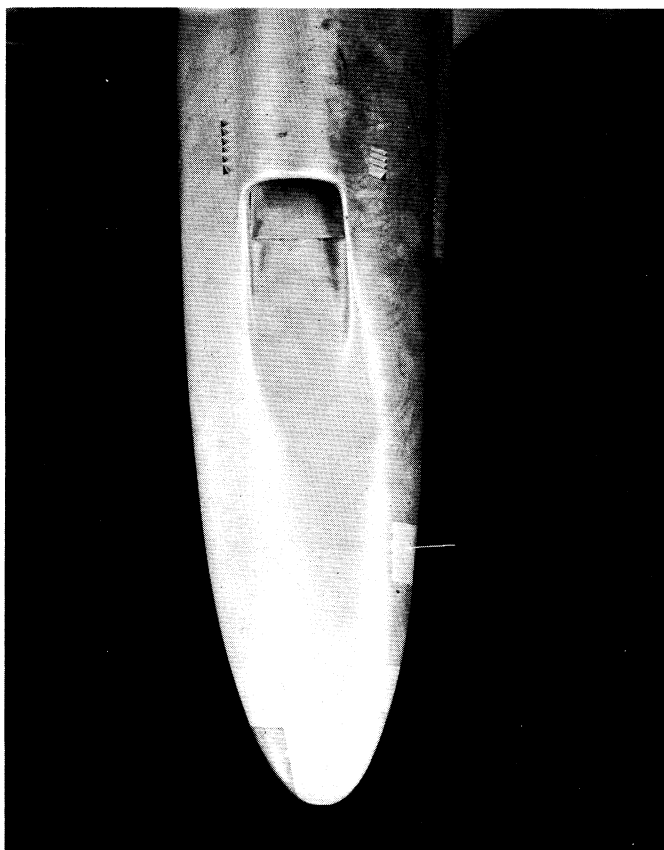


FIG. 27: $\lambda/4$ MONOPOLE ON PRECISION MODEL.

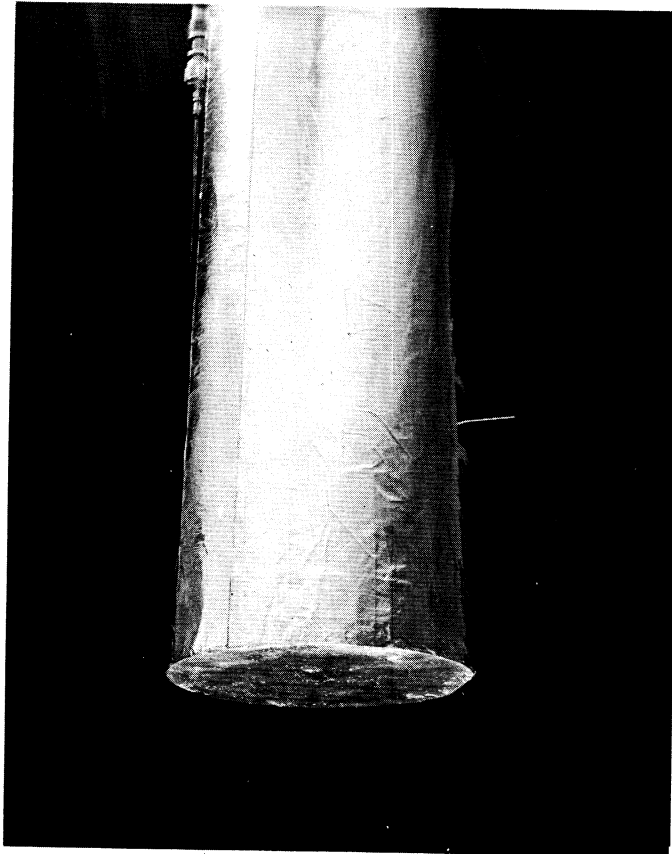


FIG. 28: $\lambda/4$ MONOPOLE ON SIMPLIFIED MODEL.

Figs. 29 through 43 it is seen that reasonably good pattern agreement still exists between the simplified model and the reference (precision) model over the full range of interest. Note the excellent agreement at the scale fundamental and first harmonic frequencies.

In this investigation emphasis was placed on the use of very simple shapes in the construction of the simplified aircraft model. This priority is exemplified in the blunt configuration of the nose of the model. In practice, it may be desirable to form conical sections at either end of the aircraft fuselage. This can be done at a minor increase in labor charge, thus maintaining the relatively low cost of this technique. The cost of the simplified model shown in Fig. 11 is \$400 - \$500. Although this model is fabricated from aluminum and wood, it may be desirable in some applications to use fiberglass as the model material (Hudson, 1964).

3.2 Simplified Partial Models

3.2.1 Introduction

Because of the scaling limitations that are associated with some antenna types, it may be desirable to obtain signature data at the full-scale fundamental, spurious and harmonic frequencies. A theoretical study has been conducted to determine the minimum size of a ground plane which can reasonably well simulate the contribution due to an aircraft frame. The study considers the analysis of the pattern of a monopole antenna in the presence of a circular cylindrical surface. The problem can be further reduced to the following mathematical model. An infinite circular cylinder of radius R , with Neumann boundary condition, in the presence of a line source at a distance r from the cylinder where $r/R \ll 1$. This model is particularly useful since the far field of the line source can be obtained by a rather straightforward approximation. It should be noted that the results obtained are valid only in the plane of the antenna.

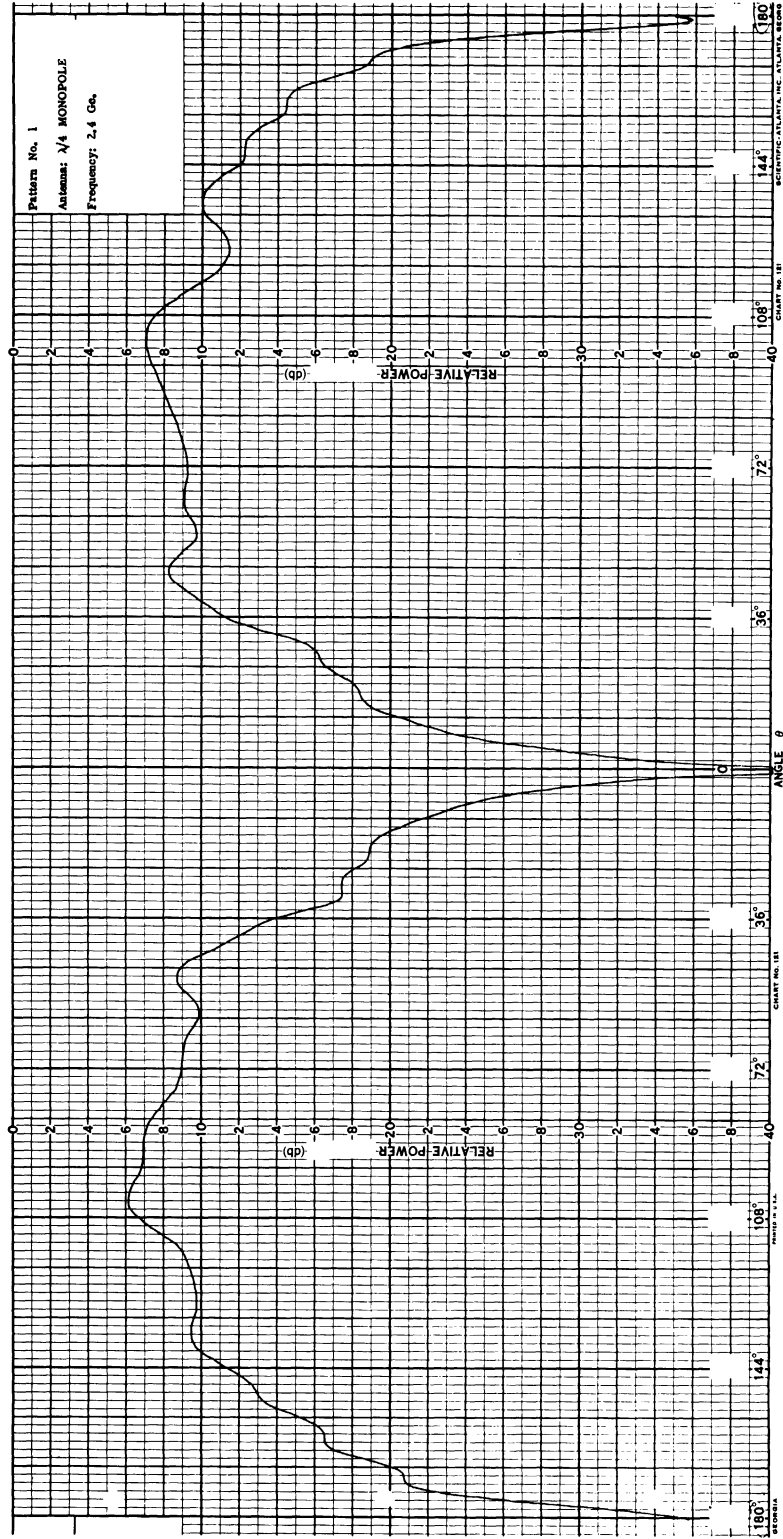


FIG. 29: PRECISION T-33 MODEL (LESS WING TANKS). FREQ. = 2.4 Gc.

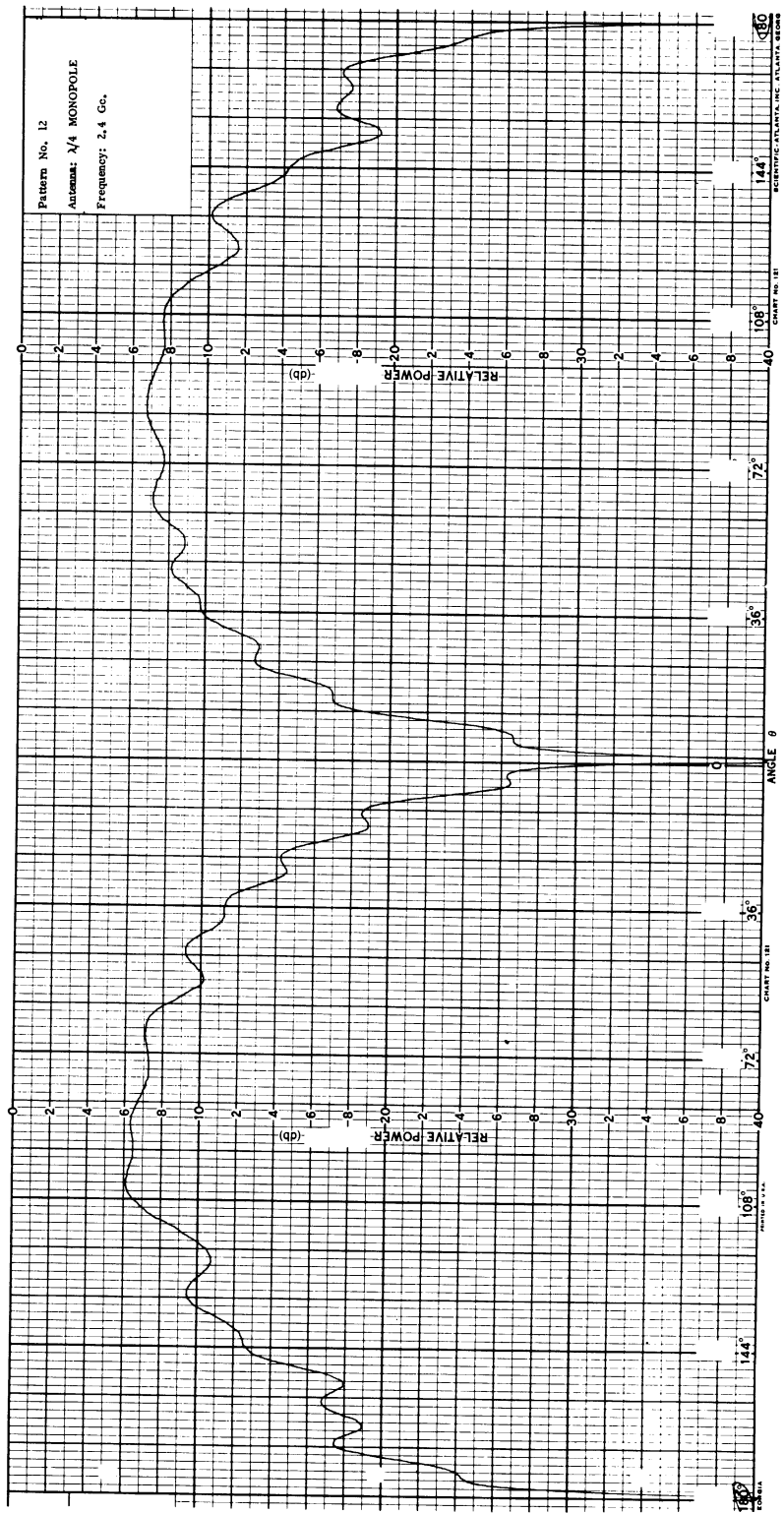


FIG. 30: SIMPLIFIED T-33 MODEL. FREQ. = 2.4 Gc.

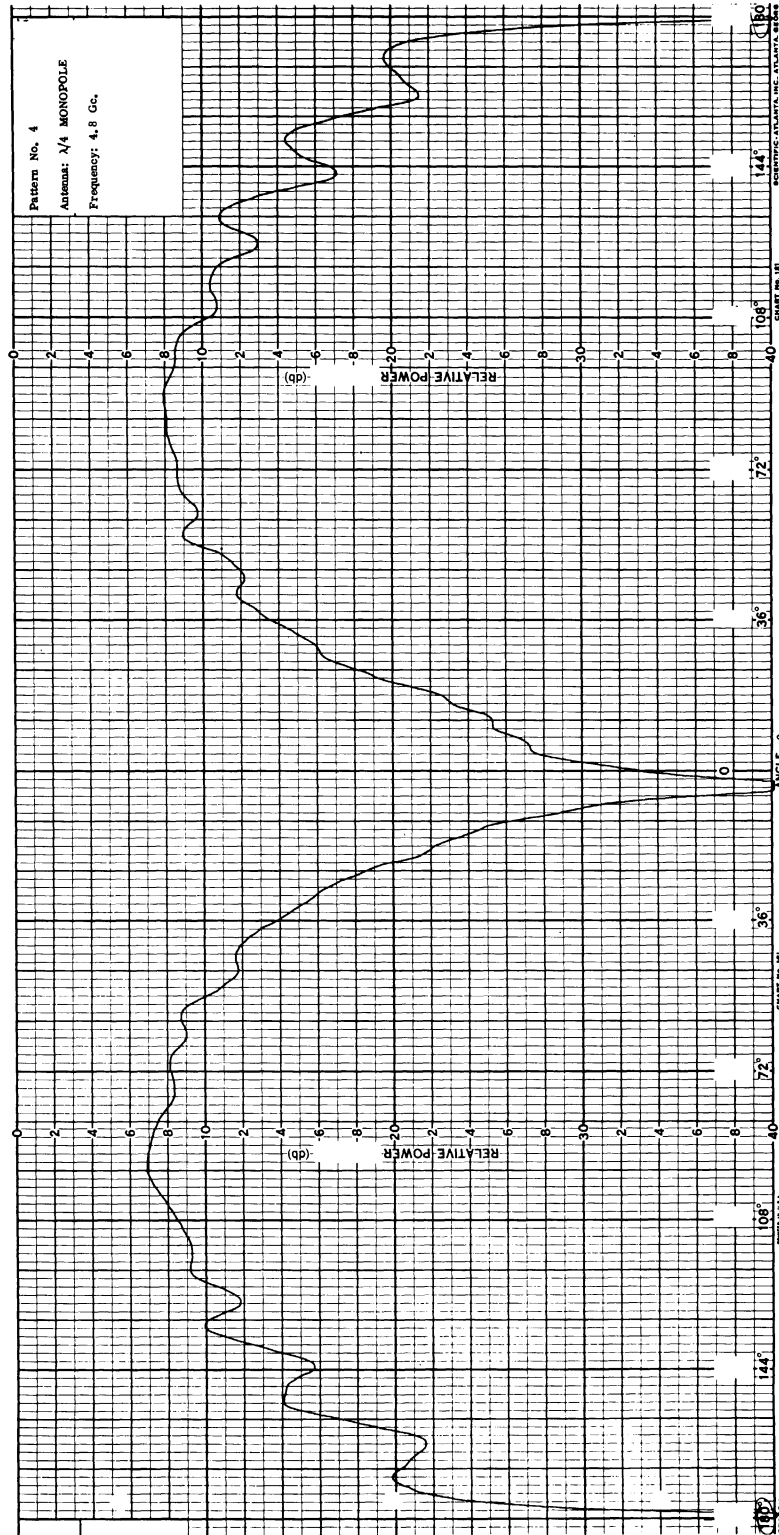


FIG. 31: PRECISION T-33 MODEL (LESS WING TANKS). FREQ. = 4.8 Gc.

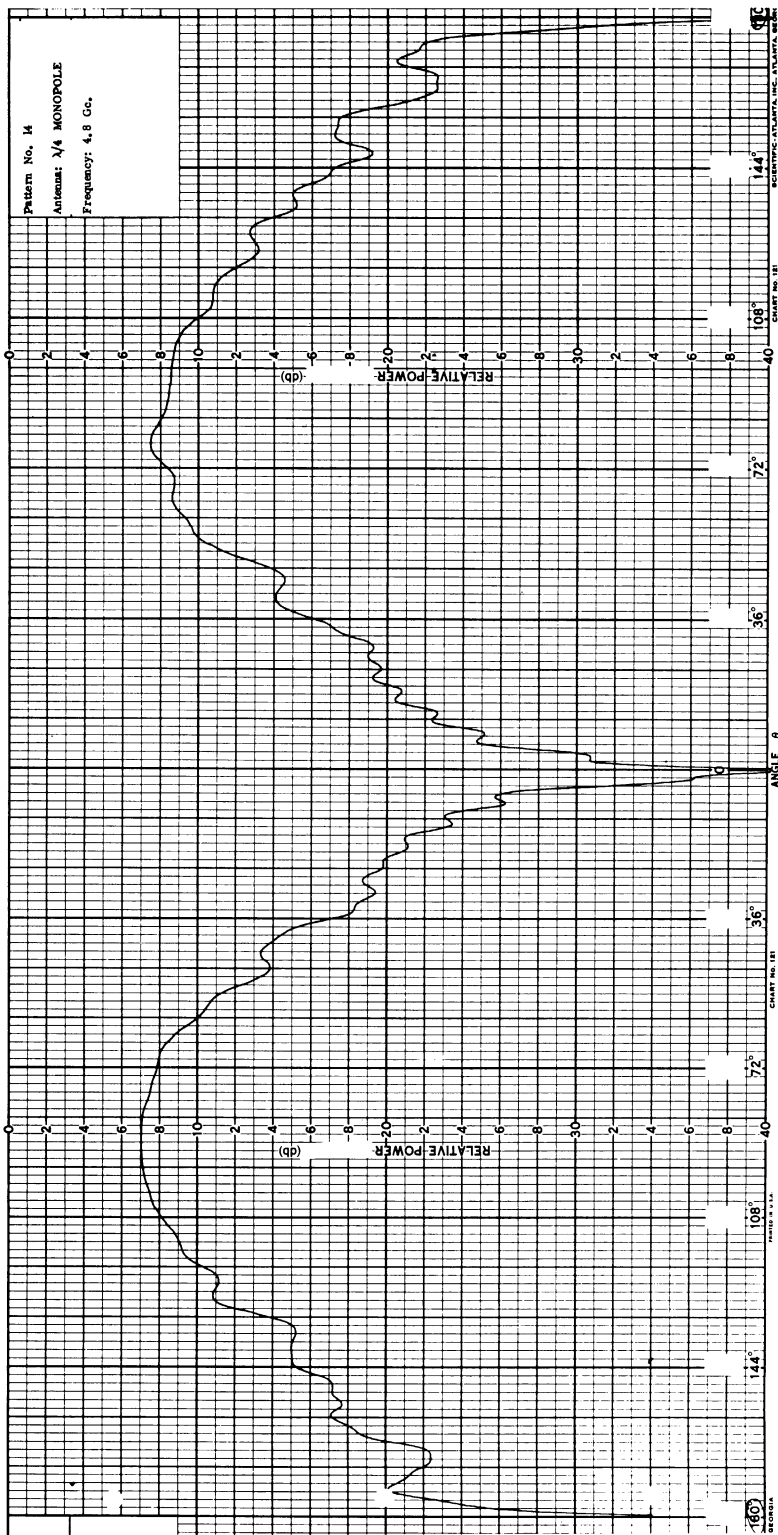


FIG. 32: SIMPLIFIED T-33 MODEL. FREQ. = 4.8 Gc.

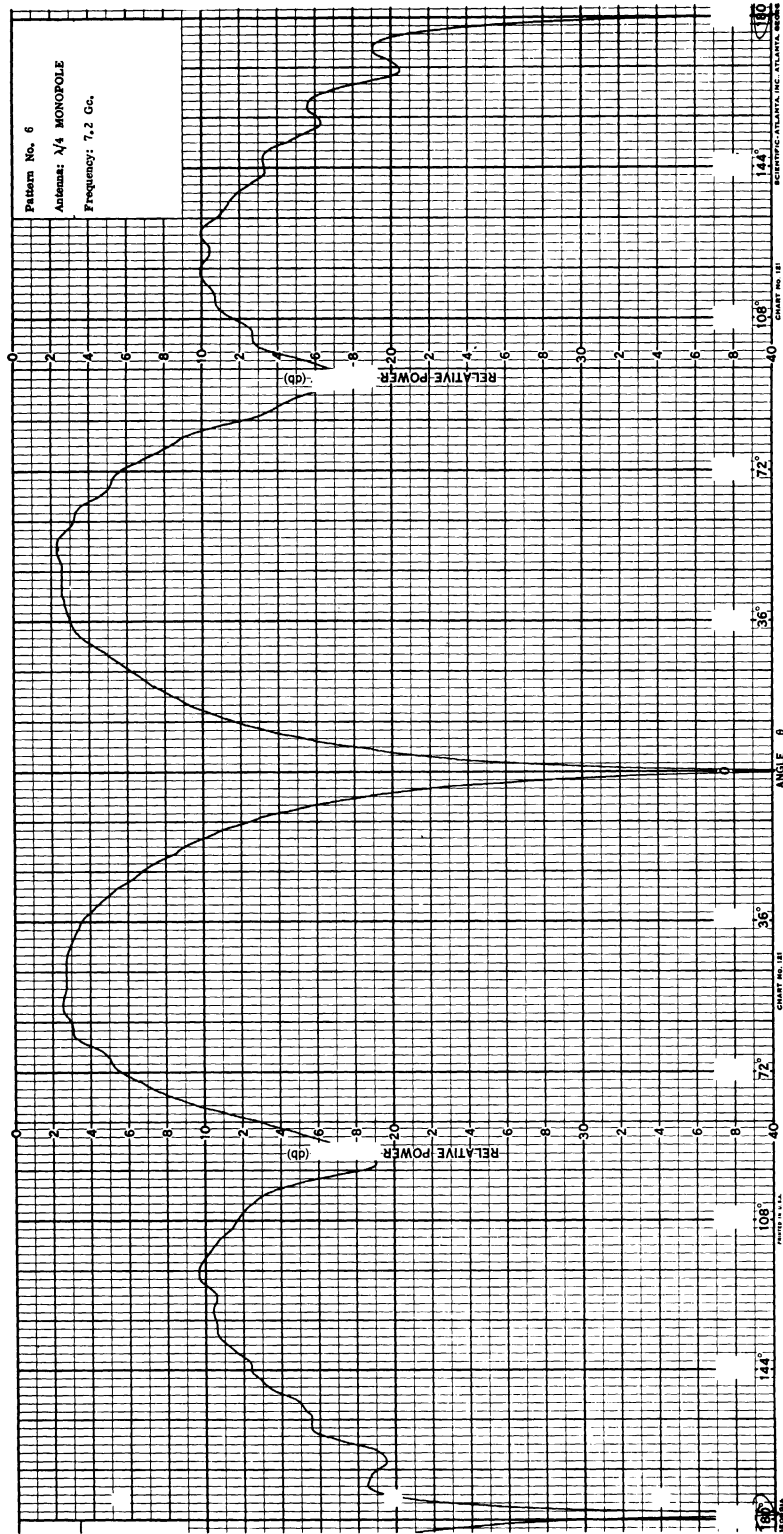


FIG. 33: PRECISION T-33 MODEL (LESS WING TANKS). FREQ. = 7.2 Gc.

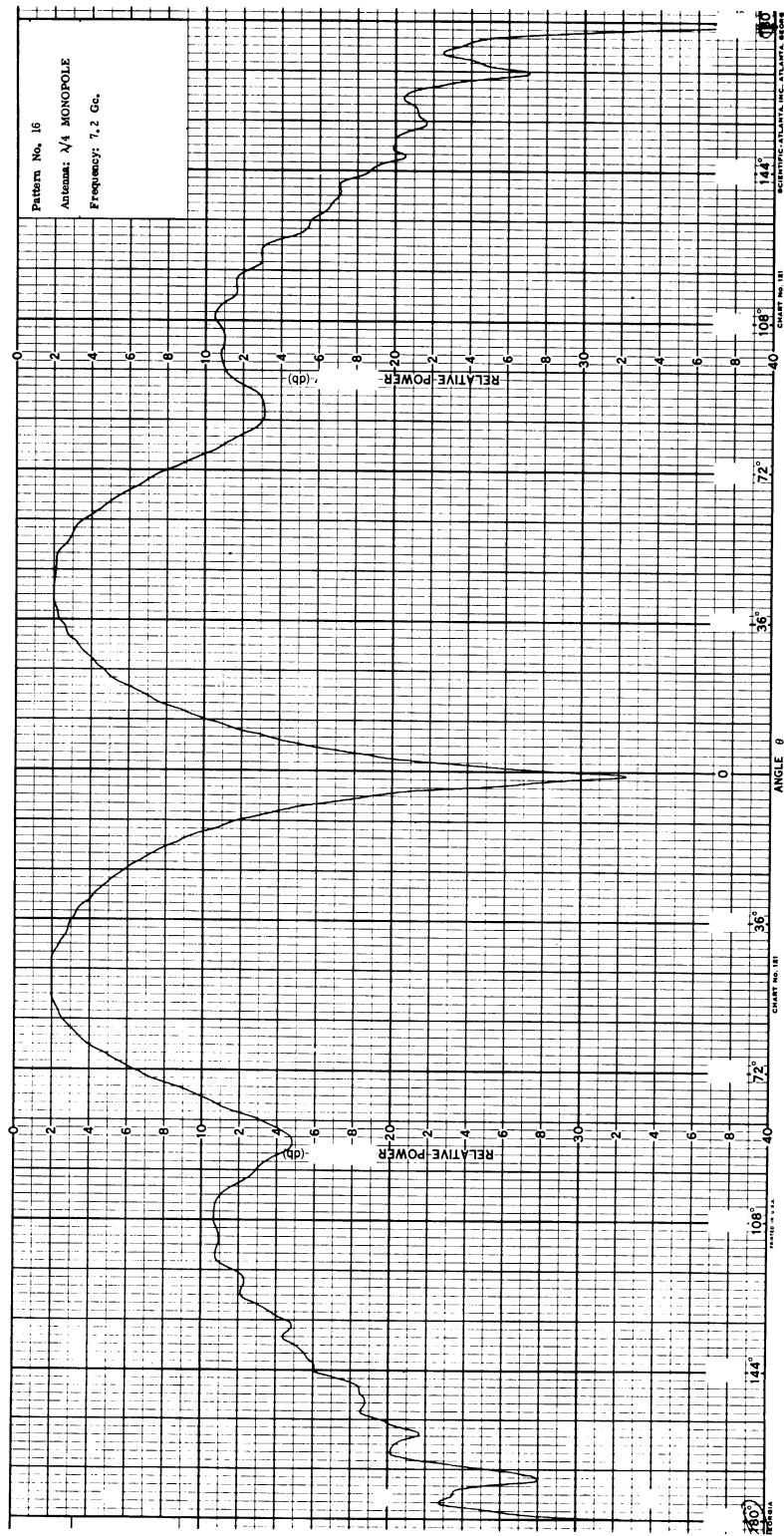


FIG. 34: SIMPLIFIED T-33 MODEL. FREQ. = 7.2 Gc.

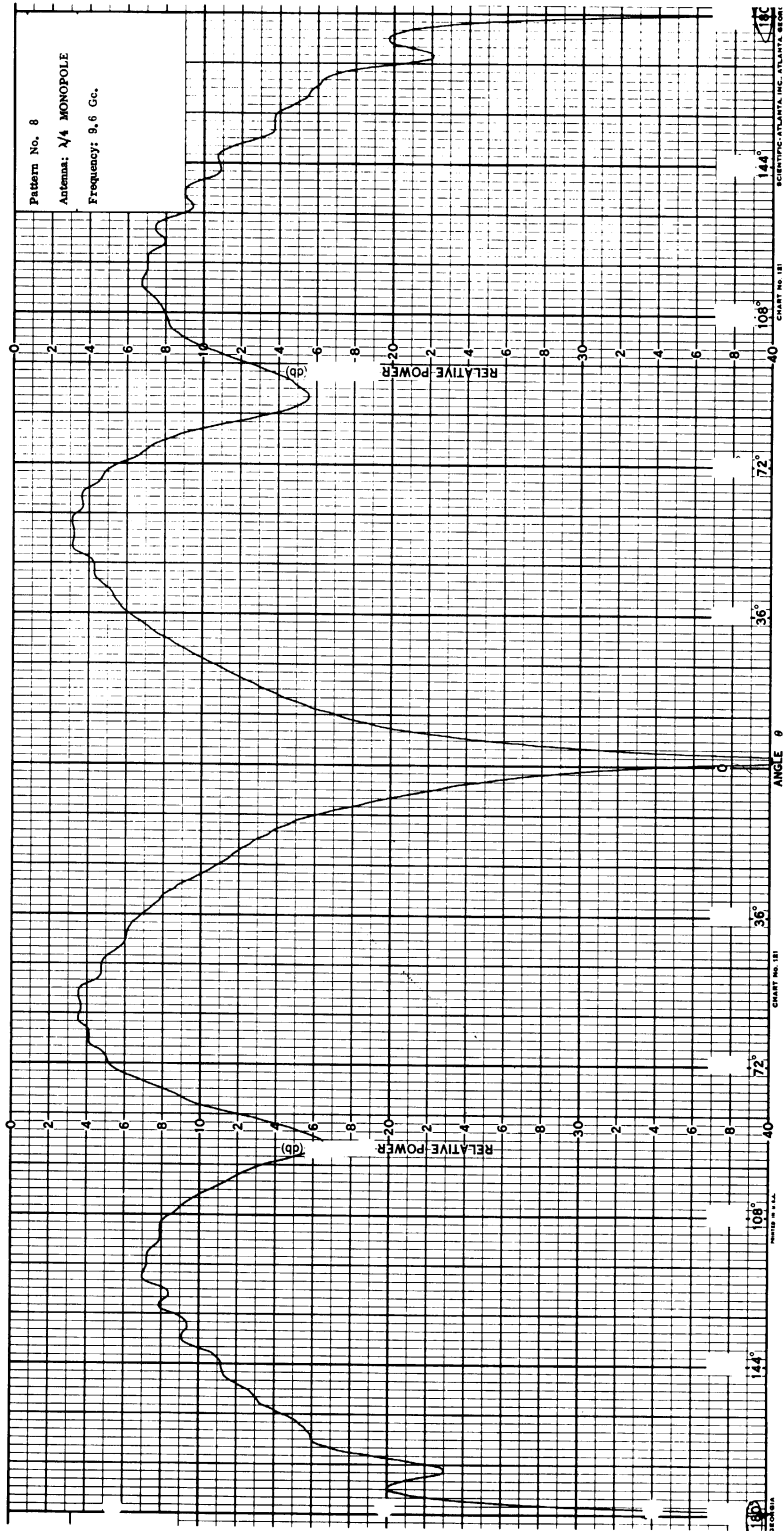


FIG. 35: PRECISION T-33 MODEL (LESS WING TANKS). FREQ. = 9.6 Gc.

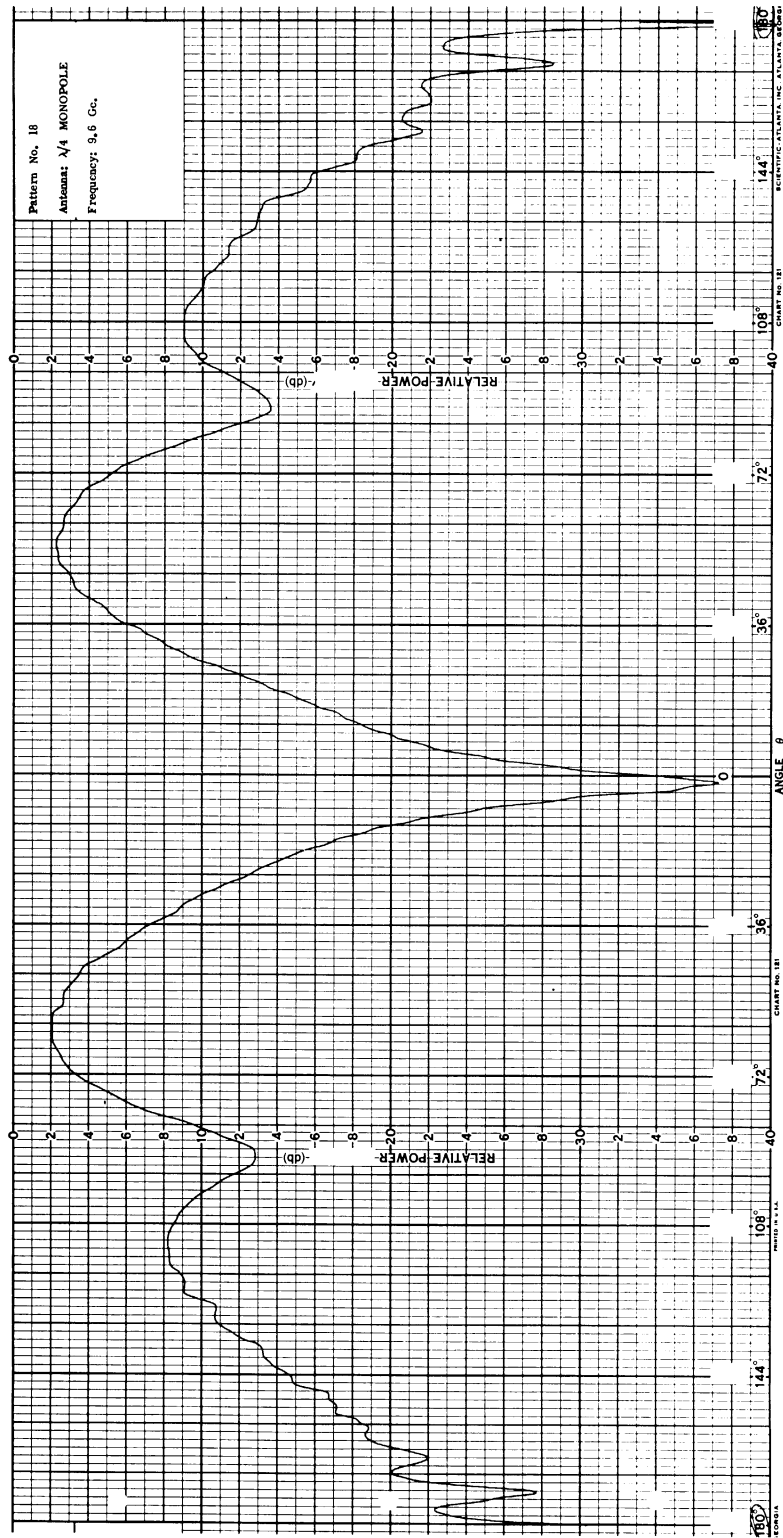


FIG. 36: SIMPLIFIED T-33 MODEL. FREQ. = 9.6 Gc.

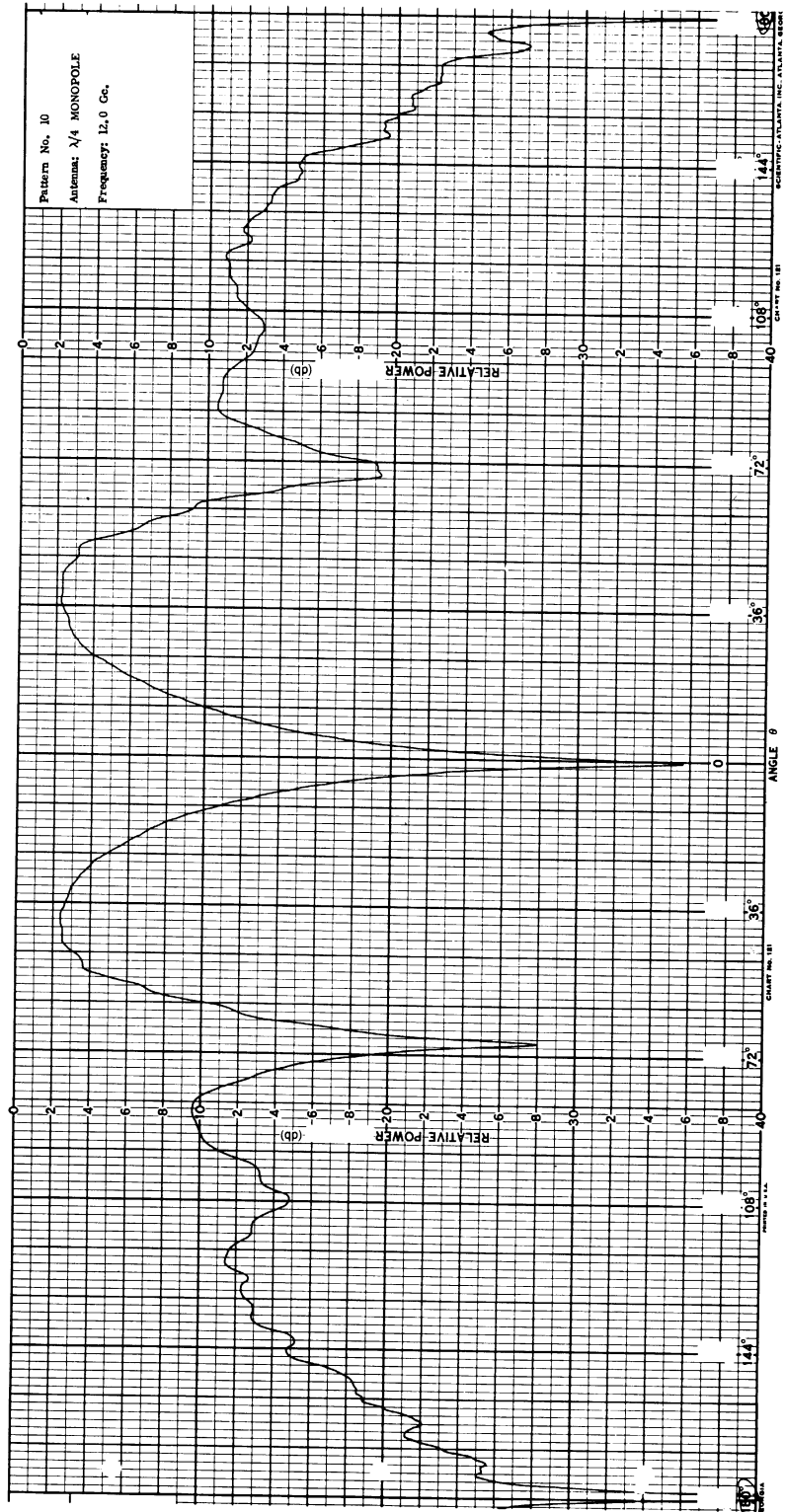


FIG. 37: PRECISION T-33 MODEL (LESS WING TANKS). FREQ. = 12.0 Gc.

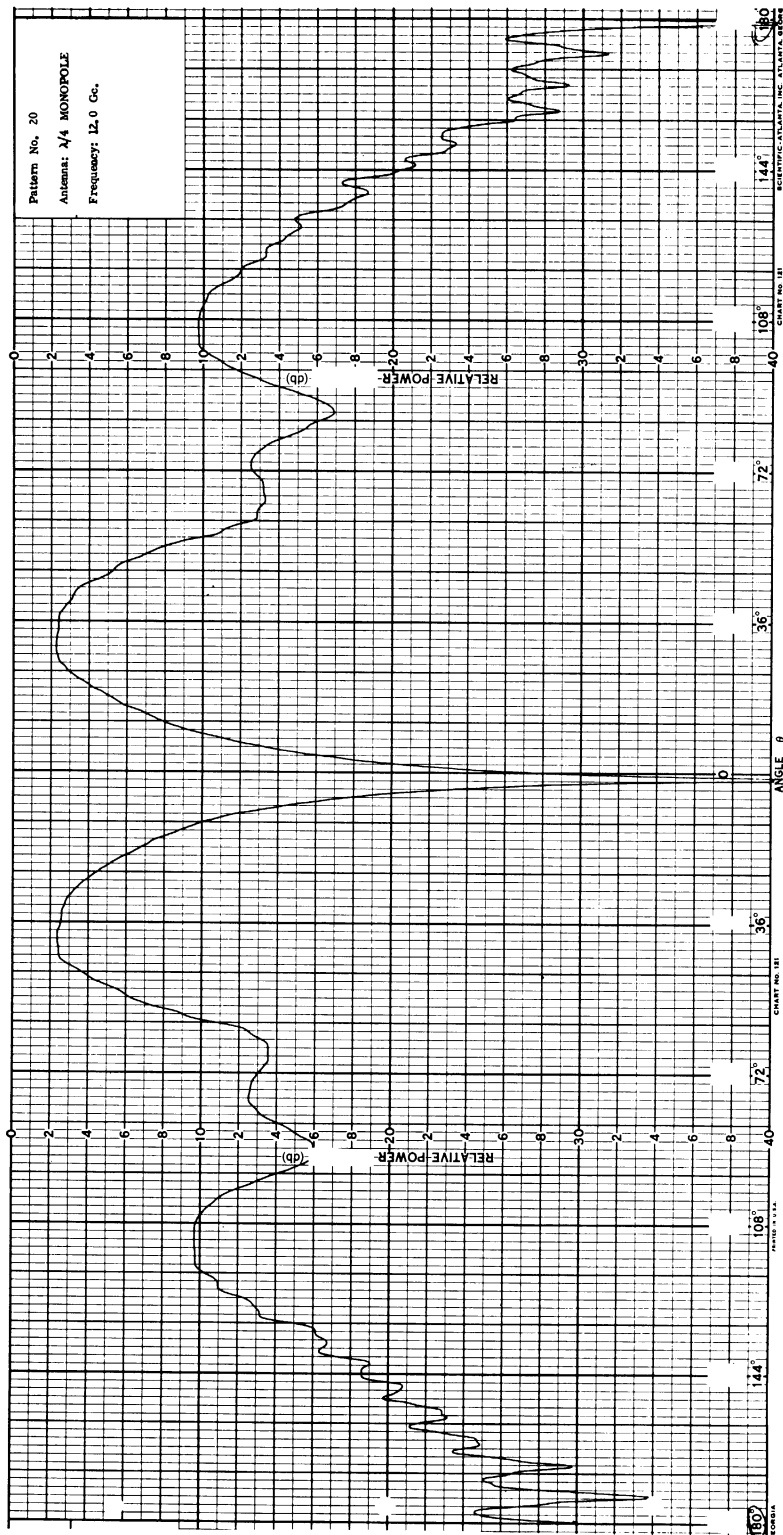


FIG. 38: SIMPLIFIED T-33 MODEL. FREQ. = 12.0 Gc.

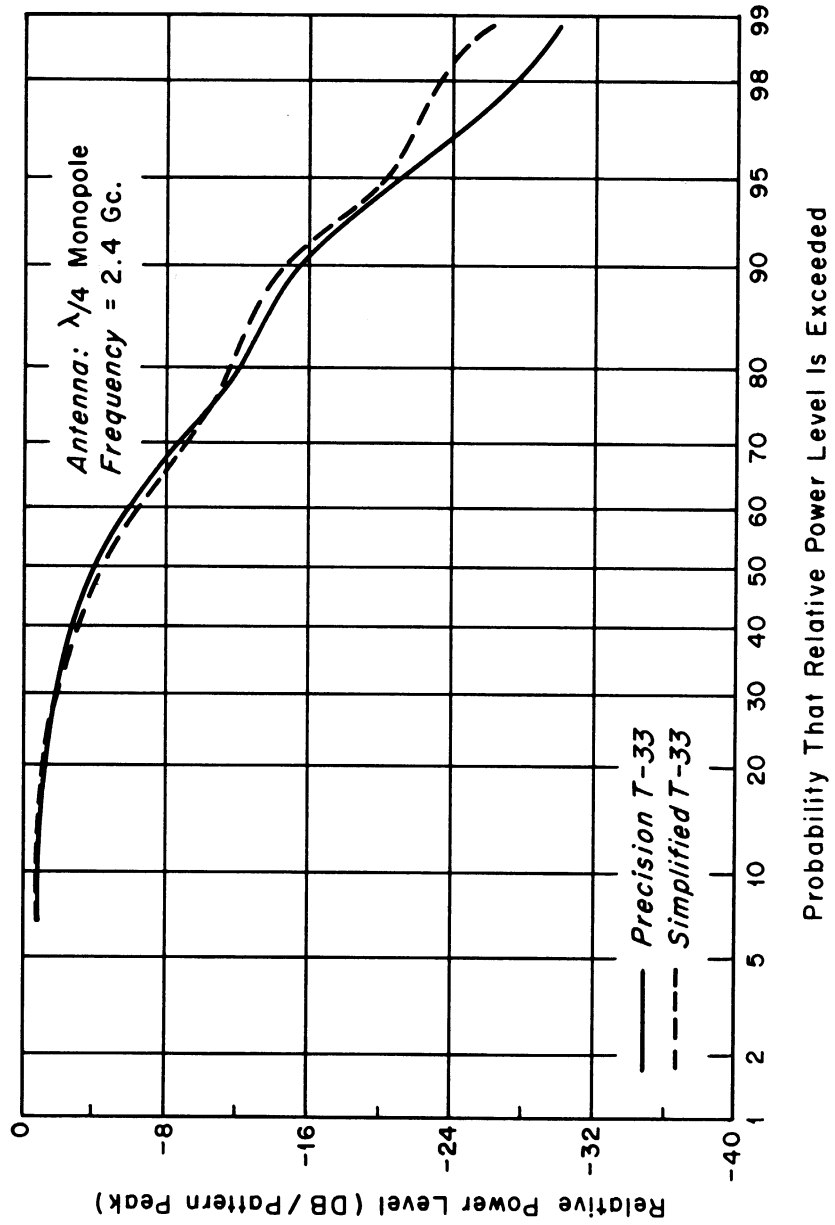


FIG. 39: CUMULATIVE GAIN DISTRIBUTIONS OF PRECISION AND SIMPLIFIED MODELS.

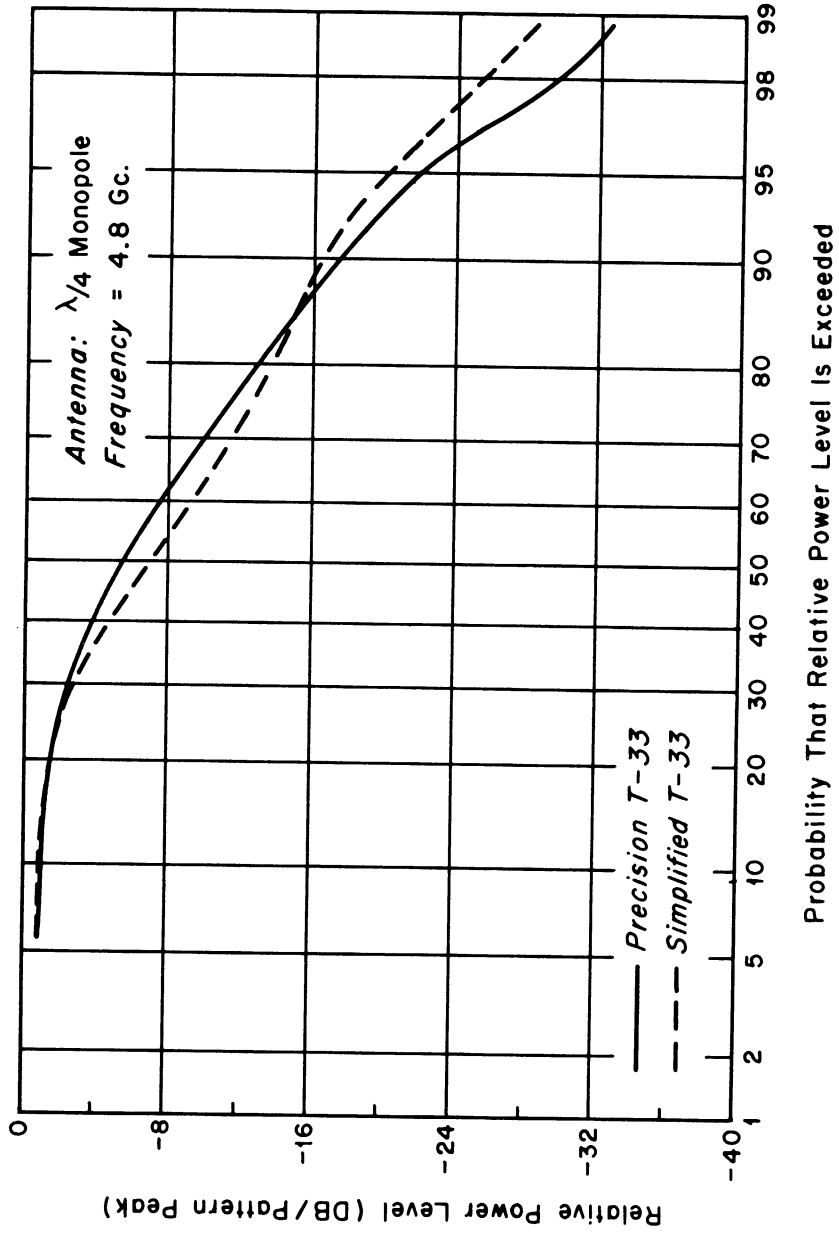


FIG. 40: CUMULATIVE GAIN DISTRIBUTIONS OF PRECISION AND SIMPLIFIED MODELS.

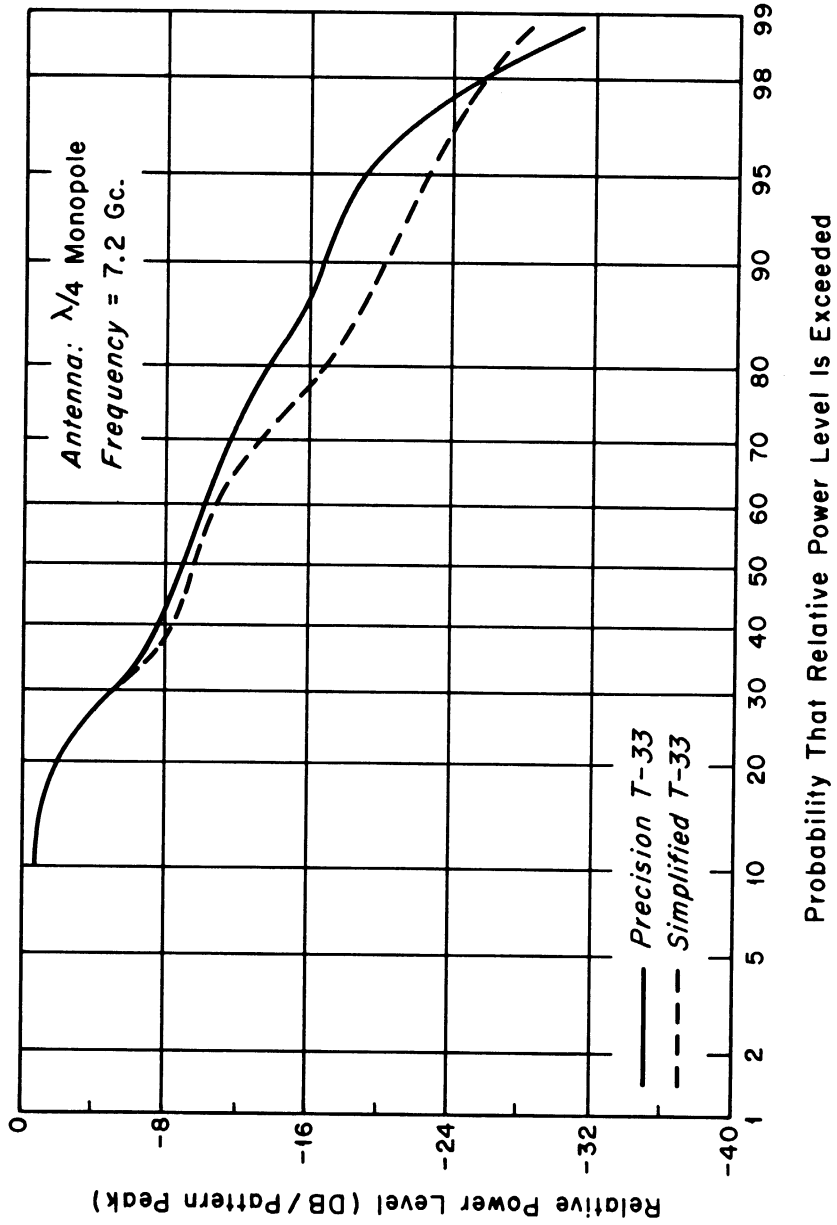


FIG. 41: CUMULATIVE GAIN DISTRIBUTIONS OF PRECISION AND SIMPLIFIED MODELS.

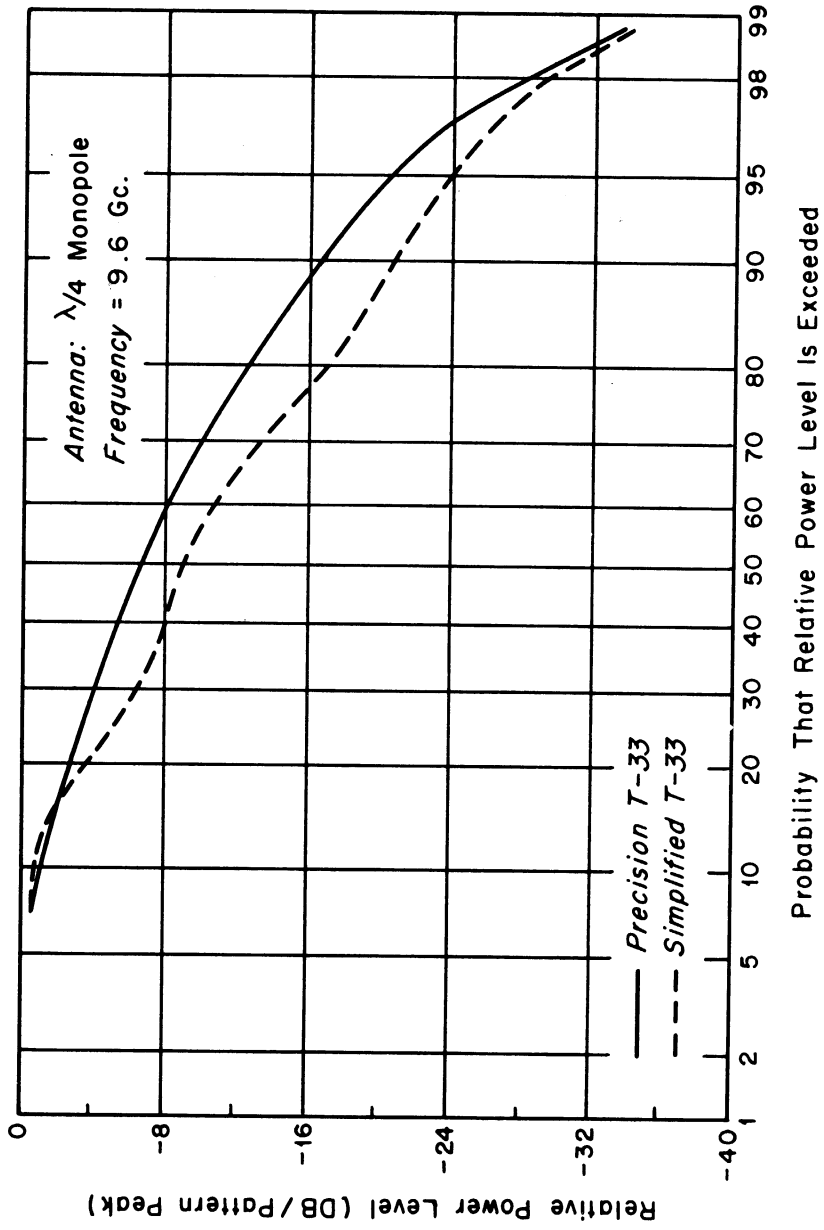


FIG. 42: CUMULATIVE GAIN DISTRIBUTIONS OF PRECISION AND SIMPLIFIED MODELS.

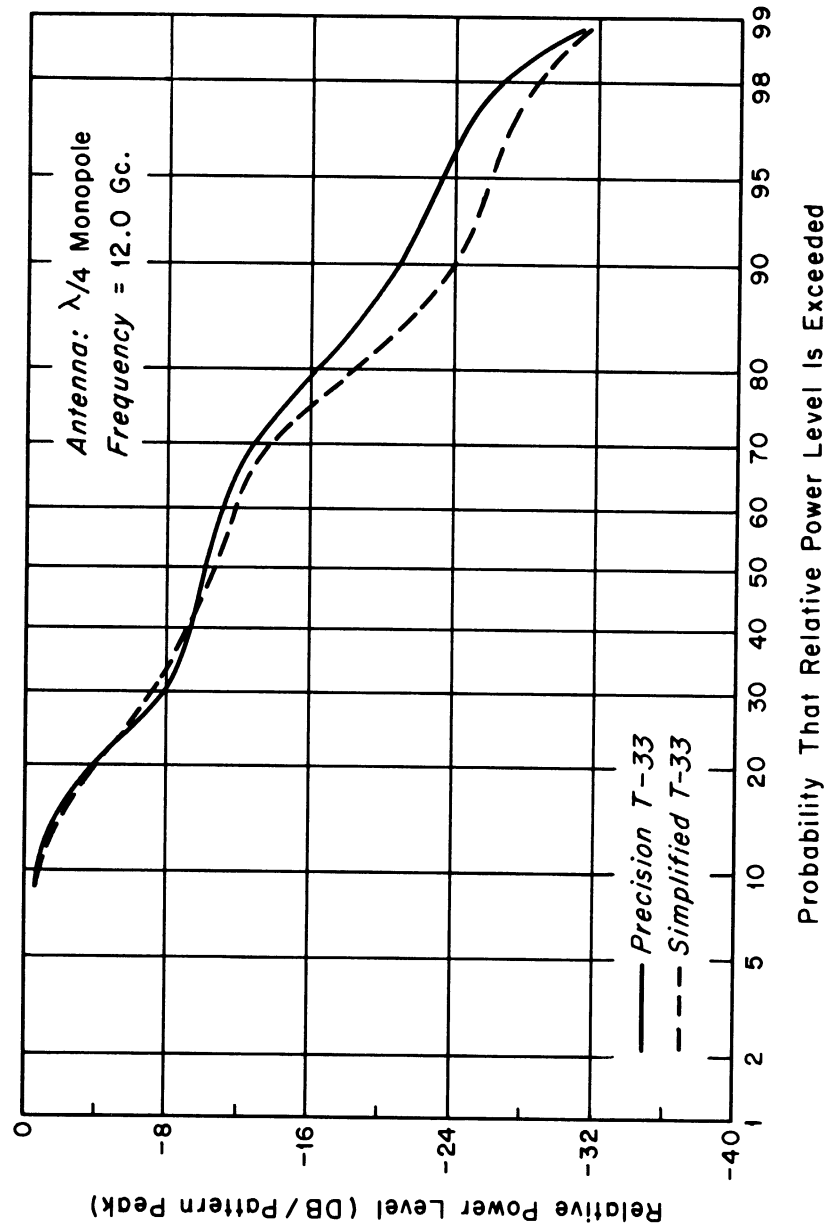


FIG. 43: CUMULATIVE GAIN DISTRIBUTIONS OF PRECISION AND SIMPLIFIED MODELS.

3.2.2 Derivation of Approximation

Consider the mathematical model described above and the usual systems of Cartesian and cylindrical coordinates (Fig. 44). For a line source at $(\rho_0 = R+r, 0)$ (time dependence $e^{-i\omega t}$ to be understood), the total field $G_0(\rho, \rho_0; \theta, 0)$ (Green's function) at (ρ, θ) satisfying $(\nabla^2 + k^2)G_0 = -4\pi\delta(\bar{\rho} - \bar{\rho}_0)$ and the radiation condition at infinity is given as (Morse and Feshbach, 1953)

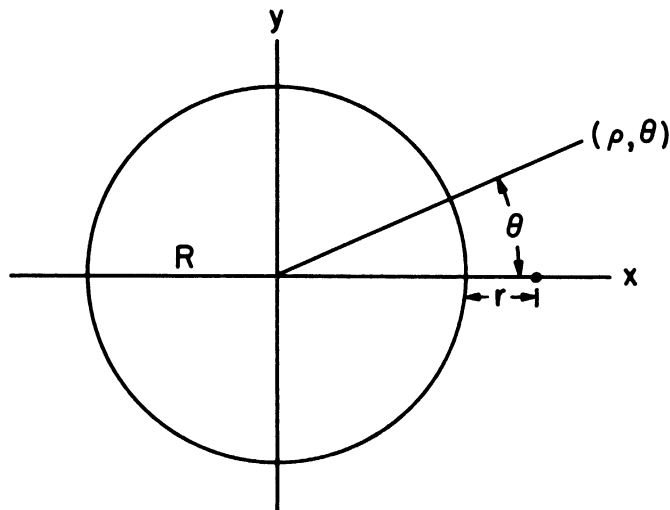


FIG. 44: CARTESIAN AND CYLINDRICAL COORDINATES

$$G_0(\rho, \rho_0; \theta, 0) = i\pi H_0^{(1)}\left(k\sqrt{\rho^2 + \rho_0^2 - 2\rho\rho_0 \cos \theta}\right)$$

$$= i\pi \sum_0^{\infty} \epsilon_m \cos m\theta \begin{cases} J_m(k\rho) H_m^{(1)}(k\rho_0) & \rho < \rho_0 \\ J_m(k\rho_0) H_m^{(1)}(k\rho) & \rho > \rho_0 \end{cases}$$

where $\epsilon_0 = 1$, $\epsilon_m = 2$, $m \geq 1$.

The total field $G(\rho, \rho_0; \theta, 0)$ at (ρ, θ) due to the line source at $(\rho_0, 0)$ in the presence of a perfectly conducting cylinder of radius R , satisfying the Neumann boundary condition $\left. \frac{\partial G}{\partial \rho} \right|_{\rho=R} = 0$ and the radiation condition at infinity, is given by (Morse and Feshbach)

$$G(\rho, \rho_0; \theta, 0) = i\pi \sum_0^{\infty} \epsilon_m \cos m\theta H_m^{(1)}(k\rho_0) \left[\frac{J_m(k\rho) H_m^{(1)'}(kR) - J_m'(kR) H_m^{(1)}(k\rho)}{H_m^{(1)'}(kR)} \right] \quad \rho < \rho_0$$

$$= i\pi \sum_0^{\infty} \epsilon_m \cos m\theta H_m^{(1)}(k\rho) \left[\frac{J_m(k\rho_0) H_m^{(1)'}(kR) - J_m'(kR) H_m^{(1)}(k\rho_0)}{H_m^{(1)'}(kR)} \right] \quad \rho > \rho_0 \quad (1)$$

where $F'(kR) = \left. \frac{d}{d(k\rho)} F(k\rho) \right|_{\rho=R}$.

Let us consider the total far field $G(\rho, \rho_0; \theta, 0)$, $k\rho \gg 1$, $\rho \gg R$. Then $\rho > \rho_0$ and the second of the expansions in (1) applies. But since $\rho_0 = R+r$ we have the following Taylor expansions:

$$J_m [k(R+r)] = J_m (kR) + \frac{kr}{kR} [kR J'_m (kR)] + \frac{(kr)^2}{2(kR)^2} [(kR)^2 J''_m (kR)] + \dots$$

$$H_m^{(1)} [k(R+r)] = H_m^{(1)} (kR) + \frac{kr}{kR} [kR H_m^{(1)'} (kR)] + \frac{(kr)^2}{2(kR)^2} [(kR)^2 H_m^{(1)''} (kR)] + \dots$$

where we have bracketed terms of the same order. Substituting these into (1), making use of the Wronskian relation (Magnus and Oberhettinger, 1949)

$$J_m (kR) H_m^{(1)'} (kR) - J'_m (kR) H_m^{(1)} (kR) = \frac{2i}{\pi(kR)},$$

yields

$$G(\rho, \rho_o; \theta, 0) = \frac{-2}{kR} \sum_0^{\infty} \epsilon_m \cos m\theta \frac{H_m^{(1)}(k\rho)}{H_m^{(1)'}(kR)} \left[1 + O \left[(r/R)^2 \right] \right] \quad (2)$$

Now since $k\rho \gg 1$ the asymptotic expansion (Magnus and Oberhettinger, 1949)

$$H_m^{(1)}(k\rho) = \left(\frac{2}{\pi k\rho} \right)^{1/2} e^{ik\rho} e^{-i\pi/4} (-i)^m \left[1 + O(1/k\rho) \right]$$

can be used. Hence

$$G(\rho, \rho_o; \theta, 0) = \frac{-2}{kR} \left(\frac{2}{\pi k\rho} \right)^{1/2} e^{ik\rho} e^{-i\pi/4} \sum_0^{\infty} \frac{\epsilon_m (-i)^m \cos m\theta}{H_m^{(1)'}(kR)} \left[1 + O \left[(r/R)^2 \right] + O(1/k\rho) \right] \quad (3)$$

We can find a very simple interpretation for this total far field. Consider a plane wave e^{-ikx} incident along $\theta = 0$ upon the perfectly conducting cylinder (Neumann boundary condition). We have the following expansion (Magnus and Oberhettinger 1949)

$$e^{-ikx} = e^{-ik\rho \cos\theta} = \sum_0^{\infty} \epsilon_m (-i)^m J_m(k\rho) \cos m\theta.$$

The total field at (ρ, θ) due to the incident plane wave and the wave scattered by the cylinder is given by (Morse and Feshbach 1953)

$$\begin{aligned} U(\rho, \cdot; \theta, 0) &= e^{-ik\rho \cos\theta} - \sum_0^{\infty} \epsilon_m (-i)^m \frac{J'_m(kR) H_m^{(1)}(k\rho)}{H_m^{(1)'}(kR)} \\ &= \sum_0^{\infty} \epsilon_m (-i)^m \cos m\theta \left[\frac{J_m(k\rho) H_m^{(1)'}(kR) - J'_m(kR) H_m^{(1)}(k\rho)}{H_m^{(1)'}(kR)} \right]. \end{aligned}$$

To find the field on the surface ($\rho=R$) of the cylinder we use the Wronskian relation. Thus

$$U(R, \cdot; \theta, 0) = \frac{2i}{\pi kR} \sum_0^{\infty} \frac{\epsilon_m (-i)^m \cos m\theta}{H_m^{(1)'}(kR)} \tag{4}$$

If we compare equation (4) with equation (3) we see that

$$G(\rho, \rho_0; \theta, 0) = i\pi \left(\frac{2}{\pi k\rho}\right)^{1/2} e^{ik\rho} e^{-i\pi/4} U(R, \cdot; \theta, 0) \left[1 + O\left[\left(\frac{r}{R}\right)^2\right] + O(1/k\rho)\right] \tag{5}$$

Hence the total far field at (ρ, θ) due to a line source at $(\rho_0 = R+r, 0)$ can be approximated using the total field on the surface at (R, θ) due to a plane wave incident along $\theta=0$. It is this relationship which we will use to further investigate the far field.

3.2.3 Analysis of the Far Field

We consider two sets of numerical values. For the first set, R , which represents the radius of curvature of aircraft fuselages, is taken to be 150 cm or

approximately 5 feet. The frequencies to be considered are 200, 400, and 1000 Mcs. Thus the wavelengths are 150 cm, 75 cm, 30 cm and $kR=2\pi$, 4π , 10π , respectively. For r we use the value $\lambda/4$ which corresponds to monopole antennas, hence $r=R/4$, $R/8$, $R/20$ for the wavelengths considered. We then have $r/R=1/4$, $1/8$, $1/20$, and $(r/R)^2=1/16$, $1/64$, $1/400$, respectively; therefore, the far field equation (5) applies and we can use the field on the surface due to an incident plane wave.

The problem of a plane wave incident upon a perfectly conducting cylinder has been widely considered in the literature. A good survey is presented in the book by King and Wu (1959). We cite only a few other papers, that of Goriainov (1958) which is similar to the one of Wetzel (1957) discussed in King and Wu. The main reason for citing Goriainov's paper is his result that for $(kR/2)^{1/3} \geq 1.36$ the "asymptotic theory" is in good agreement with the rigorous equations. In our cases $(kR/2)^{1/3}=1.47$, 1.85 , 2.50 ; therefore, we can apply the "asymptotic theory" of Wetzel which is essentially equivalent to that of Goriainov. For numerical calculations we will use Table I of the work by Logan (1959).

Solving the equation $(\frac{kR}{2})^{1/3}=1.36$ yields the value $kR=5$. Thus, the second set of numerical values will be concerned with kR below 5. In particular, we consider the value $R=100$ cm, which gives $kR=4.19$ for 200 Mcs and $kR > 5$ for 400 and 1000 Mcs. With this value of kR the values $r=\frac{1}{4}\lambda$, $r=\frac{1}{4}R$, $\frac{1}{8}R$ will be used. In addition, we examine $kR=2$, $r=\frac{1}{4}R$, $\frac{1}{8}R$, $\frac{1}{20}R$. (The reason for this latter case will be seen shortly.)

Consider a point (ρ, θ) in the far field. When the "asymptotic theory" applies to the surface field of the plane wave, it applies to the total field of the line source. Hence we can use the geometric theory of Keller and Levy (1959) to describe physically the total field of the line source. To simplify the analysis we consider a

point in the far field to be characterized by an angle alone. By symmetry we need only consider $0 \leq \theta \leq \pi$. Thus the total field at (\cdot, θ) is due to:

- (1) The incident plus reflected plus diffracted fields, if (\cdot, θ) is in the "illuminated region" of the line source (Fig. 45a)
- (2) The diffracted field if (\cdot, θ) is in the "shadow region" of the line source (Fig. 45b).

The total field at (R, θ) due to an incident plane wave is described in King and Wu (1959). The contributions to this field depend on $|g(\xi_m)|$ and $|g(\xi'_m)|$ where

$$\xi_m = (kR/2)^{1/3} \left(\theta - \frac{\pi}{2} + 2\pi m \right), \quad \xi'_m = (kR/2)^{1/3} \left(\frac{3\pi}{2} - \theta + 2\pi m \right).$$

A plot of $|g(\xi)|$ vs ξ is shown in Fig. 12 of Chapter 3, Section 15 of King and Wu. From $\xi_{2\pi} = (kR/2)^{1/3} (2\pi)$ we see that only $|g(\xi_0)|$ and $|g(\xi'_0)|$ need be considered in our cases. It remains to identify the contributions to the surface field of the plane wave with the contributions to the far field of the line source. Suppose then that half ($\pi < \theta < 2\pi$) of the cylinder is smoothly removed, by which we mean that the plane wave or line source impinges on a half cylinder and the energy at the edges is smoothly absorbed (no edge reflection on the surface or radiation into space). Then the total field of the line source at (\cdot, θ) is due to:

- (1) The incident plus reflected fields, if (\cdot, θ) is in the "illuminated region" of the line source. In Fig. 45a the diffracted field is no longer contributing since it is due to energy which has "crept" around the bottom of the cylinder.
- (2) The "upper" diffracted field, if (\cdot, θ) is in the "shadow region" of the line source. In Fig. 45b the "lower" diffracted field is no longer contributing since it is due to energy which has "crept" around the bottom of the cylinder.

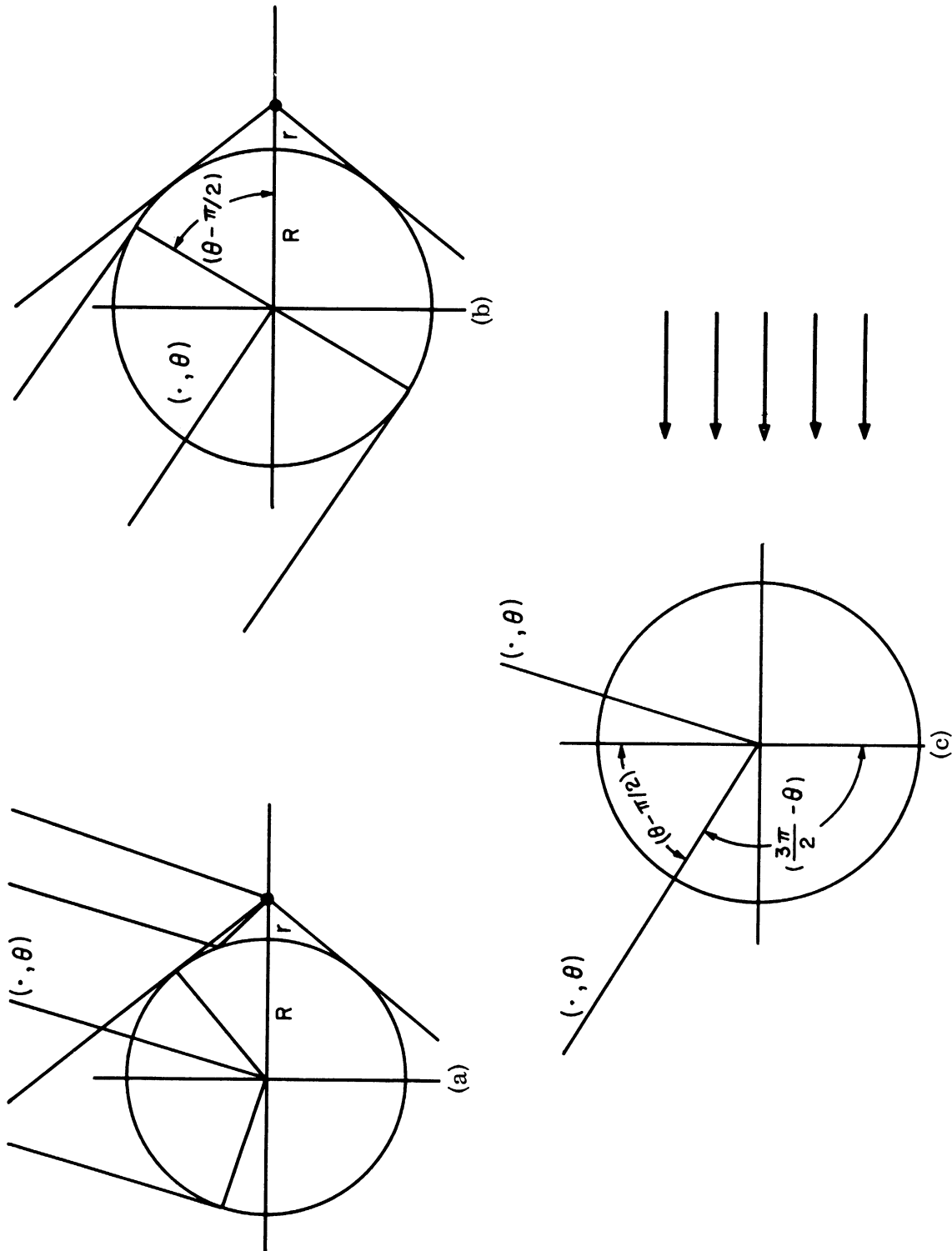


FIG. 45: (a) ILLUMINATED REGION, (b) SHADOW REGION, (c) PLANE WAVE INCIDENCE

But the only contribution to the total field of the plane wave at (R, θ) is $|g(\xi_0)|$, since again $|g(\xi'_0)|$ is due to energy which has "crept" around the bottom of the cylinder. Thus we identify $|g(\xi_0)|$ with the incident plus reflected fields if (\cdot, θ) is in the "illuminated region" of the line source, and with the "upper" diffracted field if (\cdot, θ) is in the "shadow region" of the line source. This implies that we identify $|g(\xi'_0)|$ with the diffracted field if (\cdot, θ) is in the "illuminated region" of the line source, and with the "lower" diffracted field if (\cdot, θ) is in the "shadow region" of the line source. As mentioned above, the case of the bottom half of the cylinder follows by symmetry.

For values of kR below 5, Wetzel has derived an approximation which is valid. He does not indicate the smallest value of kR for which this approximation holds, but does mention the validity at $kR=2$. Hence the reason for considering $kR=2$. The approximation consists of deriving a correction to $g(\xi)$ defined by $g_1(\xi) = g(\xi) + (\frac{2}{kR})^{2/3} c(\xi)$. $c(\xi)$ is tabulated in Wetzel and $g_1(\xi)$ is given in Appendix B. Thus the contributions to the surface field now depend on $|g_1(\xi_m)|$ and $|g_1(\xi'_m)|$. From the values of $\xi_{2\pi} = (\frac{kR}{2})^{1/3} 2\pi$ for $kR=4.19, 2$ we see that only $|g_1(\xi_0)|$ and $|g_1(\xi'_0)|$ need be considered, with relative error of less than 0.001 and 0.007 respectively. Hence, we can argue as previously to identify $|g_1(\xi_0)|$ and $|g_1(\xi'_0)|$ with the contributions to the far field of the line source. However, we must now consider to what degree of accuracy the idea of reflected and diffracted fields can be used. We know that a decrease in kR is accompanied by a decrease in accuracy of the geometric theory. This decrease in accuracy will be taken into account by the derivation of a correction term to the result calculated by assuming the notion of reflected and diffracted fields is highly accurate. Thus we will obtain uncorrected results for the first set of numerical values, then analytically derive the correction term and apply it to these numerical values. Finally we will obtain results for the second set of numerical values.

3.2.4 Uncorrected Results (First Set of Numerical Values)

In the language of our mathematical model we consider the following problem: How much of the cylinder can be smoothly removed without greatly affecting the far field in the region $-\pi/2 \leq \theta \leq \pi/2$, the "illuminated region", and the "shadow region". This problem can be solved by using the contributions $|g(\xi_o)|$ and $|g(\xi'_o)|$ to estimate the ratio of the magnitudes of the contributions to the far field.

Take first the "illuminated region" and thus the region $-\pi/2 \leq \theta \leq \pi/2$ which it contains. If we let θ_I be defined by $\cos \theta_I = R/R+r$, then the "illuminated region" is defined by $-(\theta_I + \pi/2) \leq \theta \leq \theta_I + \pi/2$. As previously we need only consider positive θ . We assert that in this region ($0 \leq \theta \leq \theta_I + \pi/2$) the far field is reasonably preserved if the arc ($\theta_I < \theta \leq \pi$) of the cylinder is smoothly removed. In practice one might have to retain a larger arc, say $0 \leq \theta \leq \theta_I + \Delta$, so that the absorbing device does not obstruct the field in the $\theta = \theta_I + \pi/2$ direction. To prove our assertion we show that the ratio

$$\frac{|g(\xi'_o)|}{|g(\xi_o)|}$$

is small for the $\theta \leq \theta_I + \pi/2$ directions. A numerical value for the largest allowable ratio will be provided later. We use the previously mentioned Table I (Logan) for the values of $|g(\xi)|$. The following table gives the ratio for the $\theta = \theta_I + \pi/2$ directions.

TABLE I

kR	$\cos \theta_I$	θ_I	$\frac{\theta_I}{180} \pi$	ξ_o	$ g(\xi_o) $	$(\frac{180-\theta_I}{180})\pi$	ξ'_o	$ g(\xi'_o) $	Ratio
2π	4/5	37°	0.645	0.95	0.75	2.50	3.68	0.071	0.095
4π	8/9	27°	0.471	0.87	0.82	2.67	4.93	0.023	0.028
10π	20/21	18°	0.314	0.79	0.87	2.82	7.05	0.004	0.005

As θ decreases from $\theta_I + \pi/2$, ξ_0 decreases and hence $|g(\xi_0)|$ increases, ξ'_0 increases and thus $|g(\xi'_0)|$ decreases; therefore the ratio $|g(\xi'_0)| / |g(\xi_0)|$ decreases from the values above. This proves our assertion. We compute the length of the arc $-\theta_I \leq \theta \leq \theta_I$ in wavelengths for the three cases.

$$\text{arc length} = 2\pi R \cdot \frac{2 \frac{\theta_I}{180} \pi}{2\pi} = 2R \left(\frac{\theta_I}{180} \pi \right)$$

TABLE Ia

kR	R	Arc Length
2π	λ	$2\lambda \left(\frac{\theta_I}{180} \pi \right) = 1.29\lambda$
4π	2λ	$4\lambda \left(\frac{\theta_I}{180} \pi \right) = 1.88\lambda$
10π	5λ	$10\lambda \left(\frac{\theta_I}{180} \pi \right) = 3.14\lambda$

If we now take a point (\cdot, θ_s) in the "shadow region" it is immediately evident (Fig. 45b) that we need at least the arc defined by $0 \leq \theta \leq \theta_s - \pi/2$, plus additional Δ as mentioned above, to reproduce the far field in $0 \leq \theta \leq \theta_s$. This is due to the contribution from the "upper" diffracted field. We make some computations (Table II) to see if the contribution of the "lower" diffracted field must be considered.

TABLE II

θ_s	kR	$(\frac{\theta - 90}{180})\pi$	ζ_o	$ g(\zeta_o) $	$(\frac{270-\theta}{180})\pi$	ζ'_o	$ g(\zeta'_o) $	Ratio
135	2 π	0.785	1.16	0.65	2.36	3.46	0.087	0.134
	4 π		1.45	0.51		4.35	0.039	0.077
	10 π		1.96	0.33		5.88	0.010	0.030
145	2 π	0.960	1.41	0.53	2.18	3.20	0.11	0.207
	4 π		1.77	0.39		4.03	0.052	0.137
	10 π		2.40	0.22		5.45	0.015	0.068
155	2 π	1.13	1.61	0.44	2.00	2.94	0.14	0.314
	4 π		2.04	0.30		3.70	0.070	0.233
	10 π		2.84	0.15		5.00	0.022	0.147

This table shows that in order to answer the above question we must decide on how accurately the far field is to be reproduced. Let us consider $(r/R)^2$ plus the ratio to be no larger than 1/5. Since the values of $(r/R)^2$ are 0.063, 0.016, 0.003 for $kR=2\pi, 4\pi, 10\pi$ respectively, we see that the computations in the "illuminated region" satisfy this requirement. However, it is not satisfied at all angles in the "shadow region". Therefore for each value of kR we seek a maximum θ_M for which the arc $0 \leq \theta \leq \theta_M - \pi/2$, plus additional Δ , reproduces the far field in $0 \leq \theta \leq \theta_M$ (subject to the 1/5 requirement).

TABLE III

kR	θ_M	$(\frac{\theta - 90}{180})\pi$	ζ_o	$ g(\zeta_o) $	$(\frac{270-\theta}{180})\pi$	ζ'_o	$ g(\zeta'_o) $	Ratio
2 π	135	0.785	1.15	0.65	2.36	3.45	0.087	0.134
4 π	150.5	1.055	1.95	0.330	2.08	3.86	0.0610	0.184
10 π	159	1.20	3.00	0.130	1.93	4.84	0.0256	0.197

For $\theta < \theta_M$, ξ_0 decreases, $|g(\xi_0)|$ increases, ξ'_0 increases, $|g(\xi'_0)|$ decreases; therefore, the ratio $|g(\xi'_0)| / |g(\xi_0)|$ decreases, and so the accuracy requirement is satisfied. For $\theta > \theta_M$, ξ_0 increases, $|g(\xi_0)|$ decreases, ξ'_0 decreases, $|g(\xi'_0)|$ increases; therefore, the ratio $|g(\xi'_0)| / |g(\xi_0)|$ increases, implying that the θ_M in Table III are the desired maximum angles. We compute the arc length of $-(\theta_M - \pi/2) \leq \theta \leq \theta_M - \pi/2$ in wavelengths.

$$\text{arc length} = 2\pi R \frac{2\left(\frac{\theta_M - 90}{180}\right)\pi}{2\pi} = 2R\left(\frac{\theta_M - 90}{180}\right)\pi$$

TABLE IIIa

kR	R	Arc Length
2π	λ	$2\lambda\left(\frac{\theta_M - 90}{180}\right)\pi = 1.57\lambda$
4π	2λ	$4\lambda\left(\frac{\theta_M - 90}{180}\right)\pi = 4.21\lambda$
10π	5λ	$10\lambda\left(\frac{\theta_M - 90}{180}\right)\pi = 12.0\lambda$

If we want the far field for $\theta > \theta_M$, subject to the accuracy requirement, we need the contribution of the "lower" diffracted field and thus (Fig. 45b) the arc $-(\frac{3\pi}{2} - \theta_M) \leq \theta \leq \frac{3\pi}{2} - \theta_M$, plus additional Δ . This arc is the minimum arc necessary to reproduce the entire far field, subject to the accuracy requirement. We compute it in wavelengths.

$$\text{arc length} = 2\pi R \frac{2\left(\frac{270-\theta}{180}\right)\pi}{2\pi} = 2R\left(\frac{270-\theta}{180}\right)\pi$$

TABLE IIIb

kR	R	Arc Length
2π	λ	$2\lambda\left(\frac{270-\theta}{180}\right)\pi = 4.72\lambda$
4π	2λ	$4\lambda\left(\frac{270-\theta}{180}\right)\pi = 8.32\lambda$
10π	5λ	$10\lambda\left(\frac{270-\theta}{180}\right)\pi = 19.3\lambda$

It is of interest to consider r as fixed and vary the frequency over the values 200, 400, and 1000 Mc. Likewise we can consider a fixed frequency and vary r over R/4, R/8, and R/20. These computations are found in the following tables. We again use the value 1/5 to limit $(r/R)^2$ plus the ratio.

$$\text{KEY: } \text{Arc}_1 = -\theta_I \leq \theta \leq \theta_I$$

$$\text{Arc}_2 = -(\theta_M - \pi/2) \leq \theta \leq \theta_M - \pi/2$$

$$\text{Arc}_3 = -\left(\frac{3\pi}{2} - \theta_M\right) \leq \theta \leq \frac{3\pi}{2} - \theta_M$$

$$r = R/4, (r/R)^2 = 1/16 = 0.063, \cos \theta_I = 4/5$$

TABLE IV

kR	$\frac{\theta_I}{180}\pi$	ζ_0	$ g(\zeta_0) $	$(\frac{180-\theta_I}{180})\pi$	ζ'_0	$ g(\zeta'_0) $	Ratio	Arc Length Arc ₁
2π	0.645	0.95	0.75	2.50	3.68	0.071	0.095	1.29λ
4π	0.645	1.19	0.063	2.50	4.62	0.031	0.049	2.58λ
10π	0.645	1.61	0.44	2.50	6.25	0.0574	0.017	6.45λ

TABLE IVa

kR	θ_M	$(\frac{\theta_M-90}{180})\pi$	ζ_0	$ g(\zeta_0) $	$(\frac{270-\theta_M}{180})\pi$	ζ'_0	$ g(\zeta'_0) $	Ratio	Arc Length Arc ₂ Arc ₃
2π	135	0.785	1.15	0.65	2.36	3.45	0.087	0.134	1.57λ 4.72λ
4π	146	0.976	1.80	0.376	2.19	4.05	0.051	0.135	3.90λ 8.76λ
10π	154	1.12	2.79	0.156	2.02	5.05	0.021	0.134	11.2 λ 20.2 λ

$$r = R/8, (r/R)^2 = 1/64 = 0.016, \cos \theta_I = 8/9$$

TABLE V

kR	$\frac{\theta_I}{180} \pi$	ξ_0	$ g(\xi_0) $	$(\frac{180-\theta_I}{180})\pi$	ξ'_0	$ g(\xi'_0) $	Ratio	Arc Length Arc ₁
2π	0.471	0.693	0.93	2.67	3.92	0.058	0.062	0.94λ
4π	0.471	0.87	0.82	2.67	4.93	0.023	0.028	1.88λ
10π	0.471	0.18	0.64	2.67	6.68	0.005	0.008	4.71λ

TABLE Va

kR	θ_M	$(\frac{\theta_M - 90}{180})\pi$	ξ_0	$ g(\xi_0) $	$(\frac{270-\theta_M}{180})\pi$	ξ'_0	$ g(\xi'_0) $	Ratio	Arc Length Arc ₂ Arc ₃
2π	142	0.906	1.33	0.565	2.23	3.28	0.103	0.183	1.81λ 4.26λ
4π	150.5	1.055	1.95	0.330	2.08	3.86	0.061	0.184	4.21λ 8.32λ
10π	158	1.19	2.97	0.134	1.95	4.88	0.0248	0.185	11.9 λ 19.5 λ

$$r = R/20, (r/R)^2 = 1/400 = 0.003, \cos \theta_1 = 20/21$$

TABLE VI

kR	$\frac{\theta_1}{180} \pi$	ζ_0	$ g(\zeta_0) $	$(\frac{180-\theta_1}{180})\pi$	ζ'_0	$ g(\zeta'_0) $	Ratio	Arc Length Arc ₁
2π	0.314	0.462	1.075	2.82	4.15	0.047	0.044	0.63λ
4π	0.314	0.58	1.005	2.82	5.22	0.0183	0.018	1.26λ
10π	0.314	0.79	0.87	2.82	7.05	0.004	0.005	3.14λ

TABLE VIa

kR	θ_M	$(\frac{\theta_M - 90}{180})\pi$	ζ_0	$ g(\zeta_0) $	$(\frac{270-\theta_M}{180})\pi$	ζ'_0	$ g(\zeta'_0) $	Ratio	Arc Length Arc ₂ Arc ₃
2π	144	0.942	1.39	0.535	2.20	3.23	0.106	0.198	1.88λ 4.40λ
4π	151.5	1.57	1.99	0.318	2.07	3.83	0.0626	0.197	4.28λ 8.28λ
10π	159	1.20	3.00	0.130	1.93	4.84	0.0216	0.197	12.0 λ 19.3 λ

3.2.5 Analytical Derivation of Correction Term

In order to investigate the decrease in accuracy of the geometric theory for the far field at (\cdot, θ) we can, according to Eq. (5), investigate it for the surface field at (R, θ) of the plane wave (providing $(\frac{r}{R})^2$ is small enough). Consider the cylinder to be divided into the "deep shadow," penumbra of width $d = (\frac{2}{K}R^2)^{1/3}$, and "brightly illuminated" regions (Fig. 46). For the "deep shadow" region the decrease in accuracy can be characterized, as a function of kR , by the difference between the phase predicted by the geometric theory and the true geometric phase. Then, providing $\theta_I + \pi/2, \theta_M$ are in the "deep shadow" we can find the correction to the arcs (Figs. 47a, 47b) as follows. The above phase difference is computed for the primary contribution in the directions $\theta_I + \pi/2, \theta_M$. This difference is then translated into arc length; it represents the desired correction for finite kR and thus is added to the arcs $-\theta_I \leq \theta \leq \theta_I, -(\theta_M - \pi/2) \leq \theta \leq (\theta_M - \pi/2)$. For the remaining arc (Fig. 47c) we compute the phase difference for the contributions in the direction π . If this difference does not exceed $\pi - \theta_M$, then no correction need be added to $-(3\pi/2 - \theta_M) \leq \theta \leq (3\pi/2 - \theta_M)$. If it does exceed $\pi - \theta_M$, say by δ , then a correction must be added only if $\delta / (\pi - \theta_M + \delta) > \frac{1}{5} - 0 \left(\left(\frac{r}{R} \right)^2 \right)$. The correction $(1 - \epsilon)\delta$, $\epsilon < 1$, is determined by the equation

$$\frac{\epsilon \delta}{\pi - \theta_M + \delta} = \frac{1}{5} - 0 \left(\left(\frac{r}{R} \right)^2 \right).$$

For the angles ϕ in the "deep shadow," the predicted phase for the primary contribution is found in Franz (1954), Wetzel, and Keller and Levy. It is

$$\left[kR + \left(\frac{kR}{6} \right)^{1/3} \cos \pi/3 q_1 - \left(\frac{6}{kR} \right)^{1/3} \cos \pi/3 \left(\frac{1}{10q_1} + \frac{q_1^2}{180} \right) \right] (\phi - \pi/2)$$

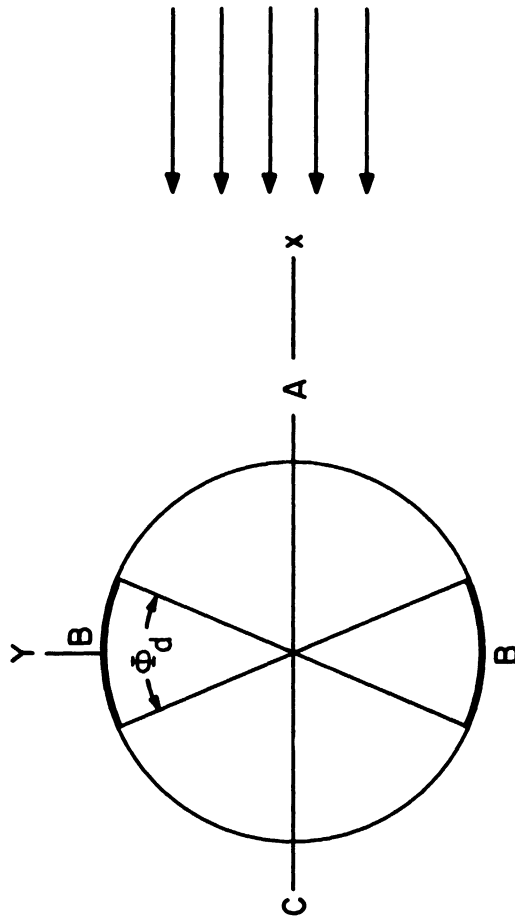


FIG. 46: A - BRIGHTLY ILLUMINATED REGION
B - PENUMBRA REGION
C - DEEP SHADOW

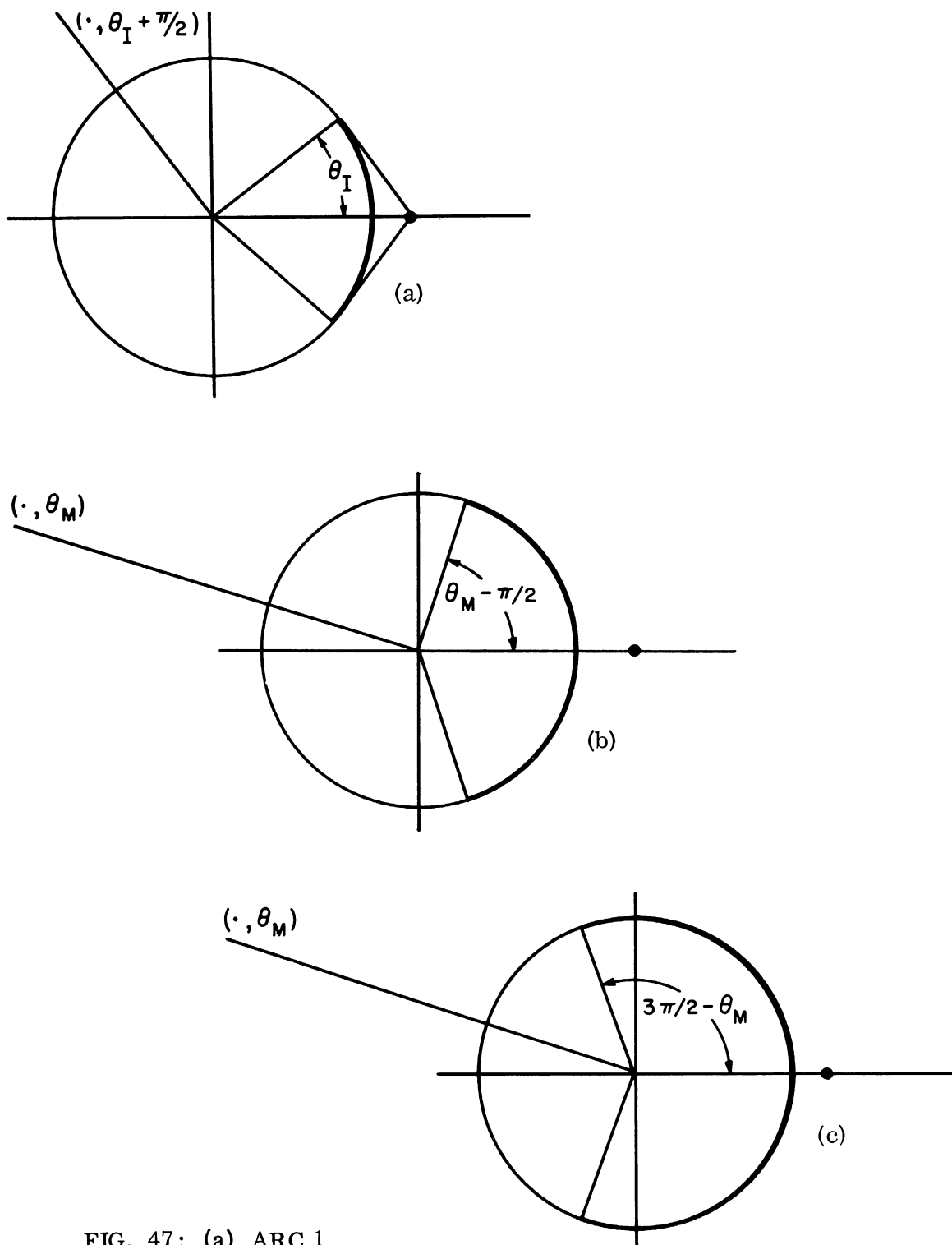


FIG. 47: (a) ARC 1
(b) ARC 2
(c) ARC 3

where q_1 is the first zero of the derivative of the Airy function $A(q)$ defined by

$$A(q) = \frac{1}{2} \int_{-\infty}^{\infty} d\xi e^{i(q\xi - \xi^2)} .$$

This can be reduced to (Franz)

$$\left[kR + 0.809 (kR)^{1/3} \cos \pi/3 - 0.145 (kR)^{-1/3} \cos \pi/3 \right] (\phi - \pi/2)$$

or

$$kR \left[1 + \frac{0.404}{(kR)^{2/3}} - \frac{0.072}{(kR)^{4/3}} \right] (\phi - \pi/2)$$

which we represent in the form $kR [1 + \gamma] (\phi - \pi/2)$. Thus $\gamma(\phi - \pi/2)$ is the difference between the predicted phase and the true geometric phase; it represents $\frac{\gamma(\phi - \pi/2)}{2\pi} 2\pi R$ or $\frac{\gamma(\phi - 90)}{360} 2\pi R$ in arc length.

If $\theta_I + \pi/2$, θ_M lie in the "penumbra region" then the correction to the arcs $-\theta_I \leq \theta \leq \theta_I$, $-(\theta_M - \pi/2) \leq \theta \leq \theta_M - \pi/2$ will be taken to be

$$\frac{\gamma \frac{\overline{\Phi}d}{2}}{2\pi} \cdot 2\pi R$$

where $\overline{\Phi}d$ is the angular width of the "penumbra region".

3.2.6 Corrections to the Arcs of IV

The corrections are tabulated in the following manner: Tables VII, VIII, IX, and X present the numerical values necessary for the corrections while Tables VIIa, VIIIa, IXa, and Xa compare the uncorrected and corrected arcs.

TABLE VII (R=150 cm, r=1/4λ)

kR	$\frac{\bar{\Phi}_d}{2}$	$(kR)^{2/3}$	γ	$\gamma\theta_I$	$\gamma\frac{\theta_I}{360}2\pi R$	$\gamma(\theta_M - 90)$	$\gamma\frac{\theta_M - 90}{360}2\pi R$	$\gamma(180-90)$
2π	19.9°	3.41	0.112	4.14°	0.072λ	5.04°	0.088λ	10.1°
4π	15.6°	5.38	0.0726	1.96°	0.068λ	4.39°	0.153λ	6.54°
10π	11.5°	9.95	0.0400	0.72°	0.063λ	2.76°	0.241λ	3.60°

TABLE VIIa

$\text{Arc}_1 = -\theta_I \leq \theta \leq \theta_I$ Corrected = $-(\theta + \gamma\theta_I) \leq \theta \leq \theta + \gamma\theta_I$
 $\text{Arc}_2 = -(\theta_M - \pi/2) \leq \theta \leq \theta_M - \pi/2$ Corrected = $-(\theta_M - \pi/2 + \gamma(\theta_M - \pi/2)) \leq \theta \leq \theta_M - \pi/2 + \gamma(\theta_M - \pi/2)$
 $\text{Arc}_3 = -(3\pi/2 - \theta_M) \leq \theta \leq 3\pi/2 - \theta_M$ Corrected = $-(3\pi/2 - \theta_M + (1-\epsilon)\delta) \leq \theta \leq 3\pi/2 - \theta_M + (1-\epsilon)\delta$

kR	Arc ₁	Corrected	Arc ₂	Corrected	Arc ₃	Corrected
2π	1.29λ	1.43λ	1.57λ	1.75λ	4.72λ	Same
4π	1.88λ	2.02λ	4.21λ	4.52λ	8.32λ	Same
10π	3.14λ	3.27λ	12.0 λ	12.48λ	19.3 λ	Same

TABLE VIII (R=150 cm, r=R/4)

kR	$\frac{\Phi_d}{2}$	$(kR)^{2/3}$	γ	$\gamma\theta_I$	$\gamma\frac{\theta_I}{360}2\pi R$	$\gamma(\theta_M - 90)$	$\gamma\frac{\theta_M - 90}{360}2\pi R$	$\gamma(180-90)$
2π	19.9°	3.41	0.112	4.14°	0.072 λ	5.04°	0.088 λ	10.1°
4π	15.6°	5.38	0.0726	2.68°	0.094 λ	4.07°	0.142 λ	6.54°
10π	11.5°	9.95	0.0400	1.48°	0.129 λ	2.56°	0.224 λ	3.60°

TABLE VIIIa

kR	Arc ₁	Corrected	Arc ₂	Corrected	Arc ₃	Corrected
2π	1.29 λ	1.43 λ	1.57 λ	1.75 λ	4.72 λ	Same
4π	2.58 λ	2.77 λ	3.90 λ	4.18 λ	8.76 λ	Same
10π	6.45 λ	6.71 λ	11.2 λ	11.65 λ	20.2 λ	Same

TABLE IX (R=150 cm, r=R/8)

kR	$\frac{\Phi^d}{2}$	$(kR)^{2/3}$	γ	$\gamma\theta_I$	$\frac{\theta_I}{\gamma} \frac{2\pi R}{360}$	$\gamma(\theta_M - 90)$	$\frac{\gamma(\theta_M - 90)}{260} 2\pi R$	$\gamma(180-90)$
2π	19.9°	3.41	0.112	3.02°	0.053 λ	5.83°	0.102 λ	10.1°
4π	15.6°	5.38	0.0726	1.96°	0.068 λ	4.39°	0.153 λ	6.54°
10π	11.5°	9.95	0.0400	1.08°	0.094 λ	2.72°	0.237 λ	3.60°

TABLE IXa

kR	Arc ₁	Corrected	Arc ₂	Corrected	Arc ₃	Corrected
2π	0.94 λ	1.05 λ	1.81 λ	2.01 λ	4.26 λ	Same
4π	1.88 λ	2.02 λ	4.21 λ	4.52 λ	8.32 λ	Same
10π	4.71 λ	4.90 λ	11.9 λ	12.37 λ	19.5 λ	Same

TABLE X (R=150 cm, r=R/20)

kR	$\frac{\Phi_I^d}{2}$	$(kR)^{2/3}$	γ	$\gamma\theta_I$	$\frac{\theta_I}{360} 2\pi R$	$\gamma(\theta_M - 90)$	$\frac{\gamma(\theta_M - 90)}{360}$	$\gamma(180-90)$
2π	19.9°	3.41	0.112	2.02°	0.035λ	6.05°	0.106λ	10.1°
4π	15.6°	5.38	0.0726	1.31°	0.046λ	4.47°	0.156λ	6.54°
10π	11.5°	9.95	0.0400	0.72°	0.063λ	2.76°	0.241λ	3.60°

TABLE Xa

kR	Arc ₁	Corrected	Arc ₂	Corrected	Arc ₃	Corrected
2π	0.63λ	0.70λ	1.88λ	1.99λ	4.40λ	Same
4π	1.26λ	1.35λ	4.28λ	4.59λ	8.28λ	Same
10π	3.14λ	3.27λ	12.0λ	12.48λ	19.3λ	Same

3.2.7 Numerical Results (Second Set of Numerical Values)

The same computations as in IV can be made for the second set of numerical values. These results are found in Tables XI, XIa, XII, and XIIa. The corrections to these arcs are found in Tables XIc and XIIc; their numerical computation in Tables XIb and XIIb.

- A. $R = 100 \text{ cm}$, $kR = 4.19$, $(\frac{kR}{2})^{1/3} = 1.29$, $\frac{\Phi^d}{2} = 23^\circ$, $(kR)^{2/3} = 2.59$, $\gamma = 0.144$
- Case 1: $r = \frac{1}{4}\lambda$, $\frac{r}{R} = \frac{3}{8}$, $(\frac{r}{R})^2 = \frac{9}{64} = 0.1405$, $\theta_I = 43.4^\circ$
- Case 2: $r = \frac{1}{4}R$, $(\frac{r}{R})^2 = \frac{1}{16} = 0.0625$, $\theta_I = 37^\circ$
- Case 3: $r = \frac{1}{8}R$, $(\frac{r}{R})^2 = \frac{1}{64} = 0.0156$, $\theta_I = 27^\circ$

TABLE XI

Case	θ	$\theta - 90$	$(\frac{\theta - 90}{180})\pi$	ζ_o	$ g_1(\zeta_o) $	$(\frac{270 - \theta}{180})\pi$	ζ'_o	$ g_1(\zeta'_o) $	Ratio
1	133.4°	43.4°	0.756	0.970	0.687	2.38	3.05	0.0957	0.139
1	$\theta_M = 110^\circ$ ⁺	20°	0.349	0.447	1.027	2.79	3.58	0.0599	0.0585
2	127°	37°	0.645	0.825	0.764	2.49	3.21	0.0860	0.113
2	$\theta_M = 133^\circ$	43°	0.750	0.960	0.693	2.37	3.06	0.0950	0.137
3	117°	27°	satisfies the accuracy requirement by above computations						
3	$\theta_M = 139^\circ$	49°	0.855	1.10	0.613	2.28	2.92	0.1113	0.182

⁺ θ_M lies in the illuminated region and hence the illuminated arc does not simulate the entire region.

TABLE XIa [Arc Length = $\frac{2\theta}{360} 2\pi R = \frac{2\theta}{360} \frac{4\pi\lambda}{3} = \frac{2\theta}{270} \pi\lambda$]

r	θ_I	Arc ₁	θ_M	Arc ₂ ($\theta_M - 90$)	Arc ₃ ($270 - \theta_M$)
1/4λ	43.4°	—	110°	0.465λ	3.72λ
1/4R	37°	0.870λ	133°	1.00 λ	3.19λ
1/8R	27°	0.628λ	139°	1.14 λ	3.04λ

TABLE XIb

r	$\gamma\theta_I$	$\frac{\gamma\theta_I}{360} 2\pi R$	$\gamma(\theta_M - 90)$ $\frac{\Phi d}{\gamma 2}$	$(\theta_M - 90)$ $\frac{\gamma}{360} \frac{\Phi d}{2} - 2\pi R$	$\gamma(180 - 90)$
1/4λ	—	—	3.31°	0.0385λ	12.95°
1/4R	5.33°	0.0620λ	6.19°	0.0720λ	12.95°
1/8R	3.89°	0.0452λ	7.05°	0.0820λ	12.95°

TABLE XIc

r	Arc ₁	Corrected	Arc ₂	Corrected	Arc ₃	Corrected
1/4λ	—	—	0.465λ	0.542λ	3.72λ	Same
1/4R	0.870λ	0.994λ	1.00λ	1.14λ	3.19λ	Same
1/8R	0.628λ	0.718λ	1.14λ	1.30λ	3.04λ	Same

B. $kR=2$, $R=\frac{\lambda}{\pi}$, $(\frac{kR}{2})^{1/3} = 1.00$, $\frac{\Phi_d}{2} = 30^\circ$, $(kR)^{2/3} = 1.59$, $\gamma = 0.226$

$r=1/4\lambda = \pi R/4$, $r/R = \pi/4$, $(r/R)^2 = \pi^2/16 > 1/5$ hence does not satisfy accuracy requirement

Case 1: $r=1/4R$ Case 2: $r=1/8R$ Case 3: $r=R/20$ $(r/R)^2 = 1/400 = 0.0025$

TABLE XII

Case	θ	$\theta - 90$	$(\frac{\theta - 90}{180})\pi = \zeta_0$	$ g_1(\zeta_0) $	$(\frac{270-\theta}{180})\pi = \zeta_1$	$ g_1(\zeta_1) $	Ratio
1	127°	37°	0.645	0.8549	2.49	0.1508	0.176
1	$\theta_M = 117^\circ^+$	27°	0.471	0.9709	2.67	0.1246	0.129
2	117°	27°	satisfies accuracy requirement computations above				
2	$\theta_M = 127^\circ$	37°					
3	108°	18°	0.690	0.8257	2.45	0.1567	0.190
3	$\theta_M = 129.5^\circ$	39.5°					

⁺ θ_M lies in the illuminated region and hence the illuminated arc does not simulate the entire illuminated region.

TABLE XIIa [Arc Length = $\frac{2\theta}{360} 2\pi R = \frac{2\theta}{360} 2\pi \frac{\lambda}{\pi} = \frac{\theta}{90} \lambda$]

r	θ_I	Arc ₁	θ_M	Arc ₂ ($\theta_M - 90$)	Arc ₃ ($270 - \theta_M$)
1/4R	37°	—	117°	0.300λ	1.70λ
1/8R	27°	0.300λ	127°	0.412λ	1.59λ
1/20R	18°	0.200λ	129.5°	0.440λ	1.56λ

TABLE XIIb

r	$\gamma \theta_I$ $\frac{\Phi d}{\gamma 2}$	$\frac{\theta_I}{360} 2\pi R$ $\frac{\Phi d}{\gamma 2} \frac{2\pi R}{360}$	$\gamma(\theta_M - 90)$ $\frac{\Phi d}{\gamma 2}$	$(\theta_M - 90)$ $\frac{\Phi d}{\gamma 2} \frac{2\pi R}{360}$	$\gamma(180 - 90)$
1/4R	—	—	6.68°	0.037λ	20.3°
1/8R	6.68°	0.037λ	8.36°	0.046λ	20.3°
1/20R	6.68°	0.037λ	8.93°	0.050λ	20.3°

TABLE XIIc

r	Arc ₁	Corrected	Arc ₂	Corrected	Arc ₃	Corrected
1/4R	—	—	0.300λ	0.374λ	1.70λ	Same
1/8R	0.300λ	0.374λ	0.412λ	0.504λ	1.59λ	Same
1/20R	0.200λ	0.274λ	0.440λ	0.540λ	1.56λ	Same

3.2.8 Limiting Case of Large R

It is possible to consider the limiting case of large R provided we are careful to maintain the far field assumption $\rho \gg R$. As R becomes large while r remains fixed the illuminated region approaches $-\pi/2 \leq \theta \leq \pi/2$, the arc length of the illuminated arc becomes infinitely large, and the width of the penumbra region becomes vanishingly small. Thus, if the results of our analysis are applied to the case of a line source near an infinite plane, we would find that the entire plane (with a zero correction since the width of the penumbra region now equals zero) is necessary to reproduce the far field pattern in the illuminated region. This, of course, is the result which is strictly valid.

To what degree the pattern can be simulated by a large (with respect to wavelength) plane depends on the analysis of the diffracted waves which can be thought of as arising from the edges. However, our analysis assumes the smooth removal of portions of the cylinder and so does not consider edge effects. Hence, it cannot be expected to give results in cases where the edges play a role.

3.2.9 Conclusions Concerning the Numerical Results

The main difference between the computations for $kR=2\pi, 4\pi, 10\pi$ and $kR=2, 4, 19$ (besides the difference in correction for finite kR) is the much smaller values of θ_M in the latter cases. We have seen two instances where θ_M lies in the "illuminated region" and thus the illuminated arc does not simulate the entire "illuminated region". This is to be expected since the smaller the cylinder, the greater the effect of the contribution due to the wave "creeping" around the cylinder.

The difference in the correction for finite kR , for the smaller values of kR , enters when we use the phase difference $\gamma \frac{\pi}{2}$ for angles which lie in the "penumbra region" of the cylinder with incident plane wave. This is only a reasonable approximation to the actual phase difference; thus the same for the correction term.

Now, in order to increase the values of θ_M we must decrease the value of r (for a fixed frequency). But, this then puts the boundary of the "illuminated region" of the line source into the "penumbra region" of the plane wave. Therefore, the correction to the illuminated arc is only the reasonable approximation. However, the larger θ_M , the further it is from the "penumbra region"; thus the better the correction term, or in other words, the better the arc $-\left(\theta_M - \pi/2 + \gamma\theta_M\right) \leq \theta \leq \theta_M - \pi/2 + \gamma\theta_M$ simulates the far field in $-\theta_M \leq \theta \leq \theta_M$ (to the given degree of accuracy).

IV

INSTRUMENTATION

The spectrum signature data required by the Electromagnetic Compatibility Analysis Center (ECAC) must be presented in a statistical form if they are to be properly processed. Since antenna spectrum signature data are generally collected in the form of conventional antenna radiation patterns (continuous plots of the antenna radiation characteristic as a function of angle), the patterns must be replotted in statistical form (e. g. cumulative gain data). Either manual or automatic techniques may be used but with the large volumes of data involved in spectrum signature studies, the manual techniques will be both time-consuming and costly. In the interest of economy, a technique has been devised so that the data may be processed automatically. This is accomplished by incorporating an analog to digital converter system in a conventional antenna pattern recorder. This converter is so designed that the pattern data are simultaneously recorded in digital form as the pattern is plotted in analog form. To facilitate later data reduction, the digital converter samples the amplitude of the analog plot at equally spaced (1°) increments so that 360 points are sampled and digitalized for each pattern. The sampled amplitude data are accurate to within a third of a db of the analog plot. The digitalized data are stored on magnetic tape for later reduction to the desired statistical form through the use of a computer (e. g. IBM 7090).

V

CONCLUSIONS AND RECOMMENDATIONS

Measurement techniques applicable to determining the three-dimensional spectrum signatures of airborne antennas have been presented in this report. The following six measurement techniques have been considered. 1) Full-scale models, 2) Partial full-scale models, 3) Instrumented flying aircraft, 4) Precision scale models, 5) Simplified scale models, and 6) Simplified partial models. Each of the above techniques has been found to be suitable for obtaining spectrum data. However, the simplified modeling techniques have been found to be more desirable from the standpoint of cost and ease of model fabrication. The use of simplified scale models and / or simplified partial models is justified since for purposes of compatibility analysis it is not the actual radiation characteristics of the airborne antenna that are used, but rather a statistical model of the radiation characteristics. To prove the validity of simplified techniques, a comparison of antenna pattern statistical data obtained from precision and simplified models of a T-33 aircraft has been made. The statistical data show excellent pattern agreement between the two aircraft models (see Figs. 22-26 and Figs. 39-43).

To evaluate the above techniques, the experimental study employed low-gain low-frequency antennas. The data presented in this report have been obtained with either a modified monopole or standard $\lambda/4$ monopole antenna. Since the radiation pattern of the monopole antenna configuration is omnidirectional split-beam, which is strongly dependent upon airframe surface currents, the simplified modeling technique has been subjected to a rather rigorous experimental evaluation. However, it is recommended that a further study of the simplified technique be conducted using an antenna having a unidirectional radiation pattern.

Since many antenna types (e. g. spirals) are not easily scaled, an analytical study has also been conducted to determine the feasibility of employing simplified full-scale partial models to obtain spectrum signature data. The results of this study are presented herein. Since these results appear encouraging, it is recommended that a short experimental study be conducted to evaluate further the theoretical data.

This report has been primarily concerned with the evaluation of various measurement techniques applicable to obtaining airborne antenna spectrum signature data suitable for Air Force requirements and in a form that may be evaluated at the Electromagnetic Compatibility Analysis Center (ECAC). It is recommended that the study now be broadened to include an investigation of techniques for 1) obtaining information on the absolute gain of airborne antennas at spurious and harmonic frequencies, and 2) predicting the radiation characteristics of such antennas.

REFERENCES

- Bruckmann, H. (1963) "Antenna Measurement by Satellite," IEEE Trans. -PGAP, pp 143-147.
- Cohen, A. and A. W. Maltese (1961) "The Lincoln Laboratory Antenna Test Range," Microwave Journal, pp 56-65.
- Dorne, A. and D. Lazarus (1947) Very High Frequency Techniques-1 (McGraw Hill, New York) pp 174-176.
- Franz, W. (1954) "On the Green's Functions of the Cylinder and Sphere," Z. fur Naturforschung, 9a, pp 705-716.
- Goodyear Aerospace Corporation (September, 1964) Brochure on Antenna and Microwave Technology.
- Goriainov, A. S. (1958) "An Asymptotic Solution of the Problem of Diffraction of a Plane Electromagnetic Wave by a Conducting Cylinder," Radiotekhnika i elektronika, 3, pp 23-29.
- Hudson, F. M. (1964) "Metal-Strayed Fiberglass Radar Target Models," Tech. Doc. Rept. No. RADC-TDR-64-25, Vol. 1, Radar Reflectivity Measurements Symposium, pp 419-425.
- Jones, E. A. (1948) "Model Techniques for Determination of the Characteristics of Low Frequency Antennas," Final Report, Contract W36-039 SC-32049.
- Keay, C. S. L. and R. E. Gray (1963) "A Practical Method for Determining the Directivity of HF and VHF Antenna Systems," NASA Tech. Memo X-940.
- King, R. W. P. and T. T. Wu (1959) "The Scattering and Diffraction of Waves," Harvard Monograph in Applied Science, No. 7.
- Levy, B. R. and J. B. Keller (1959) "Diffraction by a Smooth Object," Comm. Pure and Appl. Math., 12, pp 159-209.
- Logan, N. A. (1959) "General Research in Diffraction Theory, Vol. 2," Lockheed Missiles and Space Division Report No. 288088.
- Magnus, W. and R. Oberhettinger (1949) Functions of Mathematical Physics (Chelsea).

- Melpar, Inc., "Antenna Systems Research and Development Capabilities," Melpar Brochure TP-191.
- Morse, P. M. and H. Feshbach (1953) Methods of Theoretical Physics, Vols. I, II, (McGraw-Hill, New York).
- North American Aviation (21 October, 1964) Private communication.
- Sinclair, G., E. C. Jordan and E. W. Vaughan (1947) "Measurement of Aircraft-Antenna Patterns Using Models," Proc. IRE, pp 1451-1462.
- Turner, E. M. (1959) "Spiral Antennas Meet Needs of New Vehicles," Aerospace Elec.
- Wetzel, L. (1957) "High Frequency Current Distributions on Conducting Obstacles," Scientific Report No. 10, Harvard University Cruft Laboratory.

ACKNOWLEDGMENTS

The authors are indebted to W. De Hart and R. E. Hiatt under whose direction this work was performed, to R. Harris who was responsible for equipment modifications and antenna pattern measurements, to T. B. A. Senior who suggested the use of a simplified model and to K. Holmes for the fabrication of the simplified aircraft models.

APPENDIX A

DETERMINING ASPECT ANGLES FROM PHOTOGRAPHS

A. 1 Procedure for Obtaining Aspect Measurements

Two procedures have been developed for obtaining the aspect from which an aircraft has been viewed by examination of photographic records. The first involves measurement of the photograph, the second a comparison with a model in a shadow-graph.

The aspect or view from which the target aircraft is seen is defined with the aircraft at the center of a sphere, flying in the plane of the equator. Horizontal aspect, θ , is defined as the angle of longitude on the sphere between the axis of the aircraft (tail = 0°) and the line-of-sight from the target to the viewer, with sense as shown in Fig. A-1. Vertical aspect, ϕ , is defined as the angle between the plane of the equator and the line-of-sight from the target to the viewer, with sense as shown in Fig. A-1.

The method involving measurements taken from the photograph considers the target to be two line-segments, one the length of the fuselage along its axis and the other the distance between the wing tips.

If the viewing distance is large compared with the dimensions of the target, the ratio of the projected lengths of these two lines and the angle between them can be measured from a photograph. The ratio of the comparable dimensions of the target is known. A set of equations was derived which relate this angle and these two ratios to the aspect angles ϕ and θ (Sec. A. 2). A graph of these equations is used for rapid computation during film reduction.

The second method used to determine aspect from photographic records makes use of a shadow-graph. A model is illuminated by a distant light source, which casts a shadow of the model on an adjacent plane surface. The model is mounted on

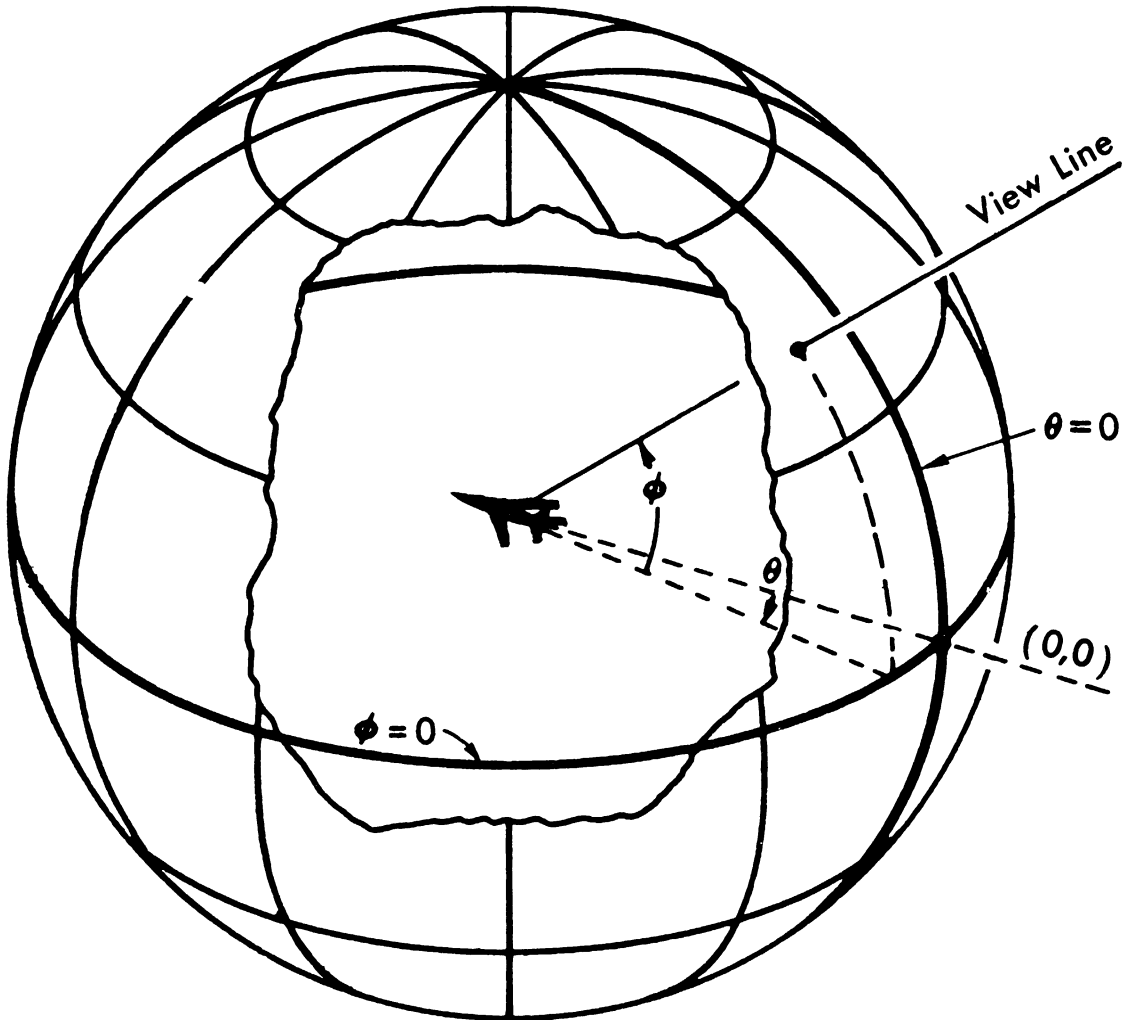


FIG. A-1: DEFINITION OF ASPECT ANGLES: ϕ = VERTICAL
 θ = HORIZONTAL.

gimbals provided with a scale for measuring aspect angles. In use, the position of the model is adjusted visually so that the shape of the shadow is identical with the photograph of the target, and the angles θ and ϕ are read from the scales on the gimbals.

A study of the error introduced by parallax due to a finite separation of the light source and the model was made. This study, which influenced the mounting design, indicated that at a distance of 13 ft, parallax error is negligible.

The model was mounted on a box containing the light source as shown in Fig. A-2. A mirror on an adjustable mount was fastened to a wall at a height of about 6 - 1/2 ft above the light source and model. The position of the source and model and the tilt of the mirror were adjusted so that the light incident upon the model was perpendicular to the two axes of rotation of the model when both aspect scales were adjusted to the zero aspect reading and the shadow of the model indicated zero aspect.

A. 2 Geometry of Ratio Method for Determining Aspect

The ratio method is based on the conclusion that for this test program there exists a unique set of aspect angles, θ and ϕ for each angle between, and the ratio of lengths of, two perpendicular lines on the aircraft seen on the film. The target is assumed to consist of two line-segments. These lines need not intersect, but a translation of one line into intersection with the other must, in the analysis to follow, form a right angle. In Fig. A-3, parts of each of the two lines representing the target are shown as \overline{OA} and \overline{OB} . One of these lines can be assumed to have been translated into intersection with the other at point O. The line \overline{OD} is the line-of-sight from the viewer to the target. The distance from the viewer to the target is assumed to be large in comparison with the projected dimensions of the target.

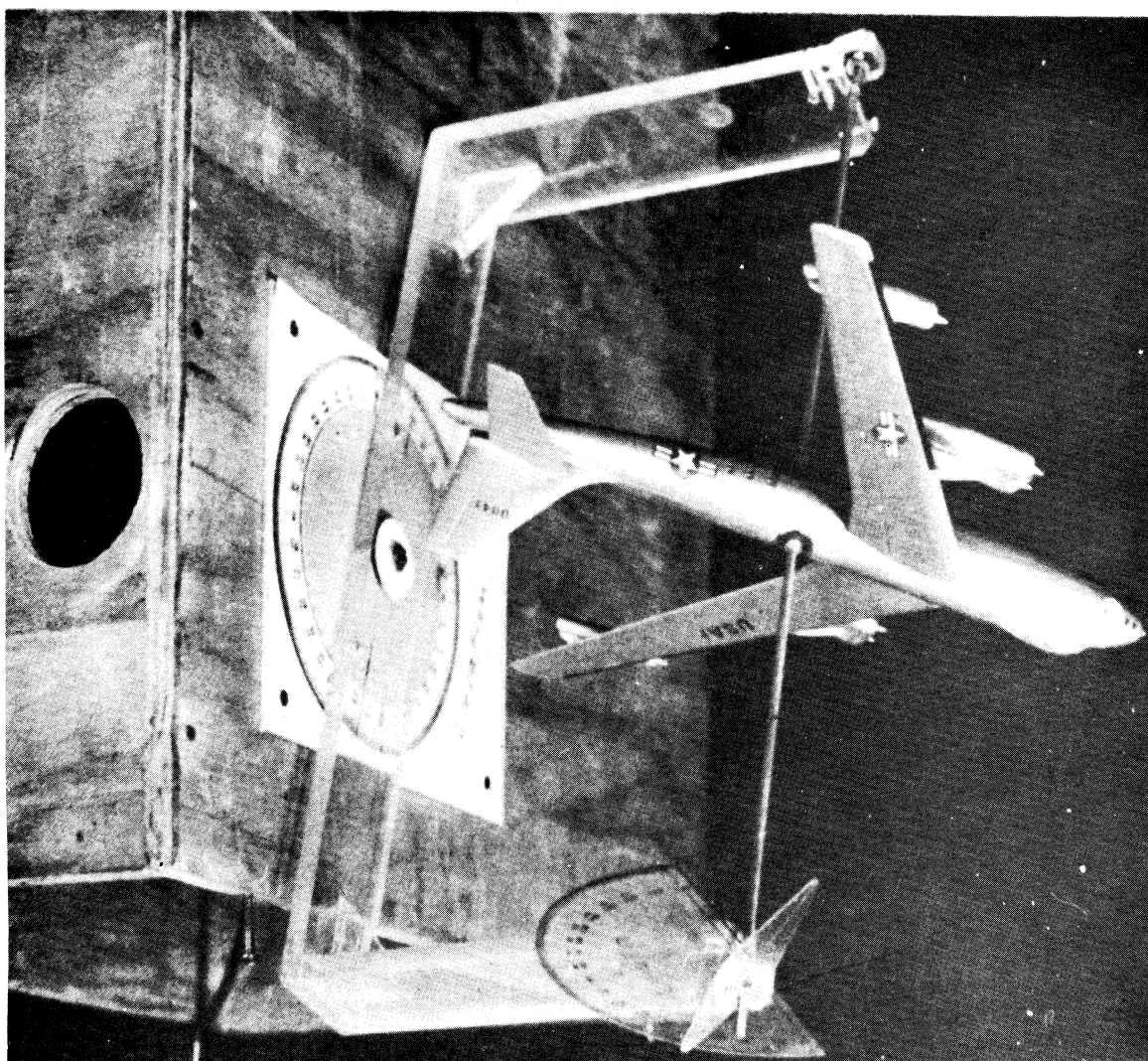
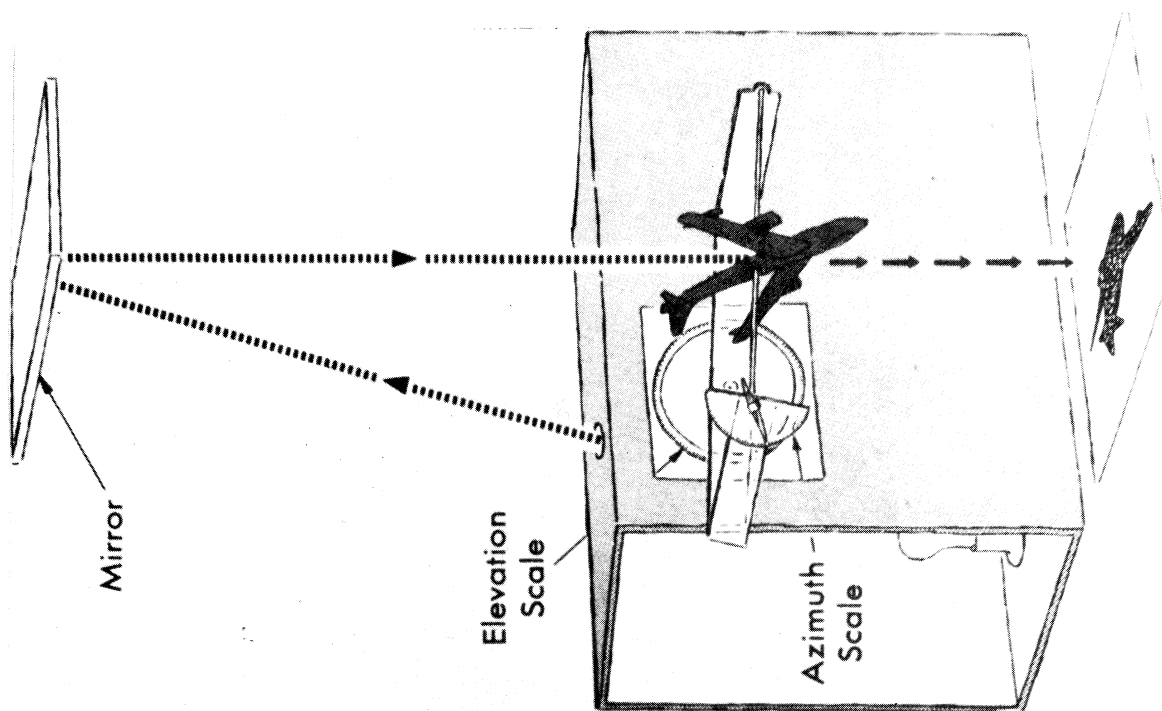


FIG. A-2: SHADOWGRAPH FOR MEASURING ASPECT

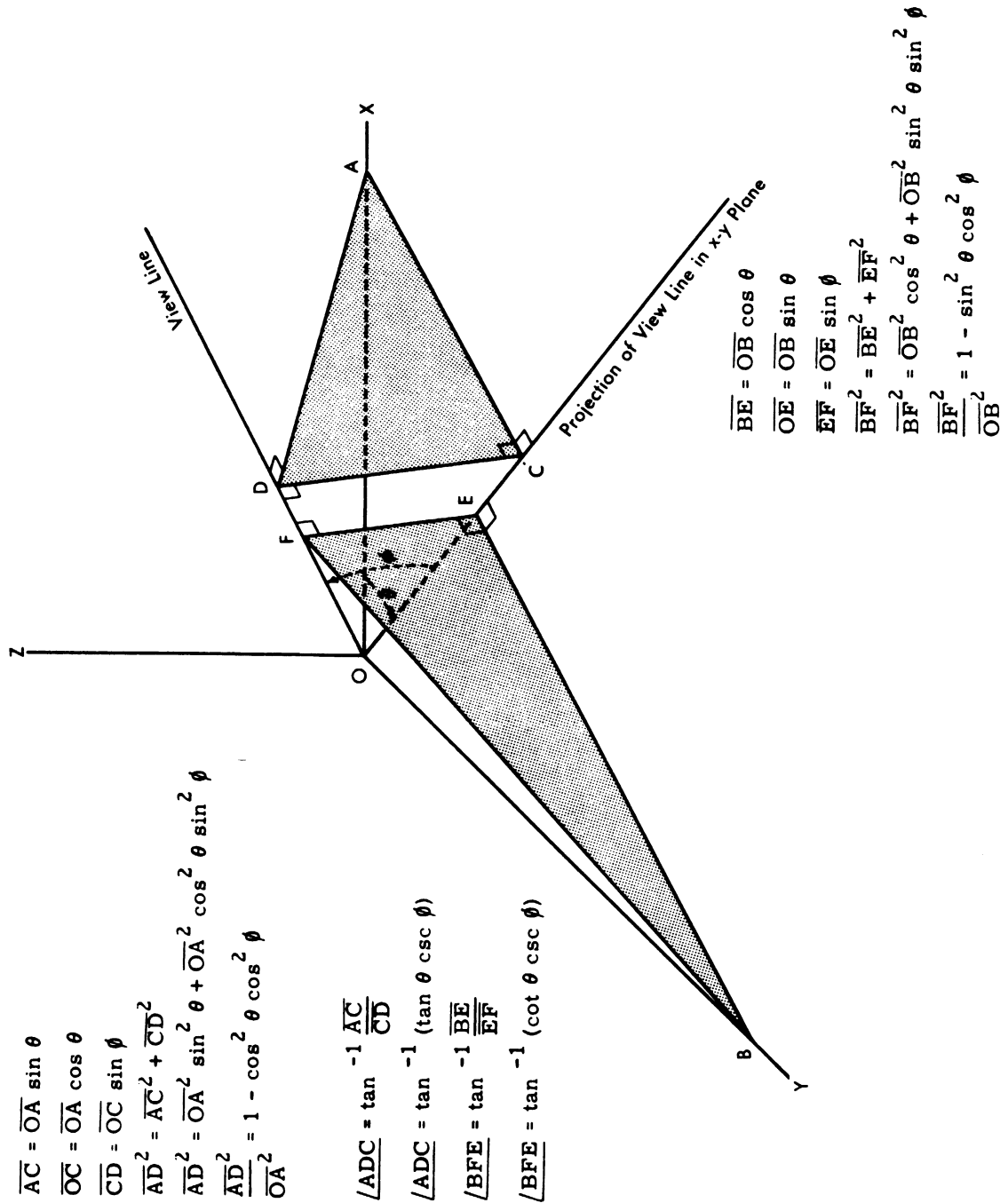


FIG. A-3: GEOMETRY OF ASPECT MEASUREMENT FROM PHOTOGRAPHS

In Fig. A-3, line \overline{OA} is defined as coincident with the axis of the fuselage of the target and \overline{OB} is defined as parallel to the line joining the wing tips of the target. The projection of the view line in the \overline{AOB} plane is line \overline{OC} . These three lines form the angles θ and ϕ , previously defined as the horizontal and vertical aspect angles.

From point A, line \overline{OD} is constructed perpendicular to the view line at point D. From point D, line \overline{DC} is constructed perpendicular to the view line at D and intersecting the projection of the view line at C. Plane \overline{ACD} is the plane of projection normal to the viewing direction. Because plane \overline{OCD} is perpendicular to plane \overline{AOB} , the intersection of plane \overline{ACD} with these planes forms two right angles denoted $\angle ADC$ and $\angle OCA$. The same procedure is used at point B to generate points E and F.

The equations of the geometry presented in Fig. A-3 express, in terms of aspect angles, ratios of the projections of \overline{OA} and \overline{OB} in the viewing plane of projection to \overline{OA} and \overline{OB} respectively and the angles between these projections and lines \overline{CD} and \overline{EF} .

If L and W represent the length of the fuselage and the distance between the wing tips of a target, respectively, and ℓ and w represent the projections of L and W in the plane normal to the viewing line, according to the previous analysis,

$$\left(\frac{\ell/w}{L/W}\right)^2 = \frac{1 - \cos^2 \theta \cos^2 \phi}{1 - \sin^2 \theta \cos^2 \phi} = \rho^2 \quad (A. 1)$$

If the viewing distance is large compared with the target dimensions, the ratio ℓ/w can be measured from a photograph. The ratio L/W is a known characteristic of the aircraft.

The angle formed in the plane normal to the viewing line is the sum of angles \overline{ADC} and \overline{BFE} . For the angle ψ defined as

$$\psi = 180^\circ - \angle ADC - \angle BFE,$$

the following equation is valid:

$$\psi = 180^\circ - \tan^{-1}(\tan \theta \csc \phi) - \tan^{-1}(\cot \theta \csc \phi).$$

If the tangent of the sum of two angles is expressed in terms of the tangents of each:

$$\psi = 180^\circ - \tan^{-1} \frac{\tan \theta \csc \phi + \cot \theta \csc \phi}{1 - \tan \theta \csc \phi \cot \theta \csc \phi},$$

$$\psi = 180^\circ - \tan^{-1} \frac{-\sin \phi}{\sin \theta \cos \theta \cos^2 \phi},$$

or

$$\tan \psi = \frac{\sin \phi}{\sin \theta \cos \theta \cos^2 \phi} \quad (A. 2)$$

A graph prepared for the solution of equations (A. 1) and (A. 2) is shown in Fig. A-4. The range of the variables in this graph is sufficient for the data reduction process. The quantities ρ^2 and ψ are obtained from the photograph. The graph yields the corresponding values of ϕ and θ .

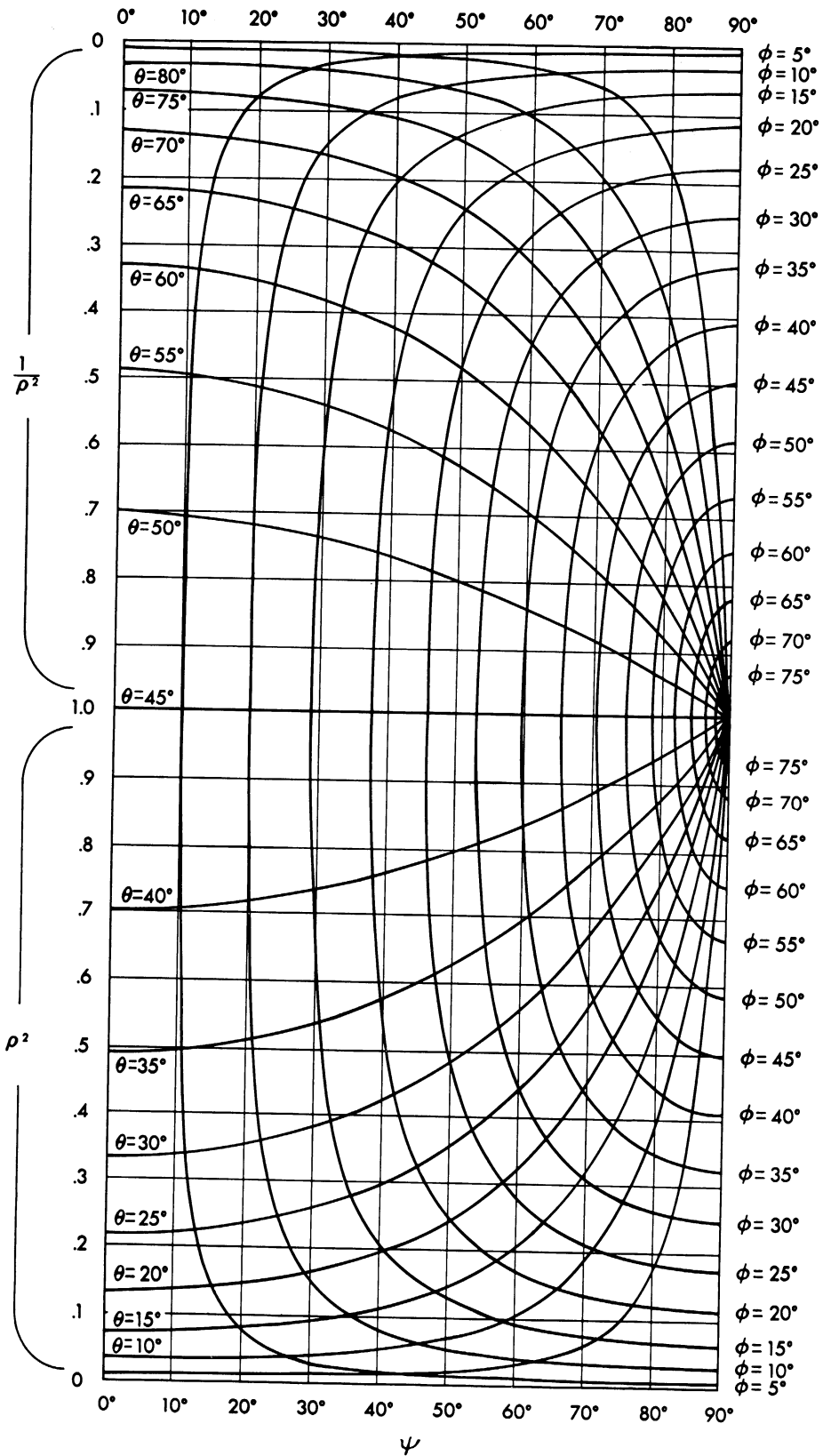


FIG. A-4: GRAPH FOR ASPECT COMPUTATION

APPENDIX B

 $g_1(\zeta)$ vs ζ (kR = 4.19)

ζ	Real Part $g_1(\zeta)$	Imag. Part $g_1(\zeta)$	$ g_1(\zeta) $
-1.0	1.794	0.3881	1.836
-0.9	1.794	0.2125	1.807
-0.8	1.772	0.0729	1.774
-0.7	1.734	0.0297	1.734
-0.6	1.689	-0.1018	1.691
-0.5	1.636	-0.1482	1.643
-0.4	1.586	-0.1712	1.595
-0.3	1.524	-0.1736	1.534
-0.2	1.465	-0.1616	1.474
-0.1	1.403	-0.1378	1.410
0.0	1.339	-0.1038	1.343
0.1	1.273	-0.06322	1.275
0.2	1.203	-0.02144	1.203
0.3	1.105	0.02195	1.105
0.4	1.059	0.06456	1.061
0.5	0.9836	0.1046	0.9892
0.6	0.9109	0.1396	0.9216
0.7	0.8372	0.1702	0.8543
0.8	0.7645	0.1952	0.7890
0.9	0.6954	0.2150	0.7278
1.0	0.6282	0.2308	0.6693
1.1	0.5635	0.2401	0.6126
1.2	0.5044	0.2465	0.5614
1.3	0.4499	0.2492	0.5143
1.4	0.3982	0.2482	0.4692
1.5	0.3527	0.2439	0.4288
1.6	0.3106	0.2376	0.3910
1.7	0.3090	0.2296	0.3850
1.8	0.2369	0.2209	0.3239
1.9	0.2049	0.2089	0.2927

THE UNIVERSITY OF MICHIGAN

6664-1-F

ξ	Real Part $g_1(\xi)$	Imag. Part $g_1(\xi)$	$ g_1(\xi) $
2.0	0.1774	0.1998	0.2672
2.1	0.1522	0.1891	0.2428
2.2	0.1307	0.1784	0.2211
2.3	0.1121	0.1676	0.2017
2.4	0.09371	0.1579	0.1836
2.5	0.07853	0.1478	0.1674
2.6	0.06546	0.1357	0.1507
2.7	0.05316	0.1267	0.1374
2.8	0.04378	0.1182	0.1260
2.9	0.03468	0.1090	0.1144
3.0	0.01588	0.09753	0.09879
3.1	0.02038	0.09029	0.09257
3.2	0.01427	0.08559	0.08678
3.3	0.01038	0.07833	0.07899
3.4	0.00607	0.07117	0.07141
3.5	0.00256	0.06460	0.06465
3.6	-0.00036	0.05863	0.05865
3.7	-0.00389	0.05255	0.05273
3.8	-0.00519	0.04830	0.04858
3.9	-0.00660	0.04515	0.04561
4.0	-0.00751	0.04006	0.04074

$g_1(\xi)$ vs ξ (kR = 2)

ξ	Real Part $g_1(\xi)$	Imag. Part $g_1(\xi)$	$ g_1(\xi) $
-1.0	1.794	0.320	1.822
-0.9	1.787	0.144	1.793
-0.8	1.759	0.004	1.759
-0.7	1.714	-0.097	1.717
-0.6	1.663	-0.168	1.672
-0.5	1.607	-0.214	1.621
-0.4	1.550	-0.237	1.568
-0.3	1.489	-0.239	1.508
-0.2	1.429	-0.227	1.447
-0.1	1.365	-0.204	1.380
0.0	1.301	-0.170	1.312
0.1	1.235	-0.129	1.242
0.2	1.165	-0.088	1.168
0.3	1.095	-0.045	1.096
0.4	1.023	-0.002	1.023
0.5	0.949	0.038	0.9497
0.6	0.879	0.073	0.8820
0.7	0.808	0.104	0.8197
0.8	0.738	0.129	0.7492
0.9	0.672	0.150	0.6885
1.0	0.608	0.167	0.6306
1.1	0.546	0.177	0.5739
1.2	0.490	0.185	0.5237
1.3	0.439	0.190	0.4783
1.4	0.390	0.191	0.4343
1.5	0.348	0.189	0.3960
1.6	0.309	0.185	0.3601
1.7	0.270	0.179	0.3239
1.8	0.240	0.173	0.2958
1.9	0.210	0.163	0.2659

THE UNIVERSITY OF MICHIGAN

6664-1-F

ξ	Real Part $g_1(\xi)$	Imag. Part $g_1(\xi)$	$ g_1(\xi) $
2.0	0.184	0.157	0.2419
2.1	0.160	0.149	0.2186
2.2	0.140	0.141	0.1987
2.3	0.123	0.133	0.1811
2.4	0.105	0.126	0.1640
2.5	0.0906	0.1186	0.1493
2.6	0.0783	0.1077	0.1330
2.7	0.0660	0.1014	0.1210
2.8	0.0574	0.0956	0.1115
2.9	0.0483	0.0884	0.1007
3.0	0.0295	0.0769	0.0823
3.1	0.0340	0.0720	0.0796
3.2	0.0275	0.0708	0.0760
3.3	0.0240	0.0651	0.0694
3.4	0.0193	0.0591	0.0622
3.5	0.0154	0.0537	0.0559
3.6	0.0121	0.0489	0.0504
3.7	0.0089	0.0436	0.0444
3.8	0.0061	0.0409	0.0414
3.9	0.0043	0.0397	0.0399
4.0	0.0028	0.0350	0.0351

DOCUMENT CONTROL DATA - R&D

(Security classification of title, body of abstract and indexing annotation must be entered when the overall report is classified)

1. ORIGINATING ACTIVITY <i>(Corporate author)</i> The University of Michigan Radiation Laboratory Department of Electrical Engineering		2a. REPORT SECURITY CLASSIFICATION UNCLASSIFIED	
		2b. GROUP ---	
3. REPORT TITLE Investigation of Measurement Techniques for Obtaining Airborne Antenna Spectrum Signatures.			
4. DESCRIPTIVE NOTES <i>(Type of report and inclusive dates)</i> Final Report June 1964 to March 1965			
5. AUTHOR(S) <i>(Last name, first name, initial)</i> Ferris, Joseph E., Stone, Stephen E and Wolford, Ronald L.			
6. REPORT DATE May 1965	7a. TOTAL NO. OF PAGES 105	7b. NO. OF REFS 19	
8a. CONTRACT OR GRANT NO. AF 33(615)-1964	9a. ORIGINATOR'S REPORT NUMBER(S) 6664-1-F		
b. PROJECT NO. 4357	9b. OTHER REPORT NO(S) <i>(Any other numbers that may be assigned this report)</i>		
c. Task No. 435703	AFAL-TR-65-104		
d.			
10. AVAILABILITY/LIMITATION NOTICES Qualified requestors may request additional copies from Defense Documentation Center, Cameron Station, Alexandria, Virginia 22314.			
11. SUPPLEMENTARY NOTES		12. SPONSORING MILITARY ACTIVITY Electronic Warfare Division, Air Force Avionics Laboratory, Wright-Patterson AFB, Ohio	
13. ABSTRACT This report presents measurement techniques applicable for determining the three-dimensional spectral radiation patterns of antennas installed in airborne vehicles. There are six possible measurement techniques that may be followed to obtain spectrum signatures of airborne antennas. These techniques are characterized by the type of models used, namely, 1) full-scale models, 2) full-scale partial mock-ups, 3) instrumented flying aircraft, 4) precision scale models, 5) simplified scale models, and 6) simplified partial models. The data obtained for electromagnetic compatibility analysis is normally required to be in a statistical form, therefore, a discussion of the instrumentation required to obtain data suitable for statistical analysis will also be presented.			

14. KEY WORDS	LINK A		LINK B		LINK C	
	ROLE	WT	ROLE	WT	ROLE	WT
Spectral Radiation Measurement Techniques Airborne Antennas						

INSTRUCTIONS

1. **ORIGINATING ACTIVITY:** Enter the name and address of the contractor, subcontractor, grantee, Department of Defense activity or other organization (*corporate author*) issuing the report.

2a. **REPORT SECURITY CLASSIFICATION:** Enter the overall security classification of the report. Indicate whether "Restricted Data" is included. Marking is to be in accordance with appropriate security regulations.

2b. **GROUP:** Automatic downgrading is specified in DoD Directive 5200.10 and Armed Forces Industrial Manual. Enter the group number. Also, when applicable, show that optional markings have been used for Group 3 and Group 4 as authorized.

3. **REPORT TITLE:** Enter the complete report title in all capital letters. Titles in all cases should be unclassified. If a meaningful title cannot be selected without classification, show title classification in all capitals in parenthesis immediately following the title.

4. **DESCRIPTIVE NOTES:** If appropriate, enter the type of report, e.g., interim, progress, summary, annual, or final. Give the inclusive dates when a specific reporting period is covered.

5. **AUTHOR(S):** Enter the name(s) of author(s) as shown on or in the report. Enter last name, first name, middle initial. If military, show rank and branch of service. The name of the principal author is an absolute minimum requirement.

6. **REPORT DATE:** Enter the date of the report as day, month, year; or month, year. If more than one date appears on the report, use date of publication.

7a. **TOTAL NUMBER OF PAGES:** The total page count should follow normal pagination procedures, i.e., enter the number of pages containing information.

7b. **NUMBER OF REFERENCES:** Enter the total number of references cited in the report.

8a. **CONTRACT OR GRANT NUMBER:** If appropriate, enter the applicable number of the contract or grant under which the report was written.

8b, 8c, & 8d. **PROJECT NUMBER:** Enter the appropriate military department identification, such as project number, subproject number, system numbers, task number, etc.

9a. **ORIGINATOR'S REPORT NUMBER(S):** Enter the official report number by which the document will be identified and controlled by the originating activity. This number must be unique to this report.

9b. **OTHER REPORT NUMBER(S):** If the report has been assigned any other report numbers (*either by the originator or by the sponsor*), also enter this number(s).

10. **AVAILABILITY/LIMITATION NOTICES:** Enter any limitations on further dissemination of the report, other than those

imposed by security classification, using standard statements such as:

- (1) "Qualified requesters may obtain copies of this report from DDC."
- (2) "Foreign announcement and dissemination of this report by DDC is not authorized."
- (3) "U. S. Government agencies may obtain copies of this report directly from DDC. Other qualified DDC users shall request through _____."
- (4) "U. S. military agencies may obtain copies of this report directly from DDC. Other qualified users shall request through _____."
- (5) "All distribution of this report is controlled. Qualified DDC users shall request through _____."

If the report has been furnished to the Office of Technical Services, Department of Commerce, for sale to the public, indicate this fact and enter the price, if known.

11. **SUPPLEMENTARY NOTES:** Use for additional explanatory notes.

12. **SPONSORING MILITARY ACTIVITY:** Enter the name of the departmental project office or laboratory sponsoring (*paying for*) the research and development. Include address.

13. **ABSTRACT:** Enter an abstract giving a brief and factual summary of the document indicative of the report, even though it may also appear elsewhere in the body of the technical report. If additional space is required, a continuation sheet shall be attached.

It is highly desirable that the abstract of classified reports be unclassified. Each paragraph of the abstract shall end with an indication of the military security classification of the information in the paragraph, represented as (TS), (S), (C), or (U).

There is no limitation on the length of the abstract. However, the suggested length is from 150 to 225 words.

14. **KEY WORDS:** Key words are technically meaningful terms or short phrases that characterize a report and may be used as index entries for cataloging the report. Key words must be selected so that no security classification is required. Identifiers, such as equipment model designation, trade name, military project code name, geographic location, may be used as key words but will be followed by an indication of technical context. The assignment of links, rules, and weights is optional.

UNIVERSITY OF MICHIGAN



3 9015 02826 7774